STUDIES
ON
PREPARATION AND CHARACTERIZATION
OF
HIGHLY DISPERSED MOLYBDENUM SULFIDE CATALYSTS

Akinori MAEZAWA

Department of Chemical Engineering

Faculty of Engineering Science

Osaka University

1988

Preface

The present thesis is a summary of the author's studies on the preparation and characterization of highly dispered molybdenum sulfide catalysts, which have been carried out at Department of Chemical Engineering, Faculty of Engineering Science, Osaka University during 1985 - 1988.

Molybdenum sulfide catalysts are widely used in industry for hydroprocessing petroleum feedstocks. Typical catalyst systems are cobalt or nikel promoted molybdenum sulfides supported on alumina. These catalysts have been extensively studied up to now because of their industrial importance and academic interests. In order to understand synergetic effects in the promoted molybdenum sulfide catalysts, it is required to characterize well the structure of sulfided molybdenum species and the configuration of catalytically active sites over such highly dispersed sulfides. The preparation of highly dispersed and well defined molybdenum sulfide catalysts are intriguing for the design of highly effective hydroprocessing catalysts.

The themes of this thesis include detailed characterization of highly dispersed molybdenum sulfides, in particular, the configuration of catalytically active sites on the sulfides and the preparation of well defined and highly dispersed molybdenum sulfide catalysts. The precursor states and their catalytic activities were also investigated to understand well the sulfided catalysts.

Contents

General Introduction

Supported molybdenum sulfide catalysts are one of the most important catalysts in industry. They are usually promoted by the addition of a proper amount of cobalt or nickel for the uses of hydrodesulfurization of fossile fuels [1]. Concerning the catalytic properties of the supported molybdenum sulfides promoted or unpromoted, extensive investigations have been conducted and reviewed [1-4] recently.

In order to understand the catalytic features of these sulfide systems, it is required to obtain information on the structure of highly dispersed molybdenum sulfides and, in particular, on the configuration of active sites. However, little information has been provided on the latter subject. With unsupported crystalline molybdenum sulfide catalysts, it is suggested [5], actually, that the coordinative unsaturation of the surface site determines the catalytic properties for the hydrogenations of olefins, dienes and acetylenes and the isomerization of olefins. In the case of dispersed molybdenum sulfides, unfortunately, the structure and dispersion degree of the sulfides are not well established.

The aforementioned features of the dispersed molybdenum sulfides depend on a support, activation conditions and preparation procedures of the catalysts. The support effects reflect the interaction modes between precursor molybdenum oxides and the functional groups on the support surface; molybdenum species in

tetrahedral or octahedral coordinations and monomeric or polymolybdate species. However, even the interaction modes between molybdenum oxide and alumina surface, the most common support employed in industry, are not fully understood [6,7].

With the sulfided forms of the catalysts, it is considered on the basis of XPS [8], EXAFS [9], and laser Raman spectroscopic (LRS) [10] studies that highly dispersed MoS_2-like species are formed on fully sulfided MoO_3/Al_2O_3 catalysts. The dispersion degree of sulfided molybdenum has not been so quantitatively determined as that of supported metal catalysts, for which relatively reasonable probe molecules are established. In addition, no information is available concerning the configuration of the catalytically active sites for hydrodesulfurization over sulfided molybdenum catalysts.

In Part I of this thesis, detailed characterization of molybdenum sulfides and their precursor oxides dispersed on various inorganic supports and prepared by conventional procedures were conducted by means of physicochemical techniques including X-ray photoelectron (XPS), infrared (IR) and LRS, and temperature programmed desorption (TPD) techniques of adsorbed probe molelules. In Chapter 1, the interaction modes between molybdenum and a support surface (alumina) and their variations induced by sulfidation were investigated by using adsorption of H_2S. The aluminas modified with fluorine or sulfate anions or various cations were also employed to clarify the adsorption sites of H_2S. In Chapter 2, characterizations of supported

molybdenum sulfide catalysts were conducted to reveal the structure of the sulfided molybdenum species and, in particular, the configuration of the catalytically active sites by means of XPS, LRS, IR and TPD of NO [12,13]. A measure of the dispersion degree of sulfided molybdenum species was proposed. It was found that TPD of NO differentiates two kinds of active sites; doubly and triply coordinatively unsaturated sites. In Chapter 3, physicochemical characterizations of ZnO/Al_2O_3 and MoO_3-ZnO/Al_2O_3 systems were carried out in connection with the structure of promoted MoO_3/Al_2O_3 catalysts such as CoO-MoO_3/Al_2O_3 [14]. The distribution and dispersion of Zn^{2+} ions and the effects of the presence of cation on the distribution of molybdenum precursor oxides were addressed.

As shown in Part I and by other workers [2,8], it is very difficult to prepare highly dispersed molybdenum sulfide catalysts at a low loading of molybdenum. This is obviously due to difficulties in the reduction and sulfiding of molybdenum species strongly interacting with support such as Al_2O_3 [2,8,15]. In order to prepare effective molybdenum sulfide catalysts, a low valent molybdenum species, $Mo(CO)_6$, was employed as a starting material in stead of ammonium paramolybdate in conventional preparations. Additionally, alkali-metal cation exchanged zeolites were chosen as supports for the purpose of the preparation of well-defined molybdenum sulfides. The use of low valent molybdenum species as a precursor has been briefly conducted by Yermakov et al. [16] by using a π-allyl molybdenum species

anchored on SiO_2 or Al_2O_3. Molybdenum hexacarbonyl supported on SiO_2 was also examined in a fragmentary work by Alper and Blais [17] for hydrodesulfurization of organic sulfur compounds.

In Part II of this thesis, it was demonstrated that dispersed molybdenum sulfides were prepared by using $Mo(CO)_6$ supported on a zeolite or Al_2O_3. It was found that molybdenum sulfides thus prepared were much more highly dispersed than those in conventional catalysts. The interaction modes between $Mo(CO)_6$ and a zeolite were characterized and specific catalytic properties of $Mo(CO)_6$-zeolite systems were explored. In Chapter 4 thermal stabilities of molybdenum carbonyls encaged in alkali-metal cation exchanged zeolites were characterized by means of IR, XPS, and temperature programmed decomposition (TPDE) of adsorbed $Mo(CO)_6$ [18-21]. The stoichiometry of a thermally stable subcarbonyl species was determined by using ^{13}CO [21,22]. In Chapter 5, the hydrogenation of 1,3-butadiene was found to provide selectively cis-2-butene over molybdenum subcarbonyl species encapsulated in zeolites [19,21,23]. In the final chapter, Chapter 6, the preparations of highly dispersed molybdenum sulfides were examined by using molybdenum subcarbonyls adsorbed on Al_2O_3 or zeolites [21]. Catalytic tests for the hydrodesulfurization of thiophene were also conducted as well as physicochemical characterization. It was found herein that highly dispersed and catalytically active molybdenum sulfide species were prepared by using $Mo(CO)_6$ encapsulated in zeolites.

References

1) B.C.Gates, J.R.Katzer, and G.C.A.Schiut, "Chemistry of Catalytic Process" McGraw-Hill, New York, 1979, p390.

2) F.E.Massoth, Adv.Catal., 27, 256 (1978).

3) P.Grange, Catal.Rev.-Sci.Eng., 21, 135 (1980).

4) H.Topsøe and B.S.Clausen, Catal.Rev.-Sci.Eng., 26, 395 (1984).

5) K.Tanaka and T.Okuhara, Catal.Rev.-Sci.Eng., 15, 249 (1977).

6) W.K.Hall, "Fourth International Conference on the Chemistry and Uses of Molybdenum" (H.F.Barry and P.C.H.Mitchell Eds.) Climax Molybdenum Comp. Ann Arbor, MI, 1982, p224

7) W.K.Hall, "Chemistry and physics of Solid surfaces IV" (R.Vanselow and R.Howe Eds.) Springer-Verlag, Berlin, 1986, p73.

8) C.P.Li and D.M.Hercules, J.Phys.Chem., 88, 456 (1984).

9) B.S.Clausen, H.Topsøe, R.Candia, J.Villadsen, B.Lengeler, J.Als-Nielsen, and F.Christensen, J.Phys.Chem., 85, 3868 (1981).

10) a) G.L.Schrader and C.P.Cheng, J.Catal., 80, 369 (1983).
b) G.L.Schrader and C.P.Cheng, J.Catal., 85, 488 (1984).

11) Y.Okamoto, M.Oh-Hara, A.Maezawa, T.Imanaka, and S.Teranishi, J.Phys.Chem., 90, 2396 (1986).

12) A.Maezawa, M.Kitamura, Y.Okamoto, and T.Imanaka, Bull.Chem.Soc.Jpn., under submission.

13) A.Maezawa, Y.Okamoto, and T.Imanaka,
in preparation for publication.

14) A.Maezawa, Y.Okamoto, and T.Imanaka,
J.Chem.Soc.,Faraday Trans. 1, 83, 665 (1987).

15) Y.Okamoto, H.Tomioka, Y.Katoh, T.Imanaka, and S.Teranishi,
J.Phys.Chem., 84, 1833 (1980).

16) Y.I.Yermakov, A.N.Startsev, V.A.Burmistrov,
and B.N.Kuznetsov, React.Kinet.Catal.Lett., 14, 155 (1980).

17) a) H.Alper and C.Blais, Fuel, 59, 670 (1980).
b) H.Alper and C.Blais, J.Chem.Soc.,Chem.Commun., 169 (1980).

18) A.Maezawa, H.Kane, Y.Okamoto, and T.Imanaka, Chem.Express,
2, 531 (1987).

19) A.Maezawa, H.Kane, Y.Okamoto, and T.Imanaka, Chem.Lett., No.2
(1988) in press.

20) Y.Okamoto, A.Maezawa, H.Kane, I.Mitsushima, and T.Imanaka,
J.Chem.Soc.,Faraday Trans. 1, (1988) in press.

21) Y.Okamoto, A.Maezawa, H.Kane, and T.Imanaka, "Proceeding of
the Nineth International Congress on Catalysis" Calgary, July
(1988) in press.

22) Y.Okamoto, A.Maezawa, H.Kane, and T.Imanaka,
J.Catal., under submission.

23) Y.Okamoto, A.Maezawa, H.Kane, and T.Imanaka,
J.Chem.Soc.,Chem.Commun., (1988) in press.

24) A.Maezawa, M.Kitamura, K.Wakamoto, Y.Okamoto, and T.Imanaka,
Chem.Express, 3, 1 (1988).

Part I

Characterization

of

Dispersed Molybdenum Sulfide Catalysts

Chapter 1

H_2S Adsorption on Al_2O_3, Modified Al_2O_3, and MoO_3/Al_2O_3

Abstract

A systematic investigation of H_2S adsorption on Al_2O_3, modified Al_2O_3, and MoO_3/Al_2O_3 catalysts was carried out by using temperature programmed desorption techniques, coupled with IR and XPS. The modified aluminas involve Na^+, Mg^{2+}, Zn^{2+}, F^-, or SO_4^{2-}/Al_2O_3 catalysts with various doping levels. SiO_2-Al_2O_3 and $AlPO_4$ were also studied for comparison. It was found that Al_2O_3 showed two distinctly different chemisorption modes of H_2S associative (α) and dissociative (β) H_2S, whereas SiO_2-Al_2O_3 and $AlPO_4$ provided predominantly α-H_2S. The heats of adsorption were 13 and 34 kcal mol^{-1} for α- and β-H_2S, respectively, and the corresponding site densities were 4.8 and 5.5 x 10^{13} cm^{-2}. The modification of Al_2O_3 with cations was found to induce a significant decrease in the desorption temperature of β-H_2S with a concomitant increase in the total amount of H_2S adsorption. On the contrary, the adsorption amounts of α- and, in particular, β-H_2S were decreased by modifying with anions. The adsorption sites are concluded to be cus (coordinatively unsaturated) Al_{tet}^{3+} cations for α-H_2S and cus Al_{tet}^{3+}-strong base pair sites for β-

H_2S. The effects of calcination and evacuation temperatures on the H_2S adsorption behavior of Al_2O_3 are also interpreted in terms of the above site models and a surface reconstruction of γ-Al_2O_3. The isomerization of 1-butene on Al_2O_3 was found to be poisoned by β-H_2S. On the basis of IR studies of CO_2-H_2S coadsorption, cus Al_{tet}^{3+}-strongly basic oxide anion pair sites are proposed to be responsible for the reaction. When the loading level of MoO_3 was low (< 3 wt%), molybdenum anions were found to react with the surface hydroxyl groups on Al_2O_3 as bidentate ligands similar to SO_4^{2-} anions, forming a monomolecular layer of molybdena over Al_2O_3. The H_2S adsorption on sulfided MoO_3/Al_2O_3 catalysts was also examined.

Introduction

The surface properties of transition aluminas have been investigated extensively, because of their industrial importance as the supports for various metals and metal oxides and because of their intrinsic catalytic activities for a variety of reactions involving C-H, H-H, and C-C bond activation [1-3]. The most modern physicochemical techniques have been progressively applied to the systems including aluminas and related catalysts; ^{27}Al magic angle spinning NMR (MAS-NMR) spectroscopic studies of the Al environments in Al_2O_3 [4] and crystalline and amorphous SiO_2-Al_2O_3 [4,5], ^{15}N MAS-NMR studies of pyridine adsorbed on Al_2O_3 [6] and SiO_2-Al_2O_3 [7], an inelastic electron tunneling

spectroscopic investigation of the adsorption of dimethyl methylphosphate on Al_2O_3 [8], and a photoacoustic spectroscopic study of n-butylamine on Al_2O_3 [9]. Furthermore, the interaction of a basic molecule, NH_3, with an alumina surface is also a subject of recent theoretical chemistry [10]. In these studies various adsorption and interaction sites are postulated, involving surface basic and acidic hydroxyl groups, exposed Al^{3+} cations and oxide anions, and their various combinations. However, the adsorption and reaction sites on Al_2O_3 seem to be still controversial as well as the metal oxide-surface functional group interactions in Al_2O_3 supported catalysts [11,12].

One of the most typical catalyst systems with Al_2O_3 as a support is a MoO_3/Al_2O_3 hydrotreating catalyst [12-14]. It is well established that MoO_3-Al_2O_3 interaction modes and, thus, molybdena species and their dispersions on Al_2O_3 depend on preparation variables; pH, loading level, calcination temperature, and so on [12,13]. The genesis of MoO_3-Al_2O_3 interactions is generally believed to be derived from acid-base interactions between molybdenum anions and the Al_2O_3 surface [12,13,15-17]. The acid-base properties of surface hydroxyl groups and their arrangements on the support surface are considered to determine the resultant configurations of molybdena species and, accordingly, their catalytic activities.

The molybdena-alumina interaction modes are expected to be varied by modifying the acid-base properties of Al_2O_3. Actually, it has been found that the catalytic performances of MoO_3/Al_2O_3

and $CoO-MoO_3/Al_2O_3$ catalysts are altered by the addition of F, Na, Zn, or B [18,19]. These alterations may result partly from the induced changes in molybdena and cobalt species and their dispersions and partly from direct changes in the catalytic properties of a bare alumina surface.

Alumina show interesting catalytic properties for many kinds of reactions; ortho-para H_2 conversion, hydrogen exchange reactions among olefins, paraffins, surface hydroxyl groups, and molecular hydrogen, and other various reactions which proceed on solid acids and bases [1,3,20]. The Claus reaction is also catalyzed effectively by aluminas [21,22]. However, little is known about the nature of the active sites for these reactions in spite of great efforts. In order to characterize the chemical properties of the active sites, selective poisoning techniques are often very informative [23,24]. Basic organic molecules, NH_3, CO_2, NO, H_2S and other various probe molecules have been examined for the reactions over Al_2O_3 [1,23-26] and MoO_3/Al_2O_3 catalysts [27-29].

One of the important reactions catalyzed by Al_2O_3 is the double bond shift reaction of olefins which involved C-H bond activations [1,24]. It is well established that the isomerization of 1-butene is selectively poisoned by H_2S [25,26]. Detailed information on the adsorptions sites of H_2S are required for understanding the site configurations of the isomerization reactions on Al_2O_3. Furthermore, knowledge of the adsorption sites of H_2S on Al_2O_3 and MoO_3/Al_2O_3 would be informative for

understanding the behavior of the Claus reaction as well as the hydrodesulfurization (HDS) reaction. Adsorbed H_2S plays an essential role for the Claus reaction to proceed [21,22,30,30]. In the case of the HDS reaction, it has been found that H_2S, the reaction product, retards the reaction by competitive adsorptions on the active sites with the sulfur compounds to be removed [32,33], that hydrocracking and isomerization reactions taking place during HDS are also affected strongly by H_2S adsorbed on bare Al_2O_3 surface and molybdenum sulfides [33], and further that the degree of sulfidation of Mo (and Co) can be evaluated only on the basis of information on the H_2S strongly held on the catalysts [34]. Therefore, detailed information on the H_2S adsorption on Al_2O_3 and MoO_3/Al_2O_3 would be very valuable in the field of catalysis on these catalysts.

The adsorption of H_2S on Al_2O_3 has been studied by using (FT-)IR [30,35-37], isothermal adsorption [38], and calorimetric measurement [39] techniques. These studies show strong adsorption of H_2S on Al_2O_3. Associative and dissociative adsorptions of H_2S are suggested to occur on Al_2O_3 by IR studies [30,35,36]. However, the respective amounts of two types of chemisorbed H_2S and their chemical nature have not been clarified yet, particularly, in connection with the 1-butene isomerization. As for the Claus reaction, it is suggested that nondissociatively adsorbed species react with SO_2 [31]. In addition, no results have been reported on the effect of additives or impurities, such as SO_4^{2-} and Na^+, on the adsorption behavior of H_2S in spite of

their industrial importance.

The configuration of H_2S adsorption sites have not been fully understood yet. It is believed on the basis of IR studies that H_2S interacts with the surface hydroxyl groups to form O-H-SH_2 complexes [37]. Other sites proposed are Lewis acid-base couples to dissociate S-H bonds, with various acid and base strengths [35,36]. The oxide ions [38] and exposed Al^{3+} cations [35] are also supposed to be the chemisorption sites for H_2S. No decisive models have been presented yet.

In the present study, the adsorption behavior of H_2S on pure Al_2O_3, Al_2O_3 modified with various anions and cations, and MoO_3/Al_2O_3 was systematically investigated by using mainly temperature programmed desorption (TPD) and IR techniques. TPD techniques provide information regarding thermal stabilities, kinetic behavior, and amounts of distinct adsorption species [11,40]. As for the H_2S adsorption, only a brief TPD study has been recently reported by Ramachandran and Massoth [41] for sulfided MoO_3/Al_2O_3 (8 wt% Mo) catalyst.

The results on alumina modified with anions such as F^- and SO_4^{2-} and with cations such as Mg^{2+}, Zn^{2+}, and Na^+ would provide information not only about the surface properties of Al_2O_3 modified with these anions or cations, which are often found in industrial aluminas as impurities, but also about the configurations of the H_2S adsorption sites. XPS techniques were also employed to characterize the modified Al_2O_3 catalysts in terms of the chemical states and dispersions of the additives. IR studies

of H_2S and CO_2 adsorptions, including CO_2-H_2S coadsorption, were also carried out.

The present study revealed that H_2S chemisorbed in two distinctly different modes, associative and dissociative, and that only the latter mode poisoned the 1-butene isomerization. The anions, F^- and, particularly, SO_4^{2-}, strongly depressed the H_2S adsorption, mainly the dissociative adsorption. On the basis of the present results, the adsorption sites are suggested to be Lewis acid-base pair sites for the dissociative adsorption of H_2S. The dispersion degree of molybdena species was also noted. A monomolecular dispersion of Mo is suggested for catalysts with a low MoO_3 content (< 3 wt%).

Experimental

Materials

Two kinds of Al_2O_3, JRC-ALO-2 and -4, were used in the present study. They were provided by the Catalysis Society of Japan as Reference Catalysts [42]. Their nominal impurity levels and some physical properties are summarized in Table 1. ALO-4 Al_2O_3, whose crystalline form was γ-phase by XRD, was mainly used here because of the higher purity. It is designated simply γ-Al_2O_3 in the present study. These aluminas were calcined at 823 K for 5 h in air before use unless otherwise noted. SiO_2 and two kinds of SiO_2-Al_2O_3 catalysts with different compositions were also examined for comparison. They were provided by the Catalysis

Table 1. List of the Catalysts Used in the Present Study

catalyst	surf. area, $m^2\ g^{-1}$	pore vol,[b] $mL\ g^{-1}$	impurity,[b] %	
γ-Al_2O_3[a] (ALO-4)	163	0.66	Na_2O	0.01
			SiO_2	0.01
			Fe_2O_3	0.01
ALO-2[a]	267	0.72	Na_2O	0.04
			SO_4^{2-}	1.72
			SiO_2	0.22
			Fe_2O_3	0.03
η-Al_2O_3[c]	270		SO_4^{2-}	0.3[c]
SiO_2–Al_2O_3[a] (Al_2O_3, 13.8%)	560	0.73	SO_4^{2-}	0.33
SiO_2–Al_2O_3[a] (Al_2O_3, 28.6%)	511	0.93	SO_4^{2-}	0.30
SiO_2[a] (SIO-1)	131	0.58	Al_2O_3	1.31
			CaO	1.73
			SO_3	0.29
$AlPO_4$	171			
MgO	55			
modified Al_2O_3				
Na^+ (5.93)[d]	163			
(11.7)	164			
Mg^{2+} (47.7)	149			
Zn^{2+} (22.6)	152			
F^- (5.05)	154			
(14.0)	152			
SO_4^{2-} (1.95)	160			
(3.93)	158			
MoO_3/Al_2O_3				
(6.38)[d]	160			
(12.7)	163			

[a] Reference catalysts provided by the Catalysis Society of Japan. [b] Given by the Catalysis Society of Japan. [c] ALO-2 treated with a 1.5 N aqueous ammonium solution. Sulfur level was estimated by XPS. [d] Doping level, $10^{13}\ cm^{-2}$.

Society of Japan, too. Their nominal properties are given in Table 1.

$AlPO_4$ was prepared by depositing $Al(NO_3)_3$ and phosphoric acid by using an aqueous ammonium solution. After aging at room temperature for 17 h, followed by filtering and washing, the cake was dried at 383 K for 20 h. Finally, it was calcined at 823 K for 5 h. The BET surface area of $AlPO_4$ thus obtained was 171 m^2g^{-1}.

MoO_3/Al_2O_3 catalysts with various MoO_3 loading were prepared by impregnating γ-Al_2O_3 with aqueous ammonium paramolybdate solutions (1.3 mL g^{-1} of Al_2O_3) containing appropriate amounts of molybdena. After addition of the solution to the Al_2O_3, a catalyst slurry was kneaded for 1.5 h at room temperature, followed by drying at 383 K for 16 h. The catalyst was finally calcined at 823 K for 5 h in air by using an electric furnace. SO_4^{2-}, Na^+, Mg^{2+}, Zn^{2+}, and F^-/Al_2O_3 catalysts were prepared in a similar way as that for the MoO_3/Al_2O_3 by using $(NH_4)_2SO_4$, Na_2CO_3, $Mg(NO_3)_2$, $Zn(NO_3)_2$, and NH_4F aqueous solutions, respectively. Another series of F^-/Al_2O_3 catalysts were prepared by an ion-exchange technique. γ-Al_2O_3 was dispersed into an aqueous solution of NH_4F (40 mL g^{-1} of Al_2O_3) with an appropriate concentration for 1 h, filtered, and washed 3 times with distilled water (60 mL g^{-1} of Al_2O_3). After drying, F^-/Al_2O_3 was calcined at 823 K for 5 h in air. The fluorine level was determined by chemical and XPS analyses. ALO-2 Al_2O_3 was treated with a 1.5 N aqueous solution of NH_4OH for 24 h at room

temperature in order to remove SO_4^{2-} anion as an impurity. The NH_3-treated ALO-2 catalyst, whose crystalline form was η-phase by XRD, is designated simply η-Al_2O_3 here. The residual impurity level of SO_4^{2-} was estimated to be ca. 0.3 wt% from the XPS analysis. F^-/η-Al_2O_3 catalyst series was also prepared by ion exchanging η-Al_2O_3. All the chemicals used here for the catalyst preparations were analytical grade.

The BET surface areas of several catalysts are summarized in Table 1.

Temperature Programmed Desorption (TPD)

TPD studies were carried out by using an apparatus similar to that reported by Cvetanovic and Amenomiya [40]. The catalyst was activated at 773 K for 2 h under a pressure of $< 10^{-3}$ Pa. After cooling to room temperature under a dynamic vacuum, the catalyst was exposed to ca. 7.7 kPa of H_2S at this temperature unless otherwise noted. The exposure time was 30 min, followed by evacuation for 15 min and subsequent standing in a deoxygenated and dehydrated He stream for 30-60 min at room temperature. The desorption of H_2S was undertaken in a He stream (20 mL STP min^{-1}) from room temperature to ca. 880 K at a constant heating rate of 23 K min^{-1}. The H_2S concentration in the effluent gas was determined by a TCD cell. The effluent gas was further analyzed by a GLC to confirm the desorption products. With the catalyst examined here, a small amount of H_2O was detected at the desorption temperature of > 670 K. The curve resolutions of the

TPD spectra were carried out on the basis of the gas analyses. The amount of desorbed H_2S was calculated from the peak area intensity calibrated by known amounts of H_2S.

The TPD spectra of NH_3 were also measured similarly to those of H_2S. The catalyst, which had been evacuated at 773 K for 2 h, was exposed to 11 kPa of NH_3 at room temperature for 30 min, followed by degassing at the same temperature.

The sulfidation of the MoO_3/Al_2O_3 catalyst in the TPD cell was carried out at 773 K for 2 h in an atmospheric pressure of a H_2S/H_2 stream (1/10, 200 mL STP min^{-1}), accompanied by an evacuation at the same temperature for 1 h. Hydrogen sulfide was adsorbed on the sulfided catalyst after cooling to room temperature under a dynamic vacuum.

Measurement of IR Spectra

The IR spectra of the aluminas and modified aluminas were recorded at room temperature on a Hitachi double beam spectrophotometer (EPI-G). The self-supporting wafer of the catalyst was activated in an IR cell at 733 K for 2 h under the same conditions employed for the TPR experiments before the exposure to H_2S and/or CO_2.

XPS Measurements

The XP spectra of the catalysts were measured on a Hitachi 507 photoelectron spectrometer equipped with a cylindrical mirror analyzer using an Al anode (9 kV, 50 mA) [29]. The sample was

mounted on a double-sided adhesive tape and evacuated at room temperature up to 10^{-3} Pa in a pretreatment chamber for measurements of the XP spectra. Binding energies (BE) were referenced to the C1s level at 285.0 eV due to contaminant carbon. The reproducibility of the BE values thus obtained was usually better than $\pm$ 0.2 eV. The peak area was used for the quantitative analysis of the catalyst surface. After the TPD experiments, the sulfidation degree of MoO_3/Al_2O_3 catalysts and sulfur level of the catalyst were estimated from the XPS intensities of the S2p, S2s, Mo3d, and Al2s bands [29]. However, it should be noted that the sulfided catalysts were exposed to air at ambient temperature when mounted into spectrometer.

Isomerization of 1-Butene

The isomerization of 1-butene over the catalyst was carried out at 298 K by using a closed circulation system with a volume of 350 mL. The catalyst was activated in a similar way as in the TPD study. The reaction pressure of 1-butene, which had been purified by freeze-thaw techniques in a vacuum, was 8.2 kPa. The products were analyzed by GLC.

For poisoning experiments, a freshly activated catalyst was contacted with an appropriate pressure of H_2S (< 2 kPa) at room temperature. After circulation for 30 min, the amount of H_2S in the gas phase was determined by GLC to elucidate the adsorption amount of H_2S on the catalyst, followed by a 15 min-evacuation before the introduction of 1-butene.

Results

H_2S Adsorption on γ-Al_2O_3

The TPD spectra of H_2S are shown in Fig. 1 for γ-Al_2O_3, SiO_2-Al_2O_3, SiO_2, and $AlPO_4$. With the Al_2O_3, two peaks are apparently observed at ca. 400 and 560 K. These peaks are designated α and β in this study, respectively. As for ALO-2 and η-Al_2O_3, both peaks were observed with slightly different intensities. These findings indicate the presence of two or more distinct adsorption modes of H_2S on Al_2O_3. The SiO_2-Al_2O_3 catalysts provided relatively weak single peaks at ca. 400 K. $AlPO_4$ also showed predominantly α-peak. On the other hand, the SiO_2 gave a weak desorption peak at 510 K, which was found, however, to be ascribable to the H_2S desorbed from an impurity, CaO, since CaO and MgO provided strong single peaks at nearly the same temperature under the identical activation and adsorption conditions. After the desorption studies of H_2S up to 870 K, XPS indicated no residual surface sulfur within the detection limit of the spectrometer ($< 0.8 \times 10^{13}$ S atoms cm^{-2}). The IR band characteristic of SO_4^{2-} anion, however, appeared at 1380 cm^{-1} after the adsorption of H_2S on γ-Al_2O_3, followed by an evacuation and an oxygen treatment (13 kPa) at 773 K. This indicates the presence of irreversibly adsorbed H_2S. On the basis of the IR band intensities at 1380 cm^{-1}, the sulfur level on γ-Al_2O_3 was estimated to be $(0.3 \pm 0.1) \times 10^{13}$ cm^{-2}. Slager and Amberg [35] also suggested irreversibly adsorbed H_2S on Al_2O_3.

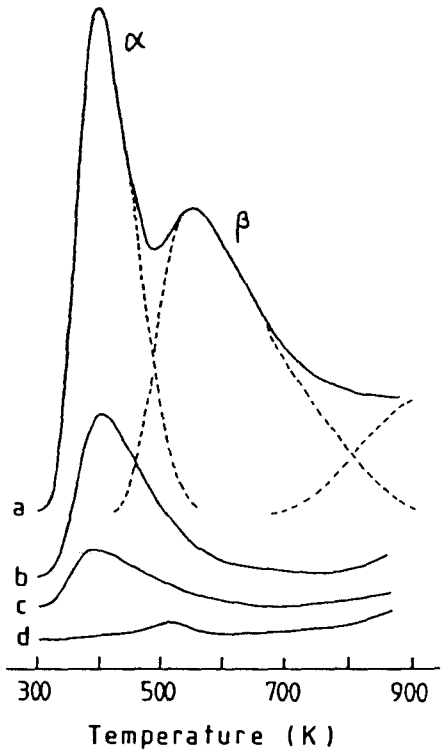

Figure 1. TPD spectra of H_2S on (a) γ-Al_2O_3, (b) SiO_2–Al_2O_3 (28.6% Al_2O_3), (c) $AlPO_4$, and (d) SiO_2. The intensities of the spectra are normalized for the catalyst weight. Dashed lines indicate the resolved spectra of α- and β-H_2S and H_2O.

The amount of H_2S desorbed from these catalysts are summarized in Table 2. They are considered to be nearly identical with those of adsorbed H_2S, since the amount of irreversibly adsorbed H_2S is considerably small (< 3% of adsorbed H_2S for γ-Al_2O_3 degassed at 773 K). The surface Al/(Al + Si) atomic ratios of the SiO_2-Al_2O_3 catalysts were calculated to be 0.15 and 0.56 for 13 wt% (Al/(Al + Si) = 0.16 in bulk) and 28 wt% Al_2O_3 (0.32) catalysts, respectively, on the basis of the XPS intensities of the Al2s and Si2p levels and their atomic cross sections [43] corrected for the escape depths [44]. It is noteworthy that the desorption amounts of α- and, in particular, β-H_2S from the SiO_2-Al_2O_3 catalysts are much lower than those expected from the surface aluminum concentrations.

A TPD study of NH_3 was also carried out for γ-Al_2O_3 and the SiO_2-Al_2O_3 catalysts. The TPD curves were similar to those reported by Amenomiya et al. [45], a strong peak at 430 K and a shoulder at ca. 530 K for γ-Al_2O_3 and the corresponding peaks at higher desorption temperature by ca. 10 K for the latter catalysts. The desorption amounts of NH_3 are also summarized in Table 2. The ratios of the amounts of desorption, NH_3/H_2S, are extremely high for the SiO_2-Al_2O_3 catalysts, compared with that for the Al_2O_3 catalysts. This is due to their very low adsorption capacities for H_2S and not to their high adsorption amounts of NH_3. These observations strongly suggest that different adsorption sites are probed by NH_3 and H_2S.

The dependencies of the amounts of α- and β-H_2S on γ-Al_2O_3

Table 2. Adsorption Amounts of H_2S and NH_3 on the Catalyst As Determined by TPD[a]

catalyst	H_2S, 10^{13} molecules cm^{-2}		NH_3, 10^{13} molecules cm^{-2}	NH_3/H_2S
	α	β		
γ-Al_2O_3	4.42	5.46	17.9	1.9
ALO-2	2.96	2.77		
η-Al_2O_3	3.29	4.54	15.8	2.0
SiO_2–Al_2O_3 (28.6%)	0.73		8.1	11
SiO_2–Al_2O_3 (13.8%)	0.33		7.0	21
SiO_2	0.10[b]			
$AlPO_4$	0.75			
MgO	7.96[b]			
modified γ-Al_2O_3				
Na^+ (5.93)[c]	4.4	5.9	16.0	1.6
(11.7)	10.4[d]		14.5	1.4
Mg^{2+} (47.7)	11.4[d]		17.7	1.6
Zn^{2+} (22.6)	10.7[d]		14.1	1.3
F^- (5.05)	3.82	4.43	19.3	2.3
(14.0)	3.86	3.06	18.5	2.7
SO_4^{2-} (1.95)	3.90	4.64	20.6	2.4
(3.93)	3.64	3.51	21.4	2.9
MoO_3/Al_2O_3				
(6.38)[c]	2.74	2.46	18.0	3.1
(12.7)	1.59	0.89	20.0	5.8

[a] Catalyst evacuated at 773 K for 2 h, followed by an exposure to H_2S (7.7 kPa) or NH_3 (11 kPa) at room temperature for 30 min. [b] See text. [c] Doping level, 10^{13} cm^{-2}. [d] Sum of the adsorption amounts of α- and β-H_2S species is shown because of the unresolved spectrum.

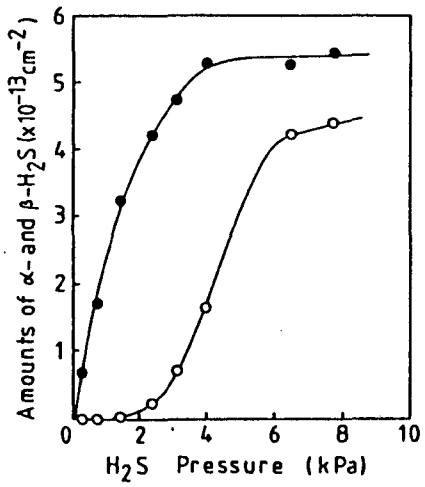

Figure 2. Amounts of α- and β-H_2S on γ-Al_2O_3 as a function of the H_2S pressure. Exposure time, 30 min at room temperature. O, α-H_2S and ●, β-H_2S.

were examined as a function of the exposure time and pressure. It was found that β-H_2S reached an equilibrium value essentially within 10 min of the exposure at a pressure of 7.7 kPa, whereas α-H_2S took much longer time to saturate the adsorption sites. At a 30-min exposure to 7.7 kPa of H_2S, β-H_2S sites were completely saturated and more than 90% of α-sites were fulfilled (4.84×10^{13} cm^{-2} at 120 min). A similar behavior was observed for η-Al_2O_3, too.

Figure 2 shows the effects of the exposure pressure on the adsorption amounts of α- and β-H_2S. It is evident that 4 kPa of H_2S saturates practically all the β-sites within 30 min, while a much higher pressure of H_2S is required for the α-site saturation. When the H_2S pressure is lower than 1.3 kPa, only β-H_2S is observed. These results evidently show that β-H_2S is formed much more easily than α-H_2S. On the basis of these observations, the H_2S adsorption conditions were chosen in the following studies to be 30 min for the adsorption time and 7.7 kPa for the adsorption pressure.

The heat of adsorption of H_2S on γ-Al_2O_3 was calculated from the slope of a linear correlation between $2\log T_M - \log\beta$ and $1/T_M$, assuming that the readsorption of desorbed H_2S occurs freely [40,46]; T_M is the desorption temperature (K) at the peak maximum and β is the rate of temperature increase (5-30 K min^{-1}). The adsorption energies were thus calculated to be 13 and 35 kcal mol^{-1} for α- and β-H_2S at the coverage of 5.5 and 4.4×10^{13} cm^{-2}, respectively. As for ALO-2 catalyst, 14 and 33 kcal mol^{-1}

were obtained for H_2S chemisorbed at the full coverages, respectively. On the basis of isothermal adsorption studies, deRosset et al. [38] calculated the heats of H_2S adsorption to be 38 and 25 kcal mol^{-1} at the coverages of 0.68 and 1.02 x 10^{13} H_2S cm^{-2}, respectively. Recent calorimetric measurement of H_2S adsorption on Al_2O_3 [39] showed 31.5 kcal mol^{-1} at an initial adsorption and 16 kcal mol^{-1} at saturation. These values are consistent with those from the present TPD experiments. In addition, their higher and lower heats of adsorption seem to correspond to those of α- and β-H_2S, respectively.

In order to obtain information on the kinetic behavior of adsorbed H_2S, the desorption order was estimated, according to Cvetanovic and Amenomiya [40] and Konvalinka et al. [46]. The dependencies of T_M and the peak width normalized by T_M, $\Delta T/T_M$, were examined with γ-Al_2O_3 upon the coverage of adsorbed H_2S. Assuming energetically homogeneous first-order desorptions, the T_M and $\Delta T/T_M$ values were theoretically estimated by using the equations derived by Cvetanovic and Amenomiya [40]. Figure 3 shows T_M and $\Delta T/T_M$ as a function of θ, the fractional coverage of H_2S, as well as the theoretical values. With α-H_2S, the experimental values are quite consistent with the theoretical ones. However, the desorption behavior of β-H_2S cannot be correlated by the simple first-order desorption kinetics.

The theoretical values of T_M and $\Delta T/T_M$ were calculated by assuming a second-order desorption kinetics and energetically homogeneous sites, according to the equations developed by

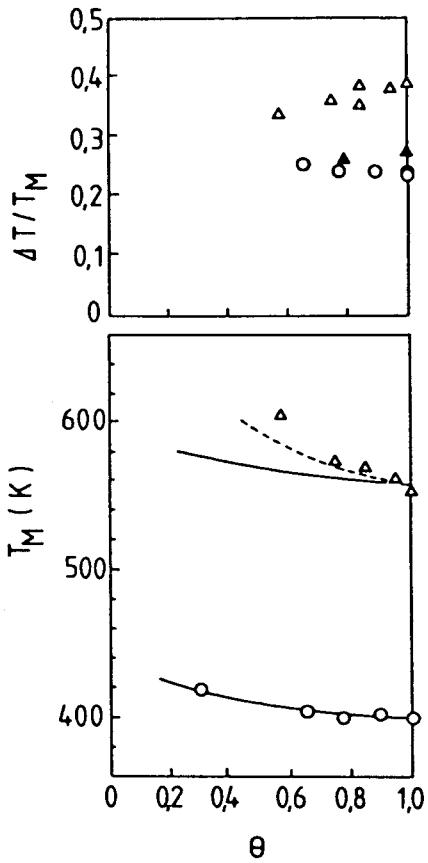

Figure 3. Dependencies of the experimental and theoretical desorption temperatures (T_M) and normalized peak widths ($\Delta T/T_M$) upon the fractional coverage of H_2S on γ-Al_2O_3. Experimental: O, α-H_2S; Δ, β-H_2S. Theoretical: solid line, T_M for the first-order desorption kinetics; dashed line, T_M for the second-order desorption kinetics; ●, α-peak width for the first-order desorption kinetics; and ▲, β-peak width for the second order desorption kinetics.

Konvalinka et al. [46]. As shown in Fig. 3, the T_M values of β-H_2S are predicted much better on the basis of the second-order kinetics than the first-order one. However, the experimental peak widths $\Delta T/T_M$ for β-H_2S are still too wide to simulate on the basis of a homogeneous adsorption of H_2S. Consequently, it is considered that α-H_2S desorbs in a first order from homogeneous sites, whereas β-H_2S desorbs, most likely, in a second order from energetically heterogeneous sites.

As shown in Fig. 4, the evacuation temperature of γ-Al_2O_3 affected the amounts of both α- and β-H_2S species. They both showed maxima at 770 K. The β/α site-density ratio decreased with increasing evacuation temperature. The effects of calcination temperature on the H_2S adsorption were also examined for γ-Al_2O_3 and are summarized in Table 3. For the catalyst calcined at 1423 K, which showed a XRD pattern characteristic of α-Al_2O_3, no clear desorption peaks were observed, probably, due to the low surface area. The amount of α-H_2S decreased gradually with the calcination temperature up to 1173 K, whereas that of β-H_2S decreased more steeply beyond 970 K. In both heat treatments, the ratio β/α decreased with increasing the temperature.

H_2S Adsorption on Modified Al_2O_3

A systematic adsorption study of H_2S was carried out with γ-Al_2O_3 catalysts doped with various amounts of F^-, SO_4^{2-}, Na^+, Mg^{2+}, or Zn^{2+} in order to examine the effect of modifying the surface functional groups upon the adsorption behavior of H_2S

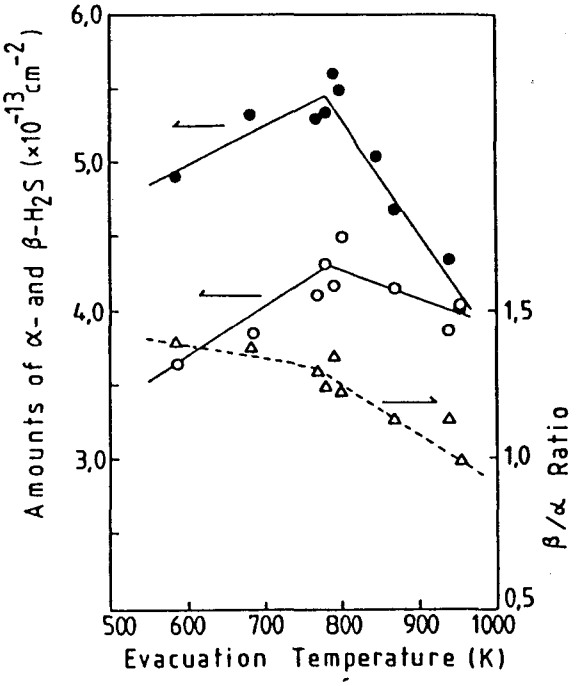

Figure 4. Dependencies of the amounts of α- and β-H_2S adsorbed on γ-Al_2O_3 upon the evacuation temperature. Evacuation time, 2 h. ○, α-H_2S; ●, β-H_2S; and △, β/α ratio.

Table 3. Effect of Calcination Temperature on the H_2S-Desorption Behavior of γ-Al_2O_3

calcination temp, K	surf. area, $m^2\ g^{-1}$	H_2S desorbed,[a] 10^{13} molecules cm^{-2}		β/α
		α	β	
823	163	4.42	5.46	1.24
973	151	4.12	5.15	1.25
1173	127	4.00	3.86	0.97
1423	8	nd[b]	nd[b]	

[a] Exposed to H_2S (7.7 kPa) at room temperature for 30 min. [b] Not determined accurately due to weak peaks under the experimental conditions employed here.

and, furthermore, to obtain some insights into the nature of the adsorption sites of H_2S.

The TPD spectra of H_2S on the F^-/Al_2O_3 catalysts are shown in Fig. 5. The desorption temperatures of α- and β-H_2S were not altered by the addition of less than 2 wt% F (ca. 40 x 10^{13} F^- cm^{-2}). The catalysts containing 2 and 5 wt% F showed lower desorption temperature by about 15 and 50 K for β-H_2S, respectively, while no appreciable change was observed for α-H_2S.

The desorption amounts of α- and β-H_2S are shown in Fig. 6 as a function of the F^- concentration. The amounts of α-H_2S and, particularly, β-H_2S decrease considerably as the doping level of F^- increases up to 10 x 10^{13} cm^{-2}. Then, they decrease more slowly with a further increase of the number of the ion on the Al_2O_3 surface. It seems that the preparation method to support F^- on Al_2O_3, the ion exchange or impregnation, does not modify the H_2S adsorption behavior of the resultant catalysts.

The chemical state of F^- ions was examined by XPS to assess the origin of the change in the slopes in Fig. 6. The F1s BE remained constant at 685.5 ± 0.1 eV up to the loading level of ca. 20 x 10^{13} F^- cm^{-2} (ca. 1 wt% F) and then shifted to higher BE by 0.7 eV at > 40 x 10^{13} F^- cm^{-2} (ca. 2 wt% F), accompanying a slight increase in the Al2s BE by 0.3 eV. Taking into account the BE values for AlF_3 [47,48], it is considered that these BE increases indicate the formation of compounds similar to AlF_3 in the surface layer of Al_2O_3 upon the addition of more than 2 wt% of F. The formation of surface "aluminum fluoride" layer is

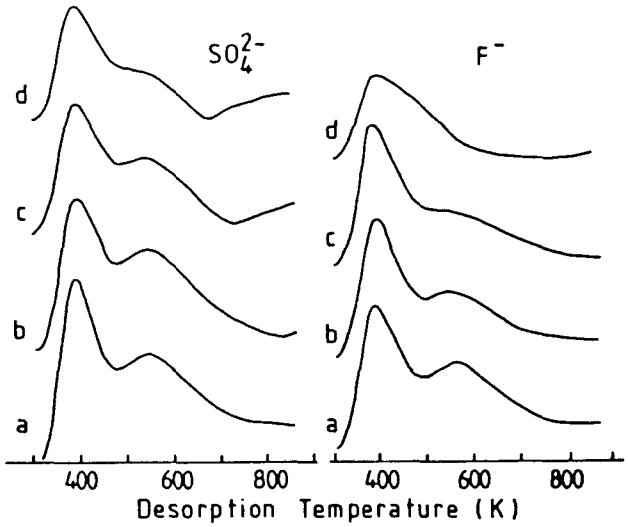

Figure 5. TPD spectra of H_2S on the SO_4^{2-} and F^-/Al_2O_3 catalysts. Doping level of SO_4^{2-}: (a) non- or γ-Al_2O_3, (b) 1.95, (c) 4.97, and (d) 9.27 × 10^{13} cm^{-2}. Doping level of F^-: (a) 5.0, (b) 11.5, and (c) 16.2, and (d) 96.7 × 10^{13} cm^{-2}.

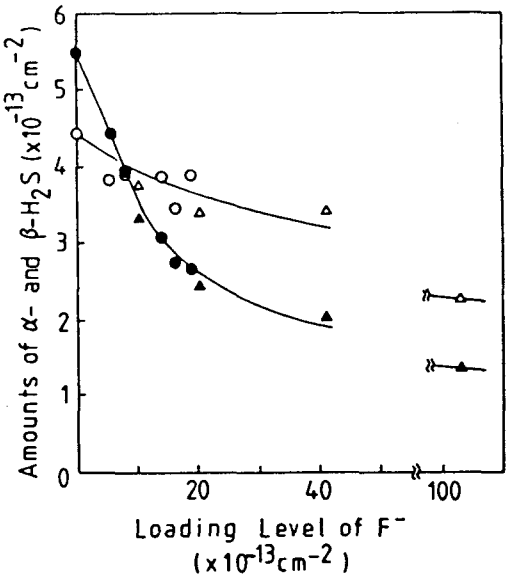

Figure 6. Amounts of α- and β-H_2S on the F^-/Al_2O_3 catalysts as a function of the loading level of F^-. α-H_2S: ○, ion-exchanged; △, impregnated. β-H_2S: ●, ion-exchanged; ▲, impregnated.

supported by the relative XPS intensities; that is, the slope of the F1s/Al2s intensity ratio against the F^- content decreased for the sample containing more than ca. 20 x 10^{13} F^- cm^{-2}.

The TPD spectra of H_2S on the SO_4^{2-}/Al_2O_3 are shown in Fig. 5. Apparently, the peak intensities of α- and β-H_2S decrease greatly with increasing the SO_4^{2-} content. It seems that the desorption peak of H_2O becomes well resolved. This is due to considerable reductions of the intensity and width of β-H_2S peak with increasing the SO_4^{2-} content. However, no appreciable change in the amount of desorbed H_2O was observed by modifying the Al_2O_3 with SO_4^{2-}.

Figure 7 shows the amounts of α- and β-H_2S as a function of the surface SO_4^{2-} concentration. Up to ca. 8 x 10^{13} SO_4^{2-} cm^{-2}, the amount of β-sites decreased linearly with the anion density, followed by a more gradual decrease with a further increase of the anion content. As for α-H_2S, a similar behavior was observed as illustrated in Fig 7. It is noteworthy that the slopes in Fig. 7 are much larger than those for the F^-/Al_2O_3, indicating that SO_4^{2-} anions block more efficiently the H_2S-adsorption sites than F^- anions.

The S2p BE was 168.8 ± 0.2 eV irrespective of the SO_4^{2-} concentration. A linear correlation between the S2p/Al2s XPS intensity ratio and the anion content was obtained up to 14 x 10^{13} cm^{-2} (4 wt% SO_4^{2-}), implying a high dispersion of the anion over the Al_2O_3. Beyond that concentration of SO_4^{2-}, a slight deviation from the linear line was observed.

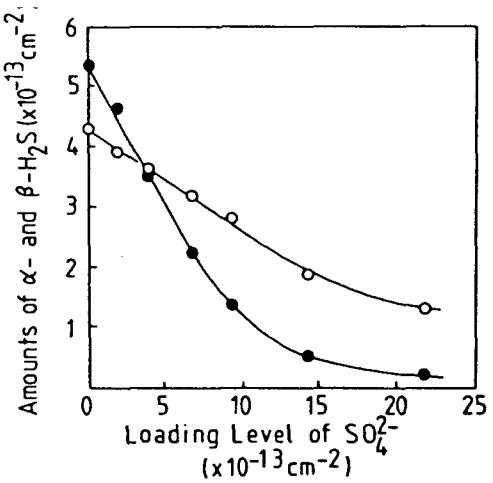

Figure 7. Correlations between the amounts of α- and β-H_2S on the SO_4^{2-}/Al_2O_3 catalyst and the loading level of SO_4^{2-}. O, α-H_2S and ●, β-H_2S.

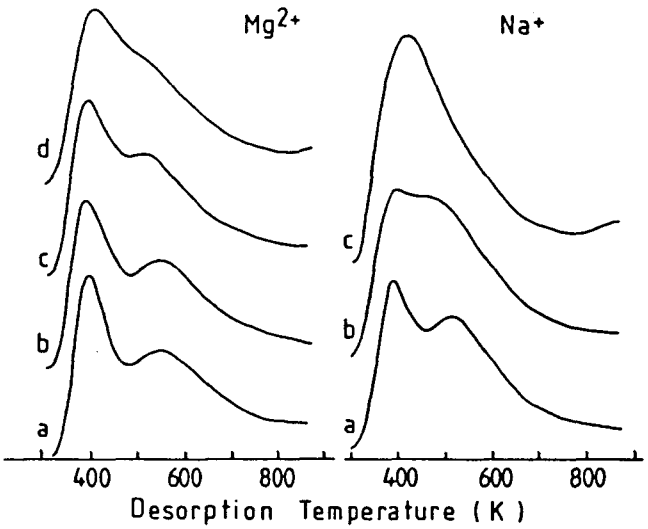

Figure 8. TPD spectra of H_2S on the Mg^{2+} and Na^+/Al_2O_3. Doping level of Mg^{2+}: (a) non- or γ-Al_2O_3, (b) 9.42, (c) 47.7, and (d) 100 × 10^{13} cm^{-2}. Doping level of Na^+: (a) 5.9, (b) 11.7, and (c) 65.6 × 10^{13} cm^{-2}.

The effects of cations on the adsorption behavior of H_2S were also examined. Figure 8 shows the TPD spectra of H_2S adsorbed on the Na^+/Al_2O_3 catalysts. It is apparent that the desorption temperature of β-H_2S decreased with increasing the Na^+ content and finally collapsed into that of α-H_2S. The desorption temperature of H_2S on Na^+/SiO_2 was ca. 370 K. Accordingly, the reduction in the β-H_2S desorption temperature is not due to a mere superposition of an additional spectra of H_2S on Na^+. As shown in Fig. 8, the reduction of the desorption temperature of β-H_2S was also observed for the Mg^{2+}/Al_2O_3 catalysts. As illustrated in Fig. 9, the total amount of desorbed H_2S increased as the Na^+ content increased up to ca. 20×10^{13} Na^+ cm^{-2}, contrary to the anions, and then became invariant with a further increase in the Na^+ content. In the case of the divalent cation, Mg^{2+}, an identical increment in the amount of H_2S adsorption was observed. The Zn^{2+}/Al_2O_3 showed a similar H_2S-adsorption behavior to the Mg^{2+}/Al_2O_3 catalysts.

A linear correlation was observed between the Na KLL/Al2s XPS intensity ratio and the Na^+ content ($< 12 \times 10^{13}$ Na^+ cm^{-2}). Beyond that doping level of Na^+, the slope of the line decreased significantly, suggesting the formation of subsurface compounds. With the Mg^{2+}/Al_2O_3, the Mg2p/Al2s XPS intensity ratio increased linearly with the MgO content (< 10 wt%).

The amounts of adsorbed NH_3 on the modified Al_2O_3 catalysts are summarized in Table 2. It is evident that the NH_3/H_2S ratio is decreased by cation addition, whereas the ratio is increased

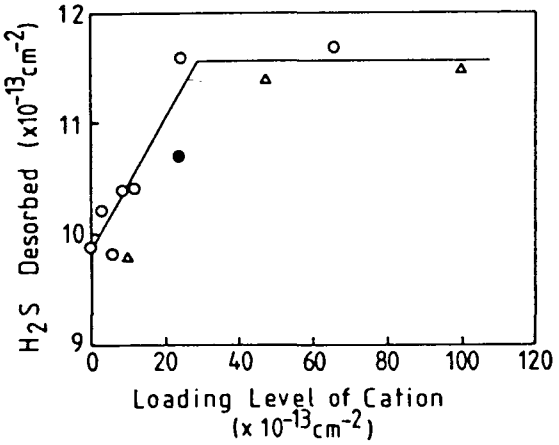

Figure 9. Dependency of the desorption amount of H_2S upon the loading level of cation. ○, Na^+; △, Mg^{2+}; and ●, Zn^{2+}.

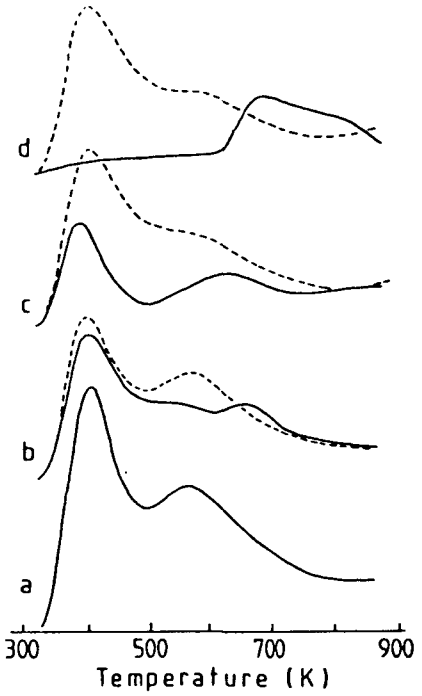

Figure 10. TPD spectra of H_2S on the oxidic and sulfided MoO_3/Al_2O_3 catalysts. Supported amount of MoO_4^{2-}: (a) non- or γ-Al_2O_3, (b) 6.38 (2.5 wt %), (c) 12.7 (5 wt %), and (d) 24.7×10^{13} cm^{-2} (10 wt %). Solid line, oxidic catalyst; dashed line, sulfided catalyst.

by anion doping.

H_2S Adsorption on MoO_3/Al_2O_3 Catalysts

Figure 10 shows the TPD spectra of H_2S for the MoO_3/Al_2O_3 catalysts. A new desorption peak can be seen at ca. 670 K, which is denoted γ-H_2S here. With increasing the MoO_3 content, the α- and β-H_2S peaks decreased in their intensities and almost disappeared for the 10 wt% catalyst, while γ-H_2S became intensified. The peak observed at ca. 820-870 K is due to H_2O as stated above. After the TPD experiments, slight sulfidation and reduction of the MoO_3/Al_2O_3 catalysts were observed by XPS. The S/Mo atomic ratios were 0.50 for 5 and 10 wt% MoO_3 catalysts.

Assuming the same spectral features, width and shape, for β-H_2S on the MoO_3/Al_2O_3 catalysts as those on γ-Al_2O_3, these spectra were graphically curve-resolved to estimate the respective amounts of α-, β-, and γ-H_2S. When slightly narrower line widths, which are observed for the SO_4^{2-}/Al_2O_3 in Fig. 5, are employed, the amounts of β-H_2S are calculated to be less by ca. 10% than those estimated above, with a concomitant increase in the amount of γ-H_2S. However, the amount of α-H_2S is obtainable with a much better accuracy than the others. These ambiguities in the curve-resolution do not affect the conclusions below. The amounts of α-, β-, and γ-H_2S thus estimated are shown in Fig. 11 as a function of the surface molybdenum concentration. The results on the SO_4^{2-}/Al_2O_3 are also cited in the figure by the dotted lines for comparison.

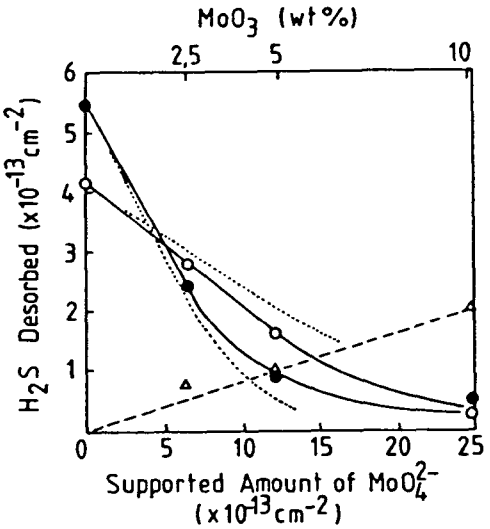

Figure 11. Correlations between the amounts of α-, β-, and γ-H_2S on the MoO_3/Al_2O_3 catalysts and the supported amount of MoO_4^{2-}. O, α-H_2S; ●, β-H_2S; Δ, γ-H_2S. Dotted lines indicate the α- and β-H_2S for the SO_4^{2-}/Al_2O_3 catalyst (see Figure 7).

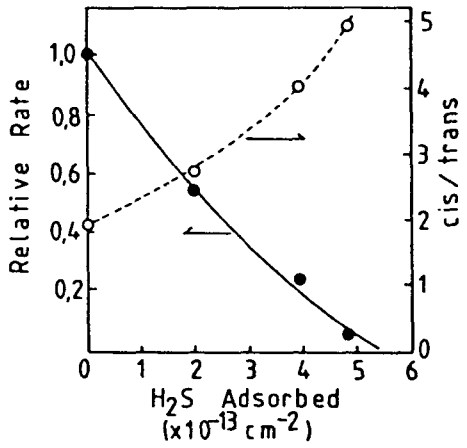

Figure 12. Correlations between the relative 1-butene isomerization rate and *cis*-/*trans*-2-butene selectivity over γ-Al_2O_3 and the amount of H_2S adsorbed. Reaction temperature, 298 K. ●, relative isomerization rate, and O, selectivity.

The effect of sulfidation on the adsorption behavior of H_2S was examined for the MoO_3/Al_2O_3 catalysts. The sulfidation degrees of Mo, S/Mo atomic ratios, were estimated from the XPS analysis to be 1.3, 1.2, and 1.4 for 2.5, 5, and 10 wt% MoO_3 catalysts, respectively. As shown in Fig. 10, the α- and β-peaks, which were lost in the oxidic catalyst, recovered partially their intensities in the sulfided catalysts. The γ-peak was not apparently observed at ca. 670 K, contrary to the oxidic catalysts. It is not decisive, however, whether the desorption temperature is shifted nearly to that of β-H_2S and/or the adsorption of γ-H_2S is suppressed by sulfidation.

The Mo3d/Al2s XPS intensity ratio for the MoO_3/Al_2O_3 catalysts increased linearly with the MoO_3 content (< 10 wt%). This suggests high dispersions of molybdena species over the Al_2O_3. On sulfidation, no significant change in the XPS intensity ratio was noted.

Isomerization of 1-Butene over γ-Al_2O_3

In order to obtain predominantly β-H_2S, the adsorption pressure of H_2S was maintained low (< 2 kPa) in the poisoning experiments. Under the conditions, the adsorption of α-H_2S is considered to be nearly neglected from Fig. 2. The results of the poisoning experiments are shown in Fig. 12. The "lethal dose" of H_2S is estimated to be 5.4×10^{13} H_2S cm^{-2}, being consistent with the values in the literature [25,26], although different aluminas are employed. Taking into account the facts that a preferential

adsorption of β-H_2S takes place under the present H_2S adsorption conditions and that the lethal dose agrees quite well with the amount of β-H_2S (5.46×10^{13} cm^{-2}), it is concluded that the isomerization sites of 1-butene are involved in the β-H_2S adsorption sites.

The cis-/trans-2-butene ratio in the reaction increased with the increase in the H_2S coverage as shown in Fig. 12. This fact indicates the heterogeneity of β-sites for both the H_2S adsorption and 1-butene isomerization and/or inductive effects of preadsorbed H_2S on the reaction as discussed below.

The isomerization activities of some of the other catalysts are summarized in Table 4. The extraordinarily high isomerization activities of the Na^+/Al_2O_3 and F^-/Al_2O_3 catalysts with a high doping level of Na^+ or F^- and the SiO_2-Al_2O_3 catalysts are attributable to the generation of extremely strong bases or acids [3,49,50]. Activity increases were also observed for the SO_4^{2-}/Al_2O_3 catalysts containing more than 2-3 wt% SO_4^{2-}.

IR Study of H_2S Adsorption

IR studies of H_2S on γ-Al_2O_3 were carried out to obtain information on the adsorption mode of H_2S. Figure 13 shows the spectra of the Al_2O_3 exposed to H_2S after an evacuation at 773 K for 2 h. When exposed to 1.3 kPa of H_2S for 30 min at room temperature, followed by an evacuation at room temperature (b), the 3785-cm^{-1} band disappeared completely as observed by other workers [30,37,38] and the 3705-cm^{-1} band was slightly perturbed,

Table 4. Activity and Selectivity of the Catalyst for the Isomerization of 1-Butene[a]

catalyst	rate const,[b] 10^{-4} min^{-1} g^{-1}	*cis*-/*trans*-2-butene ratio	TOF,[c] s^{-1}
γ-Al_2O_3	22	2.3	0.14
η-Al_2O_3	25	3.9	0.13
SiO_2–Al_2O_3 (28.6%)	580	0.77	
Na^+/Al_2O_3 (5.93)[d]	15	2.9	0.09
(65.6)	400	8.2	
Mg^{2+}/Al_2O_3 (9.42)	16	3.2	0.11
SO_4^{2-}/Al_2O_3 (3.93)	13	3.0	0.14
F^-/Al_2O_3 (103)	290	2.1	

[a] Reaction temperature, 298 K; pressure, 8.2 kPa. [b] Calculated on the basis of first-order kinetics and the initial conversion of 1-butene. [c] Turnover frequency calculated on the basis of the number of β-H_2S sites. [d] Doping level, 10^{13} cm^{-2}.

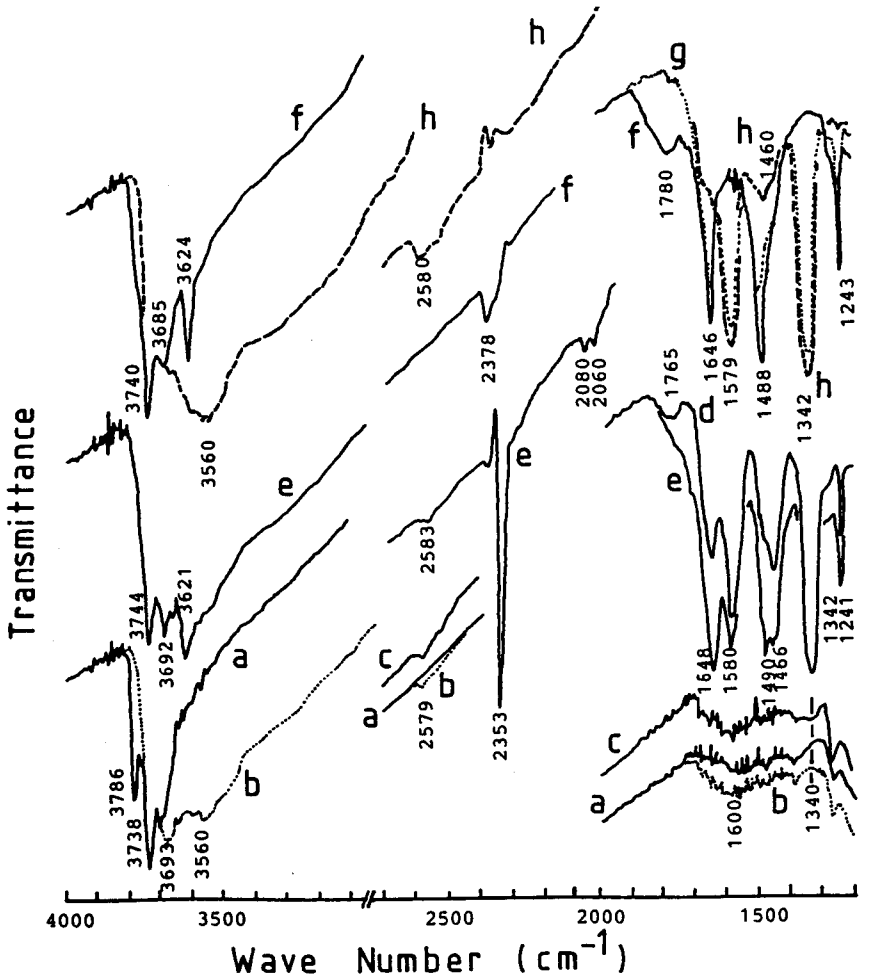

Figure 13. IR spectra of γ-Al_2O_3; (a) evacuated at 773 K for 2 h; (b) sample a exposed to H_2S (1.3 kPa) for 30 min, followed by an evacuation at room temperature for 30 min; (c) sample a contacted with H_2S (17 kPa) for 30 min, followed by an evacuation at room temperature for 30 min; (d) sample b after a 5-min exposure to CO_2 (5.3 kPa); (e) sample d after 16 h in the presence of CO_2; (f) sample a contacted with CO_2 (5.6 kPa), followed by degassing at room temperature for 1 h; (g) sample f after an 1-min exposure to H_2S (1.6 kPa); and (h) sample g after a 16-h exposure to H_2S.

whereas the 3740-cm^{-1} band was not changed appreciably. New hydroxyl bands at 3690, 3560, and at lower wave numbers appeared. Weak adsorption bands at 2580 cm^{-1} and at around 1600 cm^{-1} were additionally observed on exposure to H_2S. The former band is attributed to the S-H stretching vibration [35,37]. The appearance of the band at 1600 cm^{-1} has been noted by other workers [30] and assigned to the H-O-H bending mode. The adsorption of H_2S on deuterated γ-Al_2O_3 resulted in a rapid recovery of surface hydroxyl groups at the expense of the OD groups.

When exposed to a much higher pressure of H_2S (17 kPa), the 2580-cm^{-1} band was strengthened and a weak 1340-cm^{-1} adsorption band could be detected as shown in Fig. 13-c, in addition to the spectral changes observed for the lower pressure of H_2S. The band at 1340 cm^{-1} is ascribable to the H-S-H bending mode [30,37], suggesting molecular H_2S on the Al_2O_3.

In order to obtain more detailed information about the chemisorption sites of H_2S, coadsorption of H_2S and CO_2 were examined, since the adsorption behavior of CO_2 on Al_2O_3 had been investigated in much more detail than that of H_2S [1,24]. On the adsorption of CO_2 on γ-Al_2O_3 activated at 773 K for 1 h (f), a set of strong bands appeared at 3624, 1646, 1488, and 1243 cm^{-1} at the expense of the hydroxyl band at 3785 cm^{-1}. These bands are assigned to bicarbonate species [51-53] and designated B_2 bicarbonates here according to Morterra et al. [53,54]. Other bands were observed at 1780 and 2359 cm^{-1} with a small shoulder

at ca. 2375 cm^{-1}. They are assigned to carbonates and two kinds of weakly chemisorbed CO_2, respectively [53,54].

When CO_2 (5.3 kPa) was introduced to γ-Al_2O_3 treated with 1.3 kPa of H_2S (d), a pair of strong adsorption bands immediately appeared at 1580 and 1342 cm^{-1}, as observed by Lavalley et al. [55], together with a set of absorption bands at 3621, 1648, 1466, and 1240 cm^{-1}. The latter set of bands is ascribable to bicarbonate species B_1, which has been observed on Al_2O_3 degassed at low temperatures [53,54]. B_2 bicarbonates, which were not detected at the initial dose of CO_2, were observed to increase gradually in the intensity with the exposure time to CO_2. Finally, the intensity of B_2 bicarbonate became as strong as that of B_1 (e).

The position and intensity of the S-H stretching band did not vary upon the introduction of CO_2 on the H_2S/Al_2O_3 (e). The bands at 2350 and 1765 cm^{-1} were still observed, whereas the band at 2375 cm^{-1} was almost missing. The pair bands at 2080 and 2060 cm^{-1}, which were attributed to COS in a gas phase [55], grew gradually with increasing contact time with CO_2, while the intensity of the broad band at 1765 cm^{-1} decreased correspondingly (e). On evacuation at room temperature, the bands due to B_1 bicarbonates at 1466 and 1241 cm^{-1} decreased in intensity and the 2350-, 2080-, 2060-, and 1765-cm^{-1} bands disappeared completely. On the other hand, the ν(S-H) band at 2580 cm^{-1} remained intact. In the case of γ-Al_2O_3 that had been preadsorbed with H_2S at a pressure of 17 kPa, similar

observations were made for a subsequent adsorption of CO_2. The fate of the band at 1340 cm^{-1} could not be followed by the superposition of the strong band. These findings suggest that α-H_2S does not appreciably affect the CO_2 adsorption species.

When H_2S (1.6 kPa) was introduced to γ-Al_2O_3 (f) with pre-adsorbed CO_2, the bands characteristic to CO_2-H_2S coadsorption immediately appeared at 1580 and 1342 cm^{-1} (g). B_2 bicarbonate species disappeared gradually and only weak absorption bands ascribable to B_1 species were observed after a prolonged exposure (h). The band at 1780 cm^{-1} disappeared. Contrary to the CO_2 adsorption on H_2S/Al_2O_3, no COS was detected during the exposure to H_2S. This finding indicates that the new species characterized by the bands at 1580 and 1342 cm^{-1} are not intermediate species responsible for the formation of COS from CO_2 and H_2S. On the basis of the above observations, the adsorbed CO_2 species active for the production of COS are tentatively proposed to be the adsorbed CO_2 at 1760-1780 cm^{-1} rather than the new species [55], since the former carbonates behave correspondingly to the COS formation.

The assignment of the new adsorption species characterized by the bands at 1580 and 1342 cm^{-1} has not been established yet. Lavalley et al. [55] proposed a thiocarbonate species for the bands. However, their assignment seems suspicious, since the intensity and position of the S-H stretching band are not affected by the introduction of CO_2 into H_2S/Al_2O_3. It has been reported [54] that several pairs of bands appear in the regions

of 1700-1615 and 1450-1340 cm^{-1} at the expense of the bicarbonate species when CO_2 is adsorbed on η-Al_2O_3 evacuated at ca. 300 K and preadsorbed with pyridine. Similar bands due to carbonate species appear in the same spectral regions upon CO_2 adsorption on α-Al_2O_3 [56] and $MgAl_2O_4$ [54]. The Zn^{2+}/Al_2O_3 catalyst also provided the bands at 1600 and 1445 cm^{-1} in addition to those due to B_2 bicarbonate species. These pair bands are attributable to monodentate carbonate species, taking into consideration the splitting between the symmetric and asymmetric stretching modes [58]. This assignment is also suggested for these pair bands by other workers [54-57,59]. Accordingly, the new bands, which are formed on the CO_2-H_2S coadsorption over Al_2O_3 at the expense of bicarbonate species, are most likely assigned to monodentate carbonate species. It is considered that preadsorbed H_2S enhances the basic strength of the oxide anions by inductive effects and consumes, as substantiated by the preferential disappearance of the 3785-cm^{-1} band, strongly basic hydroxyl groups, which constitute the precursor of the bicarbonate species, thus resulting in the formation of monodentate carbonates. Inductive effects of pyridine [54] and H_2O [57] are also claimed to increase the basic strength on Al_2O_3. Consequently, the transformation of bicarbonate species to monodentate carbonates on the CO_2-H_2S coadsorption strongly demonstrates that the adsorption sites of β-H_2S involve the sites for B_2 bicarbonate formation.

Discussion

H_2S Adsorption Mode on Al_2O_3

It is evident from the present TPD studies that there are at least two distinctly different chemisorption modes of H_2S on Al_2O_3, α- and β-H_2S. The TPD parameters indicate that α-H_2S desorbs in the first-order kinetics with a relatively low adsorption energy, 13 kcal mol^{-1}. Furthermore, when γ-Al_2O_3 is exposed to a relatively high pressure of H_2S and evacuated at room temperature, the IR spectra of H_2S adsorbed on Al_2O_3 show the presence of an absorption band due to the H-S-H bending. This suggests the conservation of H_2S molecular integrity on adsorption. It is concluded on the basis of these observations that H_2S chemisorbs associatively on Al_2O_3 to form α-H_2S. Very recently, Datta and Cavell [30] have also suggested the presence of associative chemisorption of H_2S on Al_2O_3 by FT-IR studies.

As for β-H_2S, the TPD parameters indicate a somewhat complex nature of the adsorption behavior. The desorption temperature of β-H_2S is well simulated by assuming a second-order desorption kinetics, whereas the line width is much larger than those expected from the theory. The second-order desorption kinetics indicate a dissociative adsorption. The large TPD peak width implies energetically heterogeneous adsorption sites. The dissociative adsorption of H_2S on Al_2O_3 is supported by the IR results in Fig. 13: the absence of a band due to the H-S-H bending mode at a low exposure pressure of H_2S and the appearance of broad

bands at around 1600 cm^{-1} ascribable to H-O-H bending mode due to the interactions between surface hydroxyl groups and protons released from the S-H bond cleavages. The observation of B_1 bicarbonate species, which is observed only on hydroxylated aluminas [53], on the adsorption of CO_2 over the H_2S-preadsorbed Al_2O_3 shows the recovery of surface hydroxyl groups upon the β-H_2S formation. Accordingly, it is concluded that H_2S adsorbs dissociatively on energetically heterogeneous sites on Al_2O_3 to form β-H_2S. The average adsorption energy of β-H_2S is 35 kcal mol^{-1}. The rapid H-D scrambling among surface OH and adsorbed H_2S may lend additional support to the above conclusions.

Adsorption Sites of H_2S on Al_2O_3

The adsorption behavior of H_2S is strongly dependent on the adsorbent and the surface modifications. The SiO_2-Al_2O_3 catalysts showed predominantly a weak α-H_2S, while γ-Al_2O_3 showed both α- and β-H_2S in almost equal quantities as shown in Fig. 1. It is well-known that SiO_2-Al_2O_3 mixed oxides show strong Brønsted acidity, the maximum acid amount being usually attained at ca. 30 wt% Al_2O_3 [3]. On the other hand, the Lewis acidity decreases as the Al_2O_3 content decreases [3]. The Lewis acid sites on SiO_2-Al_2O_3 are characterized by CO_2 adsorption [60] and recent MAS-NMR study [7] of pyridine adsorption. Contrary to SiO_2-Al_2O_3, Al_2O_3 is well-known to show predominantly Lewis acidity with only weak Brønsted acid sites, when dehydrated at ca. 770 K [3,24,61]. As shown in Table 4, the selectivities of cis-/trans-2-butene in the

1-butene isomerization over the SiO_2-Al_2O_3 and Al_2O_3 catalysts are consistent with those anticipated from their acid-base properties [62]: about unity over Brønsted acid sites and 2-6 over Lewis acid and base sites.

On the basis of the above acid properties, it is concluded that Lewis acid sites constitute the chemisorption sites for H_2S rather than Brønsted acid sites. The extremely high NH_3/H_2S ratios for the SiO_2-Al_2O_3 catalysts in Table 2 substantiate the above conclusion, since NH_3 adsorbs on both Brønsted and Lewis acid sites [3,24]. From the ESR study of NO adsorption, Lunsford et al. [25] also strongly suggested that the exposed Al^{3+} cations are responsible for the chemisorption of H_2S on Al_2O_3.

Quantitative considerations regarding the increment of the adsorption amount of H_2S on the cation-doped Al_2O_3 lend further support for the participation of exposed or coordinatively unsaturated (cus) Al^{3+} cations as the adsorption sites. Aluminas have defect spinel structures. The unit cell contains 32 O^{2-} anions and only 21-1/3 Al^{3+} cations, so that 2-2/3 vacant cation positions are present in the unit cell [1]. Accordingly, the adsorption number is expected to increase by 13% for a perfect spinel structure, provided that the cus cations are involved as the adsorption sites. This is nearly the case in Fig. 9, where the H_2S adsorption number is increased by 18% by adding Mg^{2+}, Zn^{2+}, or Na^+ cations. These cations are incorporated into the Al_2O_3 lattice to form surface spinel compounds. In the case of Zn^{2+} or Mg^{2+}/Al_2O_3 calcined at 823 K, no formation of the bulk

oxide, ZnO or MgO, was detected by XRD, UV, and XPS-AES for the cation concentrations as low as in the present study [63]. The observation in Fig. 9 that the amount of H_2S adsorption saturates for the cation content further substantiares the participation of cations in the surface spinel.

The relatively strong and abundant adsorption of H_2S on MgO (Table 2) suggests a strong contribution of basic sites to the adsorption of H_2S on Al_2O_3 as well. MgO shows weak aprotonic acidity as evidenced by the IR study of benzonitrile adsorption [64]. The observations in Fig. 13 that the basic hydroxyl groups on the Al_2O_3, represented by the band at 3785 cm^{-1} [1], are strongly perturbed on the initial dose of H_2S demonstrates the interactions between H_2S, probably adsorbed on Lewis acid sites, and the basic sites. Taking into consideration the results in Fig. 2 and the adsorption conditions of H_2S in Fig. 13, the basic hydroxyl groups are consumed by the β-H_2S formation. Additionally, the participation of basic sites in the formation of β-H_2S is well substantiated by the considerable decrease of β-H_2S for the F^-/Al_2O_3 catalysts, since surface fluorination eliminates basic hydroxyl groups [65,66]. When these base-H_2S interactions are strong enough to polarize the S-H bonds and to abstract a proton from the bonds, dissociative adsorption of H_2S is considered to occur to form β-H_2S, the resultant fragments being stabilized as H^+-basic sites and HS^--Lewis acid sites. The former interaction species are evidenced by the appearance of the bands at 1600, 3690, and 3560 cm^{-1}, and a broad hydroxyl band at

lower wave number on the adsorption of H_2S on Al_2O_3 and the latter one by the S-H stretching band at 2580 cm^{-1}. Accordingly, it is concluded that the formation of β-H_2S takes place on strong acid-base pair sites, while that of α-H_2S on acid sites with or without weak basic sites in the vicinity. The latter conclusion may be supported by a weak dependency of the amount of α-H_2S on the surface fluorination of γ-Al_2O_3. The type of acid sites responsible for the H_2S adsorption is Lewis acid sites as discussed above. The basic sites are considered to be constituted of basic hydroxyl groups and oxide anions.

The Lewis acid sites or electron-pair-accepting sites on Al_2O_3 are undoubtedly cus Al^{3+} cations exposed at the surface. However, it is open to question as to what type of cus Al^{3+}, tetrahedral or octahedral, and what kinds of site configuration are required for the adsorption of probe molecules and for the catalytic reaction to proceed on.

The reduction of the desorption temperature T_M of β-H_2S and the concomitant increase in the total amount of H_2S adsorption were observed for the cation-doped γ-Al_2O_3 catalysts; Na^+, Mg^{2+}, and Zn^{2+}/Al_2O_3. The latter fact has been taken as the evidence of the participation of cus Al^{3+} cation for the H_2S adsorption. The decrease in T_M indicates the decrease in the adsorption strength so long as the adsorption mode is not changed [40]. It is generally accepted that these cations are incorporated preferentially into tetrahedral sites in the Al_2O_3 lattice to form spinel structures. Accordingly, it is concluded that cus Al^{3+} in

tetrahedral coordinations, cus Al_{tet}^{3+}, are responsible for the adsorption of β-H_2S on Al_2O_3. The reduced adsorption strength of β-H_2S for the cation-doped Al_2O_3 catalysts is interpretable in terms of weaker Lewis acid sites, which are comprised of mono- or divalent cations in tetrahedral sites, compared to cus Al_{tet}^{3+} cations. Inductive effects of the cation may not be neglected to reduce the acid strength of cus Al_{tet}^{3+} cation in the vicinity, since the electronegativity of the cation doped here is significantly lower than that of Al^{3+}. The MO calculation on a K^+-Al_2O_3 model system [67] suggests the inductive effect of K^+.

The α-H_2S peak was detected on the SiO_2-Al_2O_3 and $AlPO_4$ at the identical T_M with that on Al_2O_3, although in much smaller site densities. The cus Al^{3+} cations in these catalysts are located in tetrahedral coordinations as evidenced by the ^{27}Al MAS-NMR study [4] and the IR study of surface OH groups [68]. Therefore, it is concluded that cus Al_{tet}^{3+} constitutes also the chemisorption sites for α-H_2S on Al_2O_3 rather than the cus Al_{oct}^{3+} cations in octahedral coordinations. No alteration in T_M of α-H_2S was detected even for the cation-doped Al_2O_3 catalysts, although expected from the above conclusions. This is considered to be due to the experimental accuracy of the T_M measurements ($\pm$ 5 K) in the present TPD techniques rather than due to the absence of the change in T_M, since only a smaller perturbation might be anticipated for the adsorbate with a smaller heat of adsorption.

Consequently, cus Al_{tet}^{3+} cations are responsible for the

adsorption of H_2S, irrespective of adsorption mode. Quantum chemical calculations for Al_2O_3 suggest that cus Al_{tet}^{3+} cations show greater acid strength than cus Al_{oct}^{3+} cations [67], this being in agreement with the present conclusions. In addition, the coexistence of adsorbed H_2S and B_1 bicarbonates, which is believed to be adsorbed on cus Al_{oct}^{3+} [53], is consistent with the above site models. The strength of basic groups in the vicinity of the cus Al_{tet}^{3+} and, probably, the size of the anion vacancy as well would determine the adsorption mode of H_2S, associative or dissociative.

The IR study of the coadsorption of CO_2 and H_2S indicates that the sites for B_2 bicarbonate formation are involved in the sites dissociating H_2S. The bicarbonate species are supposed to be formed on Lewis acid-basic hydroxyl group pair sites [51,53] and designated X-site by Fink [51]. According to the detailed model developed by Knözinger and Ratnasamy [1], a cus Al_{tet}^{3+} cation in a double anion vacancy and basic OH^- constitute X-sites. Their X-sites fulfill the requirements for the β-H_2S chemisorption. Actually, they are involved in the β-H_2S sites. The double anion vacancy may be required for the sulfur atom to interact strongly with a cus Al_{tet}^{3+} cation in the vacancy, taking into consideration the ionic radii of S^{2-} (0.184 nm) and O^{2-} (0.132 nm) [69]. The site density of X-site has been estimated to be the order of magnitude of 10^{13} cm^{-2} as observed for the β-H_2S sites: 1.8×10^{13} cm^{-2} as measured by the HCO_3^- formation on a CO_2 adsorption, and 6.2×10^{13} cm^{-2} by the formate

formation on a CO adsorption [51].

The "α-sites" proposed by Peri [70] and characterized by the CO_2 absorption band at 2370 cm^{-1} are believed to be comprised of cus Al^{3+} and a reactive oxide ion. The cus Al^{3+} is suggested to be tetrahedrally coordinated [53,54]. The present IR study of CO_2-H_2S coadsorption actually indicates the β-H_2S sites involve, at least, most of the α-sites, since the band at 2375 cm^{-1} was found to be suppressed to a large extent by the coadsorption of H_2S. The site density of α-sites has been reported to be 5×10^{12} cm^{-2} for a γ-Al_2O_3 predried at 1073 K [70].

Other sites for β-H_2S are considered to be constituted of cus Al_{tet}^{3+} and basic oxide anions as in α-sites but with different kinds of oxide anions. The oxide ions must show high basic strength to dissociate the weak acid, H_2S (pK_a = 7.0). One of such candidates may be described by O^{2-}=Al^{3+}. Recent MO calculations on the generation of basic sites on MgO have revealed that oxide ions with a lower coordination number show greater basic strength [71].

Thus, β-H_2S sites may be composed of a variety of cus Al_{tet}^{3+}-strong base pair sites; X-sites [51], α-sites [70], and others. This can explain the energetically heterogeneous feature of β-H_2S desorption observed in the TPD studies.

Effects of Heat Treatments

The effects of evacuation and calcination temperatures on the adsorbed amounts of α- and β-H_2S and β/α site-density ratio

in Fig. 4 and Table 3 are explainable in terms of the above models for the adsorption sites of H_2S and a proposition of a surface phase transformation of γ- to α-Al_2O_3, although no significant sintering of the surface area was observed at the heat treatments below 970 K. Knözinger and Stolz [72] have explained the decrease in the number of the most energetic defects at the evacuation temperature beyond 920 K in terms of a slow formation of high-temperature forms of alumina.

Up to the evacuation temperature of 770 K, cus Al_{tet}^{3+} increases as the surface dehydroxylation proceeds, providing more adsorption sites for both α- and β-H_2S. A slight decrease in the β/α ratio is caused by the decrease in the basic OH^- density with the dehydroxylation. At the higher evacuation temperature, the surface Al_{tet}^{3+} is proposed to transform to Al_{oct}^{3+} by the surface reconstructions, resulting in the decrease in the amount of both α- and β-H_2S. The greater decrease in the β/α ratio in this region is explainable in terms of the decrease in the number of residual basic hydroxyl groups, which are supposed to be attached to Al_{tet}^{3+} cations [1], induced by the surface phase transformations as well as by an extensive dehydroxylation at the high degassing temperature.

The reductions of site densities of α- and β-H_2S with increase in the calcination temperature of γ-Al_2O_3 from 820 to 1170 K are attributable to the surface phase reconstructions. Besides, the decreasing β/α ratio with rising the calcination temperature is ascribable to a concomitant decrease in the

starting number of basic hydroxyl groups attached to Al_{tet}^{3+} cations.

H_2S Adsorption on Modified Alumina

Some of the additive effects on the H_2S adsorption behavior have already been discussed above in connection with the identification of the site configuration of the H_2S adsorption on Al_2O_3. The replacement of surface basic hydroxyl groups with F^- decreased the number of α- and, particularly, β-H_2S. Coupled with the IR results in Fig. 13, these findings provide evidence for the participation of basic hydroxyl groups in the adsorption of β-H_2S. The effects of SO_4^{2-} on the adsorption of H_2S are much greater than those of F^-. This is apparently due to a bidentate nature of SO_4^{2-} anion. The strong effects of SO_4^{2-} anions on the H_2S adsorption suggest that the sulfur content in industrial aluminas is critical when they are used as supports and catalysts (e.g., ALO-2 in Table 1).

The observations that the desorption temperature of β-H_2S did not vary with doping a small amount of F^- or SO_4^{2-} indicate the absence of strong electronic effects of the anions on the H_2S adsorption sites at a low doping level. On the other hand, a slight decrease in the desorption temperature of β-H_2S was observed for the F^-/Al_2O_3 with more than 2 wt% F. On the basis of the IR study of CO_2 and CO adsorptions over heavily fluorinated Al_2O_3, 4.5-5 wt% F, Peri [49] has suggested that the strength of Lewis acid site is enhanced by the inductive effect of F^-. The

discrepancy may be due to the large difference in the fluorine level, which strongly affects the surface species and structure as evidenced by the present and other XPS studies [47,48].

The amount of adsorbed NH_3 is increased by modifying the alumina with F^- or SO_4^{2-}, contrary to that of adsorbed H_2S, as summarized in Table 2. This is consistent with the generation of strong Brønsted acid sites [50] at the expense of Lewis acid-base pair sites.

The increase in the adsorption amount of H_2S and the concomitant decrease in the desorption temperature of β-H_2S on the Na^+, Mg^{2+}, or Zn^{2+}/Al_2O_3 catalysts are regarded as evidence for the direct participation of cus Al_{tet}^{3+} in the adsorption of β-H_2S. The impurity levels of ca. 1 wt% of Na_2O are usually found in industrial aluminas. These Na^+ cations may affect strongly the nature of aluminas as catalysts and supports as well as SO_4^{2-} anion.

On the basis of the systematic study of H_2S adsorption on Al_2O_3, it is revealed that the modifications of Al_2O_3 with cations or anions affect strongly the properties of acid-base pair sites on Al_2O_3.

Isomerization of 1-Butene on Al_2O_3

The isomerization of 1-butene over Al_2O_3 is selectively poisoned by H_2S as reported by other workers [25,26]. The lethal dose of H_2S is 5.4×10^{13} H_2S cm^{-2}, being consistent with the values found by Lunsford et al. [25] and Rosynek et al. [26] in

spite of the independent aluminas. Poisoning experiments using SO_2 and CH_3SH provided the same density of the isomerization sites [26]. These findings suggest that the number of active sites are determined by the intrinsic nature of the Al_2O_3 surface rather than by the extrinsic properties such as a defect concentration and an impurity level. Taking into consideration the present poisoning conditions and the amount of the lethal dose, it is concluded that β-H_2S sites are responsible for the isomerization over Al_2O_3. This conclusion further suggests that 1-butene isomerization proceeds on Lewis acid-base pair sites. Other workers [25,26,70] have also proposed such pair sites for the reaction. The observation that SO_2 poisons the isomerization over Al_2O_3 [26] is related to the decreased number of β-H_2S sites on the SO_4^{2-}/Al_2O_3 catalysts.

The turnover frequencies (TOF) of the 1-butene isomerization over the modified aluminas were calculated on the basis of the number of β-H_2S adsorption sites. They are summarized in Table 4. It is evident that γ-Al_2O_3, η-Al_2O_3, and SO_4^{2-}/Al_2O_3 with a low SO_4^{2-} content show almost the identical TOF. These findings lend further support for the above conclusions that β-H_2S sites are involved in the isomerization. The reduced TOF values in the Na^+ and Mg^{2+}/Al_2O_3 catalysts can be related to the fact that the strength of Lewis acid sites is reduced by modifying with the cations, as evidenced by the decrease in the desorption temperature of β-H_2S.

From the above discussions, it is concluded that the cus

Al_{tet}^{3+}- strong base pair sites constitute the catalytically active sites. However, this might not necessarily mean that all the adsorption sites for β-H_2S are I-sites [73], the isomerization sites. Actually, this is the case, since the isomerization of 1-butene over Al_2O_3 is almost independent of CO_2 adsorption [24,26,73,74] in spite of the formation of bicarbonate species. Accordingly, the cus Al_{tet}^{3+}-basic OH^- pair sites responsible for the formation of both bicarbonate species B_2 and β-H_2S are catalytically inactive for the isomerization. Although the precise configuration of I-sites is not revealed in the present work, it is concluded that I-sites should be composed of cus Al_{tet}^{3+}-basic oxide pair sites. Lunsford et al. [25] have reached the same conclusions.

H_2S Adsorption on MoO_3/Al_2O_3

As shown in Fig. 11, the amounts of α- and β-H_2S adsorbed on the MoO_3/Al_2O_3 catalysts depend on the surface concentration of molybdenum anion in the manner identical with those for the SO_4^{2-}/Al_2O_3 catalysts. These findings lead us to the conclusion that molybdenum ions interact with an Al_2O_3 surface as bidentate ligands similar to SO_4^{2-} anions, when the concentration of MoO_3 is very low (< 3 wt%). These interactions would induce a monomolecular layer of molybdena over Al_2O_3. In this range of a loading level of MoO_3, the interaction modes of MoO_4^{2-} and hydroxyl groups could be written as shown in Fig. 14. These interaction modes are generally accepted by many workers [12-14].

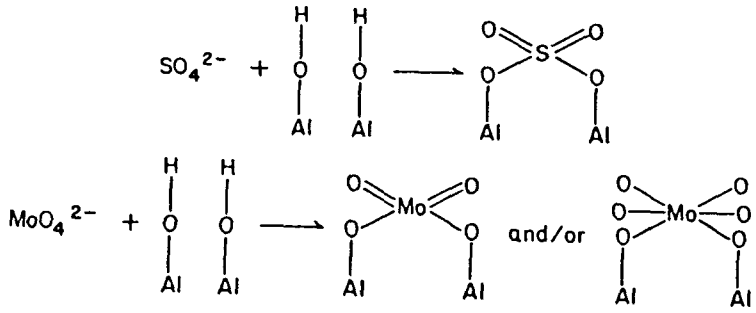

Figure 14. The interaction modes of MoO_4^{2-} and hydroxyl groups.

As for the γ-peak observed for the MoO_3/Al_2O_3 catalysts, the amount of γ-H_2S increased with increasing the MoO_3 content and the desorption temperature was very high. Accordingly, it is considered that γ-H_2S desorbs from the Mo sites, probably Mo^{6+}. After the TPD experiments, some reduction and sulfidation of molybdenum were observed by XPS. Therefore, complex reactions during the TPD experiments, such as a ligand exchange, would render the analysis of γ-H_2S unfruitful.

The amounts of H_2S adsorbed on the MoO_3/Al_2O_3 catalysts were greatly increased by sulfidation. This fact suggests the recovery of the bare Al_2O_3 surface and basic OH^- upon sulfurization. No severe sintering of molybdenum phase was detected by XPS for the low level of MoO_3. These findings are interpretable in terms of a partial cleavage of the Al-O-Mo bonds induced by the reduction and sulfidation. These processes are proposed by Millman et al. [75] and further supported by the recovery of bicarbonate species on the CO_2 adsorption for reduced MoO_3/Al_2O_3 catalysts [12,27]. However, it cannot be ruled out that the rearrangements of molybdena species over the Al_2O_3 surface, such as a homogeneous dispersion and a one-dimensional chain [76] into an island or cluster of sulfided molybdenum species, also take place on sulfidation, while the molybdenum remains dispersed monomolecularly.

The γ-H_2S observed for the oxidic MoO_3/Al_2O_3 catalysts was not detected apparently for the sulfided catalysts. However, this does not exclude the possibility of H_2S adsorption on sulfided

molybdenum, since the desorption temperature might shift toward that of β-H_2S because of the lowered valence states of molybdenum (Mo^{4+}).

Conclusions

The adsorption behavior of H_2S on Al_2O_3, modified Al_2O_3, and MoO_3/Al_2O_3 catalysts were systematically investigated to obtain information about the acid-base properties in connection with the isomerization of 1-butene on Al_2O_3, additive effects of anions and cations, and dispersion of molybdena species. Temperature programmed desorption techniques were employed in this study as well as IR and XPS techniques. The following conclusions have been drawn from the experimental results.

1) Two chemisorption modes of H_2S are differentiated on Al_2O_3 and modified Al_2O_3 catalysts; one is associative chemisorption (α-H_2S) and the other dissociative (β-H_2S). The site densities of α- and β-H_2S are 4.8 and 5.5 x 10^{13} cm^{-2}, respectively, and the corresponding heats of adsorption are 13 and 34 kcal mol^{-1}.

2) The adsorption sites of α-H_2S on Al_2O_3 are constituted of cus Al_{tet}^{3+}, while those of β-H_2S cus Al_{tet}^{3+}-strong base pair sites. The β-H_2S sites are most likely energetically heterogeneous.

3) The effects of calcination or evacuation temperature on the adsorption behavior of H_2S are interpretable in terms of the

above adsorption models and a surface reconstruction from γ- to α-phase.

4) Modifications of γ-Al_2O_3 with Na^+, Mg^{2+}, or Zn^{2+} cation induce a significant reduction in the desorption temperature of β-H_2S with a concomitant increase in the adsorption amount of H_2S. The doping of anions, F^- or SO_4^{2-}, decreases the adsorption amounts of α- and, in particular, β-H_2S.

5) The isomerization of 1-butene is selectively poisoned by β-H_2S. The catalytically active sites are proposed to be composed of cus Al_{tet}^{3+}-strongly basic oxide anion pair sites.

6) When the MoO_3 content is low (< 3 wt%), molybdenum anions react with surface hydroxyl groups on Al_2O_3 as bidentate ligands similar to SO_4^{2-} anions, forming a monomolecular layer. On sulfidation of MoO_3/Al_2O_3 catalysts, the bare Al_2O_3 surface recovers greatly, suggesting cleavage of Mo-O-Al bonds and rearrangements of molybdenum species.

References

1) H.Knözinger and P.Ratnasamy, Catal.Rev.-Sci.Eng., 17, 31 (1978).

2) D.L.Cocke, E.D.Johnson, and R.P.Merrill, Ibid, 26, 163 (1984).

3) K.Tanabe, "Solid Acid and Bases", Kodansha, Tokyo, 1970.

4) J.M.Thomas, J.Klinowski, P.A.Wright, and R.Roy, Angew.Chem.,Int.Ed.Engl., 22, 614 (1983).

5) a) C.A.Fyfe, J.M.Thomas, J.A.Klinowski, and G.C.Gobbi, Ibid, 22, 259 (1983).
b) A.P.M.Kentgens, K.F.M.G.Scholle, and W.S.Veeman, J.Phys.Chem., 87, 4357 (1983).

6) J.A.Ripmeester, J.Am.Chem.Soc., 105, 2925 (1983).

7) G.E.Macial, J.F.Haw, I-S.Chung, B.L.Hawkins, T.A.Early, D.R.McKay, and L.Petrakis, Ibid, 105, 5529 (1983).

8) M.K.Templeton and W.H.Weinberg, Ibid, 107, 97 (1985).

9) K.Jagannathan, P.Ganguly, and C.N.R.Rao, J.Catal., 75, 262 (1982).

10) H.D.Simpson, J.Phys.Chem., 89, 982 (1985).

11) H-P.Boehm and H.Knözinger, "Catalysis-Science and Technology" (J.R.Anderson and M.Boudart, Eds.) Springer-Verlag, New York, 1983, vol.4, p393.

12) W.K.Hall, "Proc. Climax Fourth Intern. Conf. on the Chemistry and Uses of Molybdenum" (H.F.Barry and P.C.H.Mitchell, Eds.) Climax Molybdenum Co., Ann Arbor, Michigan, 1982, p224.

13) F.E.Massoth, Adv.Catal., 27, 265 (1978).

14) a) B.C.Gates and G.C.A.Schuit, AIChE J., 19, 417 (1973).
b) B.C.Gates, J.R.Katzer, and G.C.A.Schuit, "Chemistry of Catalytic Processes" McGraw Hill, New York, 1979, p390.
15) M.Dufaux, M.Che, and C.Naccache, J.Chim.Phys., 67, 527 (1970).
16) A.Iannibello, S.Merengo, F.Trifiro, and P.L.Villa, "Preparation of Catalysts, III" (B.Delmon, P.Grange, P.Jacobs, and G.Poncelet Eds.) Elsevier, Amsterdam, 1979, p65.
17) L.Wang and W.K.Hall, J.Catal., 77, 232 (1982).
18) a) A.Lycourghiotis, C.Defosse, F.Delannay, J.Lemaitre, and B.Delmon, J.Chem.Soc.,Faraday Trans. 1, 76, 1677 (1980).
b) A.Lycourghiotis, C.Defosse, F.Delannay, and B.Delmon, Ibid, 76, 2052 (1980).
c) J.L.G.Fierro, A.Lopez Agudo, P.Grange, and B.Delmon, "Proc.8th Intern.Congr.Catal.", DECHEMA, Franfurt am Main, 1984, vol.2, p363.
19) a) F.E.Massoth and G.Muralidhar, "Proc. Climax Fourth Intern. Conf. on the Chemistry and Uses of Molybdenum" (H.F.Barry and P.C.H.Mitchell, Eds.) Climax Molybdenum Co., Ann Arbor, Michigan, 1982, p343.
b) G.Muralidhar, F.E.Massoth, and J.Shabtai, J.Catal., 85, 44 (1984).
c) F.E.Massoth, G.Muralidhar, and J.Shabtai, Ibid, 85, 53 (1984).
20) W.K.Hall, Acc.Chem.Res., 8, 257 (1975).

21) a) H.G.Karge, R.W.Tower, Z.Dudzik, and Z.M.George, "Proc. 7th Intern. Congr. Catal." (T.Seiyama and K.Tanabe, Eds.) Kodansha, Tokyo, 1981, p643.
b) H.G.Karge, I.G.Dalla Lana, and S.T.deSuazez, "Proc. 8th Intern. Congr. Catal." DECHEMA, Frankfurt am Main, 1984, vol.3 p453.
22) A.Datta, R.G.Cavell, R.W.Tower, and Z.M.George, J.Phys.Chem. 89, 443 (1985).
23) J.G.Larson and W.K.Hall, Ibid, 69, 3080 (1965).
24) H.Knözinger, Adv.Catal., 25, 184 (1976),
25) J.H.Lunsford, L.W.Zingery, and M.P.Rosynek, J.Catal., 38, 179 (1975).
26) M.P.Rosynek and F.L.Strey, Ibid, 41, 312 (1976).
27) K.Segawa and W.K.Hall, Ibid, 77, 221 (1982).
28) a) S.W.Weller, Acc.Chem.Res., 16, 101 (1983).
b) S.J.Tauster, T.A.Pecoraro, and R.R.Chianelli, J.Catal., 63, 515 (1980).
c) M.Millman and W.K.Hall, J.Phys.Chem., 83, 427 (1979).
d) E.A.Lombardo, M.LoJacono, and W.K.Hall, J.Catal., 64, 150 (1980).
e) J.B.Peri, J.Phys.Chem., 86, 1615 (1982).
f) N-Y.Topsøe and H.Topsøe, J.Catal., 84, 386 (1983).
29) Y.Okamoto, H.Tomioka, Y.Katoh, T.Imanaka, and S.Teranishi, J.Phys.Chem., 84, 1833 (1980).
30) A.Datta and R.G.Cavall, Ibid, 89, 450 (1985).
31) A.Datta and R.G.Cavall, Ibid, 89, 454 (1985).

32) H.C.Lee and J.B.Butt, J.Catal., 49, 320 (1977).

33) R.Ramachandran and F.E.Massoth, Ibid, 67, 248 (1981).

34) F.E.Massoth, K.S.Chung, and R.Ramachandran, Fuel Process. Technol., 2, 57 (1979).

35) T.L.Slager and C.H.Amberg, Can.J.Chem., 50, 3416 (1972).

36) O.Saur, T.Chevreau, J.Lamotto, J.Travert, and J.C.Lavalley, J.Chem.Soc.,Faraday Trans.1, 77, 427 (1981).

37) A.V.Deo, I.G.Dalla Lana, and H.W.Habgood, J.Catal., 21, 270 (1971).

38) A.J.deRosset, C.G.Finstrom, and C.J.Adams, Ibid, 1, 235 (1962).

39) R.W.Glass and R.A.Ross, J.Phys.Chem., 77, 2576 (1973).

40) R.J.Cvetanovic and Y.Amenomiya, Adv.Catal., 17, 103 (1967).

41) R.Ramachandran and F.E.Massoth, Can.J.Chem.Eng., 60, 17 (1982).

42) Y.Murakami "Preparation of Catalysts, III" (G.Poncelet, P.Grange, and P.A.Jacobs, Eds.) Elsevier, Amsterdam, 1983, p775.

43) J.H.Scofield, J.Electron.Spectrosc.Relat.Phenom., 8, 129 (1976).

44) W.J.Carter, G.K.Schweitzer, and T.A.Carlson, Ibid, 5, 827 (1974).

45) Y.Amenomiya, J.H.B.Chenier, and R.J.Cvetanovic, J.Phys.Chem., 68, 52 (1964).

46) J.A.Konvalinka, J.J.F.Scholten, and J.C.Rasser, J.Catal., 48, 365 (1977).

47) F.P.J.M.Kerkhof, H.J.Reitsma, and J.A.Moulijn, React.Kinet.Catal.Lett., 7, 15 (1977).

48) P.O.Scokart, S.A.Selim, J.P.Damon, and P.G.Rouxhet, J.Colloid Interface Sci., 70, 209 (1979).

49) J.B.Peri, J.Phys.Chem., 72, 2917 (1968).

50) I.D.Chapman and M.L.Hair, J.Catal., 2, 145 (1963).

51) P.Fink, Rev.Roum.Chim., 14, 811 (1969).

52) N.D.Parkyns, J.Chem.Soc.A, 410 (1969).

53) C.Morterra, A.Zecchina, S.Coluccia, and S.Chiorino, J.Chem.Soc.,Faraday Trans.1, 73, 1544 (1977).

54) C.Morterra, S.Coluccia, E.Garrone, and G.Ghiotti, Ibid, 75, 289 (1979).

55) J.C.Lavalley, J.Travert, J.Chevrean, J.Lamotto, and O.Saur, J.Chem.Soc.,Chem.Commum., 146 (1979).

56) a) C.Morterra, G.Ghiotti, E.Garrone, and F.Boccuzzi, J.Chem.Soc.,Faraday Trans.1, 72, 2722 (1976).
b) C.Morterra, S.Coluccia, G.Ghiotti, and A.Zecchina, Z.Phys.Chem. (Wiesbaden), 104, 275 (1977).

57) C.Morterra, G.Ghiotti, F.Boccuzzi, and S.Coluccia, J.Catal., 51, 299 (1978).

58) M.P.Rosynek, J.Phys.Chem., 79, 1280 (1975).

59) N.D.Parkyns, Ibid, 75, 526 (1971).

60) J.B.Peri, "Proc.3rd Intern.Congr.Catal." 1964, vol.2, p1100.

61) F.E.Kiviat and L.Petrakis, J.Phys.Chem., 77, 1232 (1973).

62) a) D.M.Brouwer, J.Catal., 1, 22 (1962).

b) H.R.Gerberich and W.K.Hall, Ibid, 5, 99 (1966).

c) J.W.Hightower, H.R.Gerberich, and W.K.Hall, Ibid, 7, 57 (1967).

d) J.W.Hightower and W.K.Hall, Chem.Eng.Prog.Symp.Ser., 63, 122 (1967).

63) a) A.Maezawa, Y.Okamoto, and T.Imanaka, J.Chem.Soc.,Faraday Trans.1, 83, 665 (1987).

b) B.R.Strohmeier and D.M.Hercules, J.Catal., 82, 266 (1984).

64) N.E.Tretyakov and V.N.Filimonov, Kinet.Catal., 11, 815 (1970).

65) H.R.Gerberich, F.E.Lutinski, and W.K.Hall, J.Catal., 6, 209 (1966).

66) N.Yamagata, Y.Owada, S.Okazaki, and K.Tanabe, Ibid, 47, 358 (1977).

67) a) P.Ya.Gokberg, A.O.Litinskii, A.P.Khardine, V.M.Lazauskas, and A.V.Berzhyunas, Kinet.Catal., 21, 669 (1980).

b) P.Ya.Gokberg, A.O.Litinskii, A.P.Khardine, and A.V.Berzhyunas, Ibid, 22, 911 (1981).

68) a) J.B.Peri, Discuss.Faraday Soc., 52, 55 (1971).

b) J.B.Moffat, Catal.Rev.-Sci.Eng., 18, 199 (1978).

69) "Handbook of Chemistry and physics" 46th ed., CRC, Boca Raton, FL, 1965-66.

70) J.B.Peri, J.Phys.Chem., 70, 3168 (1966).

71) a) S.Yoshida and H.Kawakami, Hyomen, 21, 737 (1983).

b) H.Kawakami, S.Yoshida, and T.Yonezawa, Shokubai (Catalyst), 25, 160 (1983).

72) H.Knozinger and H.Stolz, Fortschnittsber.Kolloide Polym, 55, 16 (1971).

73) M.P.Rosynek, W.D.Smith, and J.W.Hightower, J.Catal., 23, 204 (1971).

74) M.P.Rosynek and J.W.Hightower, "Proc. 5th Intern. Congr. Catal." 1973, vol.2, p851.

75) W.S.Millman, M.Crespin, A.C.Cirillo, S.Abdo, and W.K.Hall, J.Catal., 60, 404 (1979).

76) F.E.Massoth, Ibid, 36, 164 (1975).

Chapter 2

Characterization of Active Sites on Supported Molybdenum Sulfide Catalysts

Abstract

The site configuration of supported molybdenum sulfides catalytically active for hydrodesulfurization (HDS) of thiophene has been investigated as a function of pretreatment conditions (H_2S/H_2 = 0-0.2) and support by using X-ray photoelectron, laser Raman and IR spectroscopies and temperature-programmed desorption of adsorbed NO. It has been found that when molybdenum catalysts are presulfided with H_2S/H_2 , MoS_2-like species are formed, whereas when prereduced and subsequently sulfided during the HDS reaction, molybdenum oxysulfide or highly dispersed amorphous molybdenum sulfides are produced. The turn-over frequency of the HDS reaction calculated on the basis of the NO adsorption was shown to increase with decreasing the dispersion degree of sulfided molybdenum irrespective of the support material; Al_2O_3 or TiO_2. It is proposed that two kinds of NO adsorption sites are present; triply and doubly cus (coordinatively unsaturated) molybdenum sites. It is considered that both sites are catalytically active, possibly, the triply cus species being more

active. The presence of triply and doubly sites and their dependences on molybdenum concentration explain well the activity of the supported molybdenum sulfides for the hydrogenation of 1,3-butadiene. It is concluded that the HDS activity of sulfided molybdenum catalysts is determined by the structure, dispersion and coordinative unsaturation of sulfided molybdenum cluster.

Introduction

Supported molybdenum catalysts are widely used in industry for hydrodesulfurization (HDS). Cobalt and/or nickel are employed to promote the molybdenum catalysts. The synergic effects of the promoters have been studied by many workers [1-6] and reviewed by several authors [7-12]. Recently, Topsøe et al. have shown by using Mossbauer emission spectroscopy that a Co-Mo-S phase on promoted sulfide catalysts is responsible for thiophene HDS reaction [12-15]. In this model, it is considered that molybdenum is present as a MoS_2-like structure. EXAFS studies indicated the presence of MoS_2-like structures on sulfided Mo/Al_2O_3 and $Co-Mo/Al_2O_3$ catalysts [16-18]. However, the configurations of active sites on these dispersed molybdenum sulfides have not been unveiled yet. They are functions of the degree of the molybdenum sulfidation [19] and support [20].

In order to characterize the catalytically active molybdenum sulfide sites, several molecules are used as a probe; NO [21-26], O_2 [14,27-32], CO [33,34], and pyridine [19,35,36]. The amount of

NO chemisorption is relatively well correlated to HDS activities [15]. In addition, NO is one of the most convenient molecule for the IR studies due to its high extinction coefficient and for differentiating adsorption sites. It is well established that NO adsorbs on multiply cus (coordinatively unsaturated) molybdenum sites as a dinitrosyl [21] or dimeric [23] complex. Valyon and Hall [22] have suggested that cus Mo sites in reduced catalysts are Mo^{2+} from the IR study of the coadsorption of NO and O_2.

In order to reveal the configuration of the active sites on molybdenum sulfides responsible for the thiophene HDS reaction, a NO adsorption study was carried out herein for supported molybdenum catalysts sulfided under various conditions, coupled with X-ray photoelectron (XPS), laser Raman (LRS) and IR spectroscopies and temperature-programmed desorption techniques. The catalyst supports emplyed here were Al_2O_3, SiO_2, TiO_2, and Nb_2O_5. The hydrogenation of 1,3-butadiene was carried out to obtain some insights into the configuration of the active sites.

Experimental

γ-Al_2O_3 and SiO_2 were supplied by the Catalysis Society of Japan as a reference catalyst (JRC-ALO-4 and SIO-4 [37]; the B.E.T. surface areas of Al_2O_3 and SiO_2 were 163 and 347 m^2g^{-1}, respectively). TiO_2 was provided by Nippon Areosil Co. (Degussa, P-25; 50 m^2g^{-1}). Nb_2O_5 was provided by CBMM Co. (119 m^2g^{-1}).

Supported molybdenum catalysts were prepared by an incipient impregnation method. The loading level of MoO_3 was adjusted to be 5-120 x 10^{13} Mo cm^{-2} (2.5-30 wt%) with respect to the support. An aqueous solution of the appropriate concentration of ammonium paramolybdate (Nakarai Chemicals) was added to the support and kneaded for 10 min at room temperature. Subsequently, the catalyst slurry was dried at 383 K for 18 h, followed by calcination in air at 823 K for Al_2O_3 and SiO_2 or at 773 K for TiO_2 and Nb_2O_5 for 5 h.

The presulfidation of the catalyst was carried out at 673 K for 1.5 h in a stream of an atmospheric pressure of H_2S/H_2 (H_2S/H_2; 0-0.20, 500 mL STP min^{-1}). Subsequently, the HDS reaction of thiophene was carried out at the same temperature in an atmospheric pressure of a thiophene/H_2 stream (1.6% thiophene, 1 L STP min^{-1}), followed by measurements of catalytic activity at the reaction time of 1 h. The reaction gas was analyzed by GLC. The catalyst was, then, treated with an atmospheric pressure of a deoxygenated and dehydrated H_2-stream at 673 K for 1 h and evacuated for 1 h at the same temperature. After being cooled to room temperature under a dynamic vacuum, the amount of NO chemisorption was measured at room temperature (exposed to NO for 0.5 h and evacuated for 1 h, accompanied by NO physisorption experiments). After that, the XP spectra of the catalyst was measured without exposing the catalyst to air. The XPS measurements were made on a Hitachi 507 photoelectron spectrometer using Al $K\alpha_{1,2}$ radiation (1486.6 eV). The anode was

operated at 9 kV and 50 mA. Assuming linear backgrounds, the intensity ratios were determined by using the integrated areas of the Mo3d, S2p, S2s, Al2p, Si2s, Ti2p, and Nb3d levels. The binding energies were referenced to the Al2p (74.5 eV), Si2s (154.8 eV), $Ti2p_{3/2}$ (459.5 eV), or $Nb3d_{5/2}$ (207.4 eV) band.

Hydrogenation of 1,3-butadiene was carried out at 273 K by using a circulation system (ca. 200 mL) over the sulfided catalyst. The H_2/butadiene ratio was adjusted to 2. The initial reaction pressure was 1 kPa.

The measurements of IR, temperature-programmed desorption (TPD) of NO and LR spectra were made in situ for the activated catalyst samples. The samples were exposed to NO and/or H_2S at room temperature for the IR and TPD studies. The IR spectra of the catalyst were recorded in a transmittance mode at room temperature on a Hitachi EP1-G double beam spectrophotometer by employing self-supporting wafers. The TPD study of NO adsorbed on the sulfided catalyst was conducted in a dynamic vacuum at a rate of 1.8 K min^{-1} from room temperature to ca. 570 K and evolved gases were continuously and repeatedly analyzed by a mass filter (ULVAC, MSQ-105A). The LR spectra were obtained by using an in situ cell at room temperature with a JASCO R-800 spectrometer equipped with a double monochrometer. The 514.5 nm line of a NEC GLS-3200 Ar^+ laser was used for excitation at the intensity of 150-200 mW at the source. A spectral resolution was 5 cm^{-1}.

Results and Discussion

The HDS activities of the MoO_3/Al_2O_3 catalysts for thiophene are shown in Fig. 1 as a function of the H_2S/H_2 ratio in the presulfidation and the loading level of MoO_3. It is apparent that when the catalyst (5-30 wt% MoO_3) is presulfided at an increasing H_2S/H_2 ratio, the activity decreases steeply at a low H_2S/H_2 ratio (< 0.02) and then diminishes gradually at a further increase in the ratio. At H_2S/H_2 = 0, the MoO_3/Al_2O_3 catalyst was reduced with H_2 and then sulfided with thiophene and/or resultant H_2S during the HDS reaction. At 2.5 wt% MoO_3 content (6.4×10^{13} Mo cm^{-2}), on the other hand, the HDS activity increases as the H_2S/H_2 ratio increases. Accordingly, it is evident that the thiophene HDS activity markedly varies with both the H_2S/H_2 ratio of the sulfidation conditions and the loading level of MoO_3. It has been previously found that the activation mode of the catalyst affects the activity of the sulfided catalyst [19]. It is considered that the dependences of the HDS activity on the sulfidation conditions and the loading level of MoO_3 are correlated to the differences in the structure and dispersion degree of Mo sulfides formed on the catalyst surface.

As shown in Fig. 1, the HDS activity increases up to a loading level of 15 wt% MoO_3 and becomes independent of the MoO_3 loading level regardless of the sulfidation conditions. This is attributable to a formation of well-dispersed Mo species up to 15 wt% MoO_3 and in accord with the XRD and XPS results; no

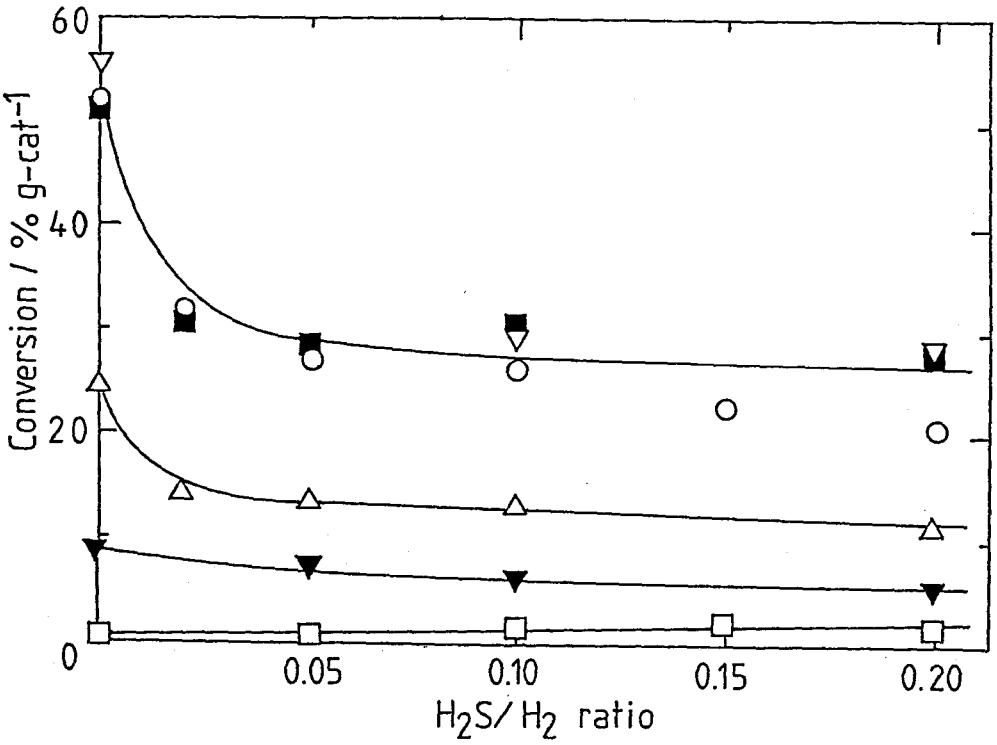

Figure 1 Dependence of the thiophene HDS activity of sulfided MoO_3/Al_2O_3 catalyst on the H_2S/H_2 ratio in sulfiding.

□, 2.5 wt%; ▼,5 wt%; △,10 wt%; ○,15 wt%;

▽, 20 wt%; ■,30 wt%.

detection of crystalline MoS_2 by XRD and a linear correlation between the Mo3d/Al2p XPS intensity ratio and the surface concentration of Mo at < 15 wt% MoO_3 as observed previously [19]. No significant change in the Mo3d/Al2p ratio was observed on the sulfidation of the catalyst with H_2S/H_2. The previous observations [19] of a considerable variation in the XPS intensity ratio on sulfidation may be attributed to the use of CS_2/H_2 for sulfiding instead of H_2S/H_2 and/or to different levels of impurities on Al_2O_3 surfaces which greatly modify the surface properties of Al_2O_3 as shown previously for the H_2S adsorption [38].

The thiophene HDS activities of the supported molybdenum catalysts are shown in Fig. 2 as a function of the Mo surface concentration and the H_2S/H_2 ratio in presulfidation. As for the TiO_2-supported catalyst, the HDS activity decreases with the increase in the surface concentration. The decrease in the activity is attributed to the formation of bulk-like MoO_3 as a result of the decrease in the dispersion degree of Mo species according to the XRD and XPS results. As illustrated in Fig. 3, the Mo3d/Ti2p XPS intensity ratio increases linearly up to the loading level of 5 wt% MoO_3 (ca. 40×10^{13} Mo cm^{-2}), followed by a deviation from the linear line. The activity at $H_2S/H_2 = 0$ is higher about two times than that at $H_2S/H_2 = 0.1$. This result is similar to that for the Al_2O_3-supported catalyst in Fig. 1. However, the activity of TiO_2-supported catalyst is much higher than that of Al_2O_3-supported catalyst. The HDS activities of

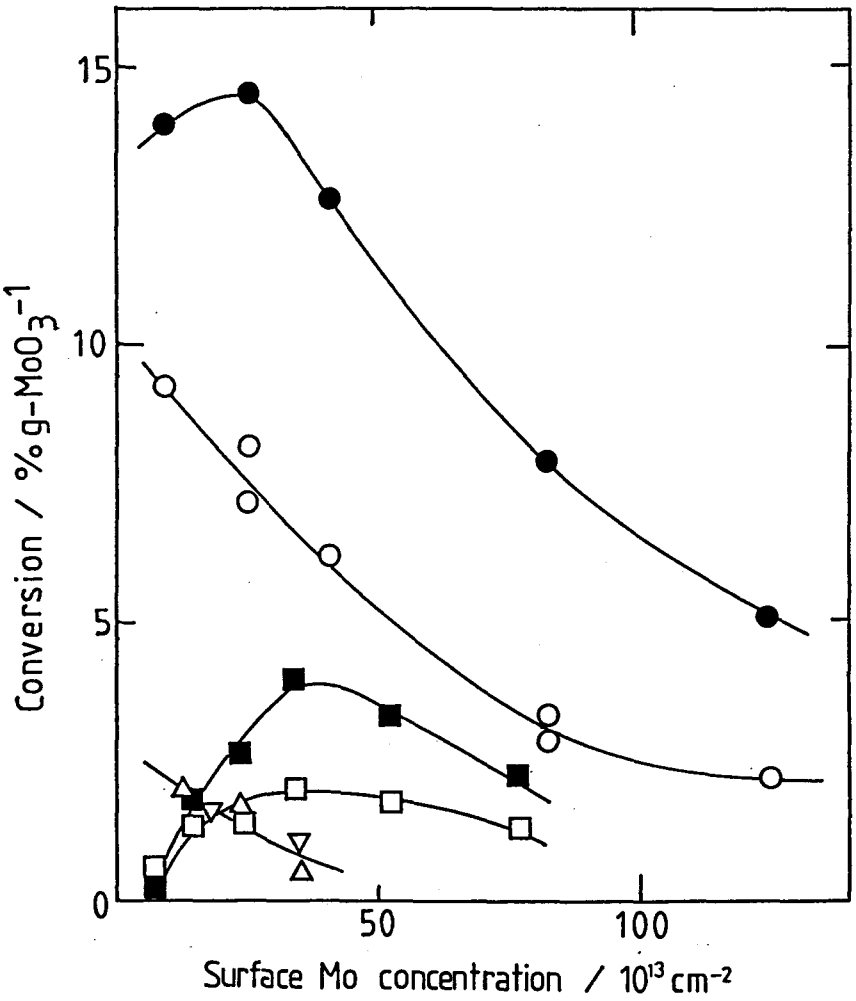

Figure 2 Dependence of the thiophene HDS activity of sulfided molybdenum catalysts on the surface concentration of molybdenum, support, and pretreatment conditions.

■, Al_2O_3, H_2S/H_2 = 0; □, Al_2O_3, 0.1;
●, TiO_2, 0; ○, TiO_2, 0.1;
△, SiO_2, 0.1; ▽, Nb_2O_5, 0.1.

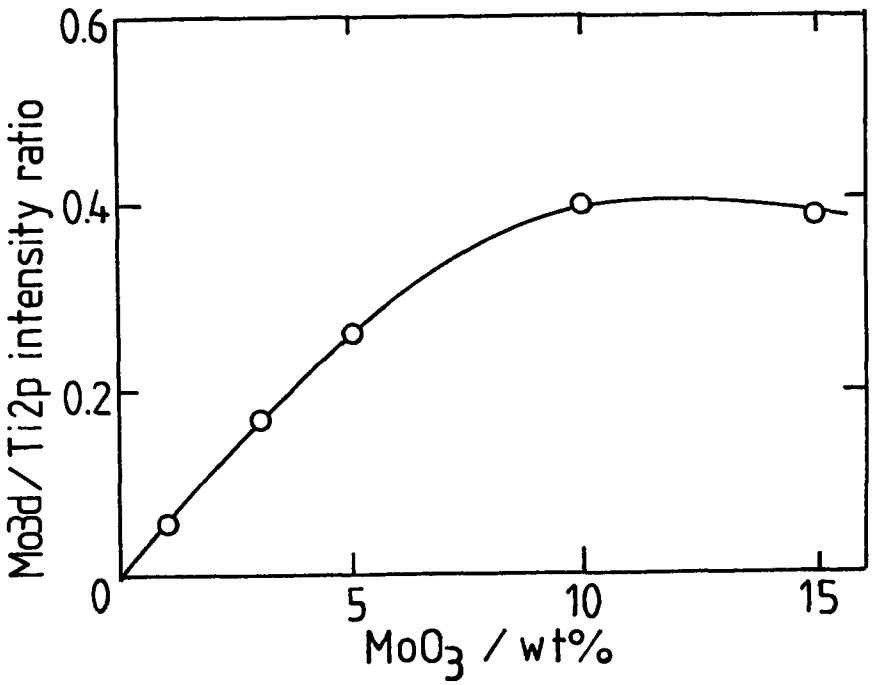

Figure 3 Mo3d/Ti2p XPS intensity ratio as a function of MoO_3 content for MoO_3/TiO_2 catalyst.

SiO_2- and Nb_2O_5-supported catalysts are nearly equivalent to that of Al_2O_3-supported catalyst. It is appearent from Fig. 2 that the dependence of the HDS activity of the Al_2O_3-supported catalysts on the surface concentration of Mo is different from those of the catalysts supported on the TiO_2, SiO_2, and Nb_2O_5; the Al_2O_3-supported catalyst shows an activity maximum at ca. 35×10^{13} Mo cm^{-2} (15 wt% MoO_3). The dependencies of the HDS activity of SiO_2- and Nb_2O_5-supported catalysts on surface concentration are similar to that of TiO_2-supported catalyst; as the surface concentration of Mo increases, the activity decreases.

The degree of sulfidation of Mo ions, S/Mo atomic ratio, is depicted in Figs. 4 and 5 as a function of MoO_3 content for the sulfided MoO_3/Al_2O_3 catalyst and for the sulfided catalysts at H_2S/H_2 = 0.1, respectively. The S/Mo ratio was calculated from the S2p/Mo3d XPS intensity ratio [19]. Apparently, as for the MoO_3/Al_2O_3 catalyst, the S/Mo ratio is increased by the H_2S/H_2-presulfidation and becomes almost independent of the H_2S/H_2 ratio at > 0.05. The S/Mo ratio gradually increases with the MoO_3 content up to 40×10^{13} Mo cm^{-2} or 10 wt% (except a considerably low S/Mo ratio for the 2.5 wt% MoO_3/Al_2O_3 catalyst at 0.05) and becomes constant (S/Mo = 1.6-1.7). It is evident from Fig. 5 that the S/Mo ratio is lower than two for the catalysts irrespective of the support examined here, this suggesting an incomplete transformation of supported molybdenum to MoS_2.

As shown in Fig. 4, under the conditions of H_2S/H_2 = 0, however, the S/Mo atomic ratio for the Al_2O_3-supported catalyst

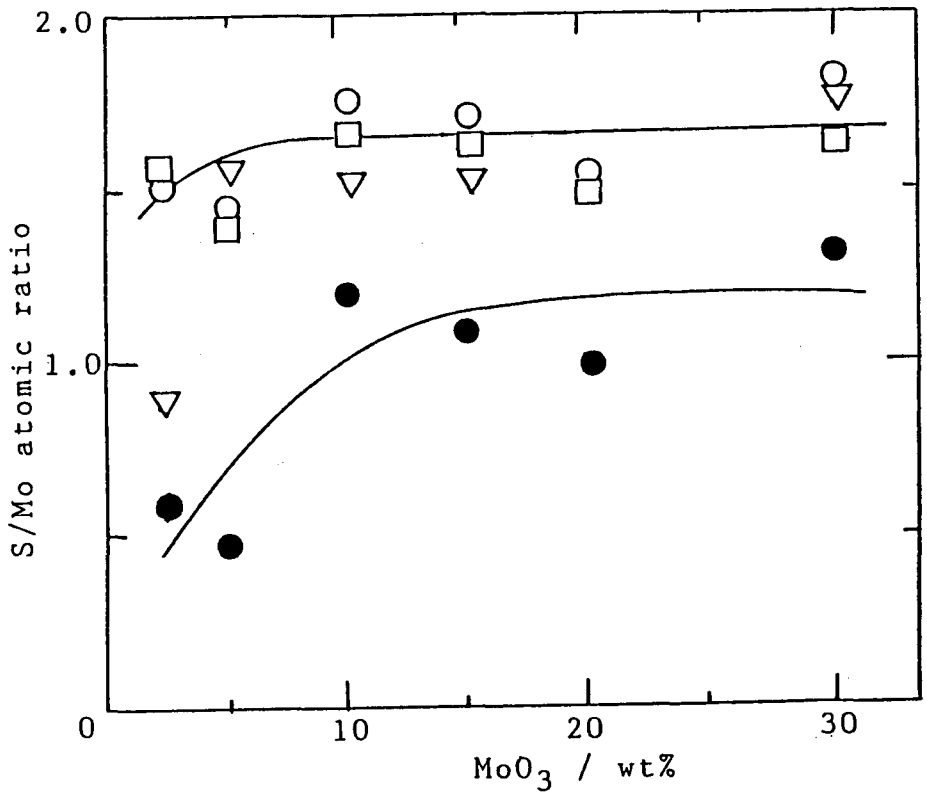

Figure 4 S/Mo atomic ratio as a function of the MoO_3 content for the sulfided MoO_3/Al_2O_3 catalyst after the HDS of thiophene at 673 K.

●, H_2S/H_2 = 0; ▽, 0.05; ○, 0.1; □, 0.2.

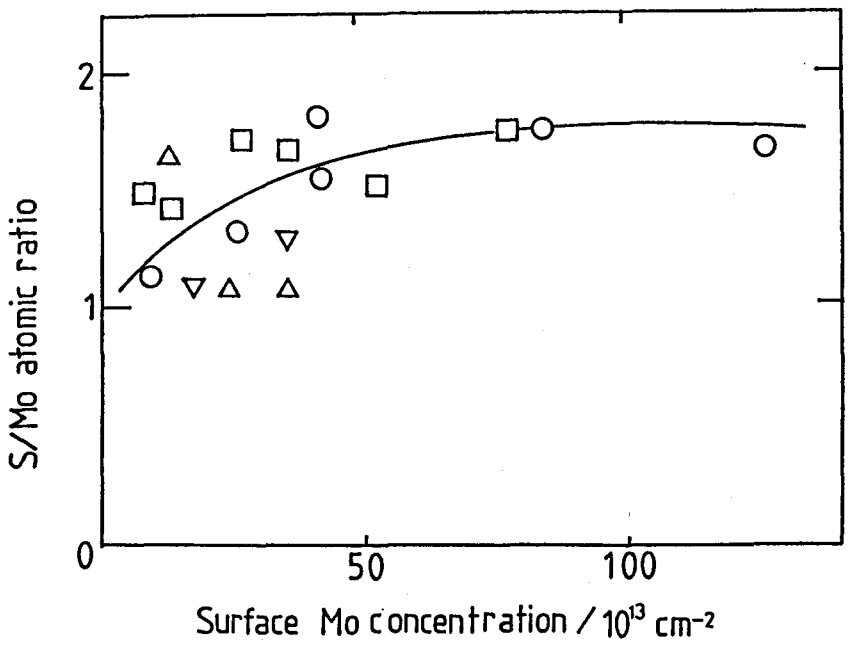

Figure 5 Degree of the sulfidation of molybdenum as a function of the surface Mo concentration and support (H_2S/H_2 = 0.1).
□, Al_2O_3; ○, TiO_2; △, SiO_2; ▽, Nb_2O_5.

increases with increasing the MoO_3 content up to 15 wt% and levels off at a lower S/Mo ratio (1.0-1.2) compared with that attained when presulfided. This suggests that the structures of sulfided Mo species formed on the catalyst surface are significantly different between the presulfidation and prereduction conditions.

These findings suggest that a considerable portion of Mo species which resists sulfiding exists in the low MoO_3 content catalysts, especially, for the 2.5 wt% MoO_3/Al_2O_3 catalyst. Zingg et al. [38] have reported with MoO_3/Al_2O_3 catalysts that the molybdenum occupies mainly tetrahedral sites at a low MoO_3 content and that two types of tetrahedral Mo species are present on the oxidic catalyst; monomeric and dimeric species. The monomeric species resists sulfiding, while the dimeric species are readily sulfided to MoS_2. Our results are in line with their model.

It is well established that NO adsorbs on cus Mo sites in a pair [21]. Therefore, the dispersion degree of Mo was assessed by the amount of NO chemisorption. The fraction of cus Mo thus obtained for the Al_2O_3-supported catalyst is shown in Fig. 6 against the MoO_3 content. The fraction varied with the H_2S/H_2 ratio, too. At a H_2S/H_2 ratio of > 0.1, the proportion of the adsorption site decreases as the MoO_3 content increases. As for the 2.5 wt% MoO_3 catalyst, 25-30% of Mo adsorb two NO molecules when properly activated. While, at low H_2S/H_2 ratios, the fraction of NO-adsorption sites shows a maximum (at 10 and

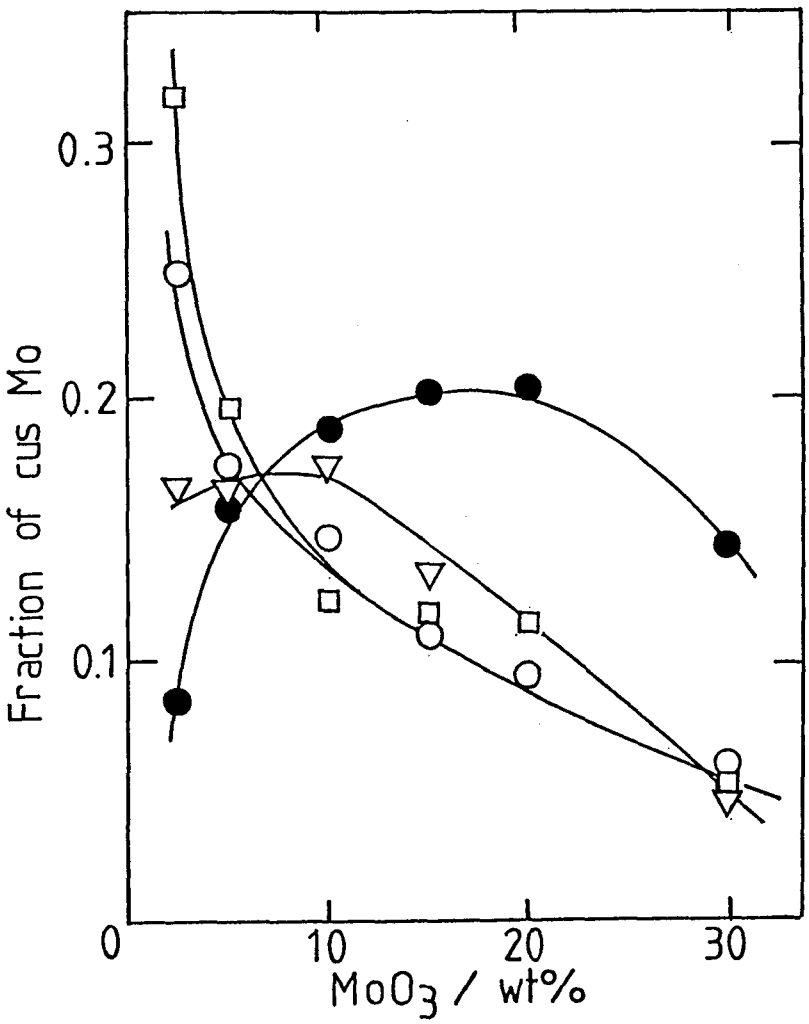

Figure 6 Fraction of cus Mo (a half of the NO/Mo molecular ratio) measured after the HDS of thiophene at 673 K vs. MoO_3 content for the MoO_3/Al_2O_3 catalysts.

●, H_2S/H_2 = 0; ▽, 0.05; ○, 0.1;

□, 0.2.

20 wt% MoO_3 for H_2S/H_2 = 0.05 and 0, respectively). The proportion of cus Mo sites in the low MoO_3 content catalysts (2.5 and 5 wt%) increases with increasing the H_2S/H_2 ratio, while the fraction decreases for the catalysts containing 10-30 wt% MoO_3.

The fraction of cus Mo at H_2S/H_2 = 0.1 is depicted in Fig. 7 for the sulfide catalysts supported on TiO_2, SiO_2, and Nb_2O_5 as a function of the surface concentration of Mo. The fractions of cus Mo for the TiO_2-, SiO_2-, and Nb_2O_5-supported catalysts decrease regularly as the surface concentration of Mo increases. On the other hand, the Al_2O_3-supported catalyst shows a maximum when sulfided by the thiophene/H_2 stream after prereduction. It is considered that the reduction behavior of Mo ions is different between the TiO_2- and Al_2O_3-supported catalysts. Temperature programmed reduction experiments for the MoO_3/TiO_2 catalysts showed that the reduction temperature and the average oxidation number of reduced molybdenum were lower than those for the MoO_3/Al_2O_3 catalysts (643 vs. 693 K, and 4 vs. 5 at ca. 40 x 10^{13} Mo cm^{-2} for TiO_2 and Al_2O_3, respectively). The low reducibility of Mo species for the Al_2O_3-supported catalyst is attributed to the presence of monomeric tetrahedral species which resist sulfiding [39].

The turn-over frequency (TOF) of the thiophene HDS reaction on the sulfided molybdenum catalyst was obtained on the basis of the amount of NO chemisorption. The TOF is shown in Figs. 8 and 9 as a function of the MoO_3 content. As shown in Fig. 8, when the MoO_3/Al_2O_3 catalyst was presulfided with H_2S/H_2, the TOF

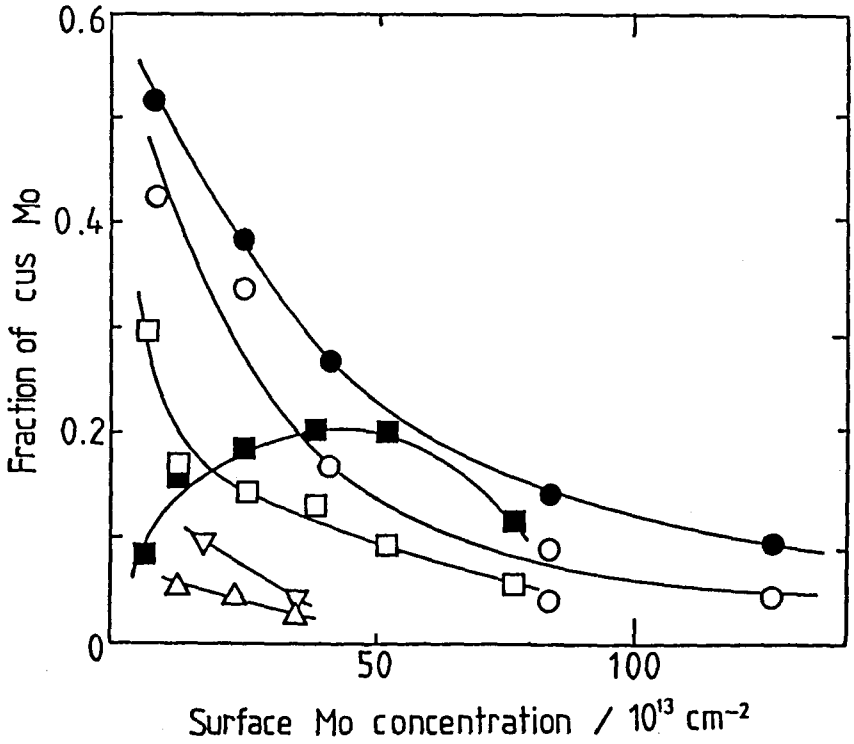

Figure 7 Fraction of NO-adsorption sites on sulfided molybdenum catalysts as a function of the surface concentration of Mo, support, and pretreatment conditions.

■, Al_2O_3, H_2S/H_2 = 0; □, Al_2O_3, 0.1;
●, TiO_2, 0; ○, TiO_2, 0.1;
△, SiO_2, 0.1; ▽, Nb_2O_5, 0.1.

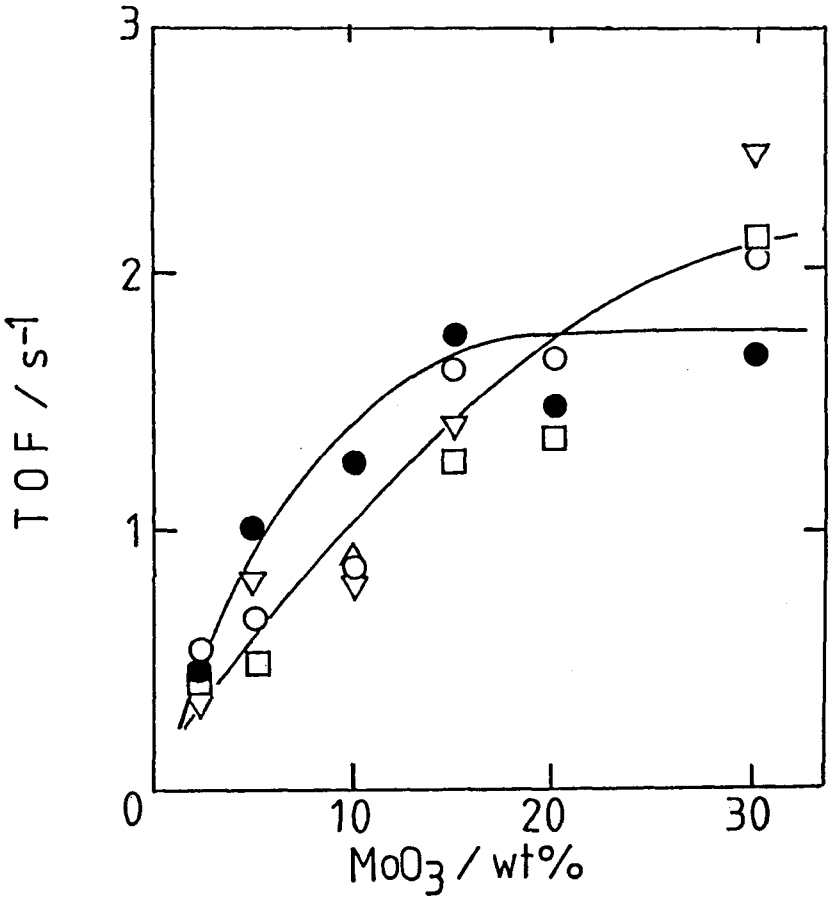

Figure 8 Dependence of the TOF of thiophene HDS reaction over the sulfided MoO_3/Al_2O_3 catalyst upon the MoO_3 content.

●, H_2S/H_2 = 0; ▽, 0.05; ○, 0.1; □, 0.2.

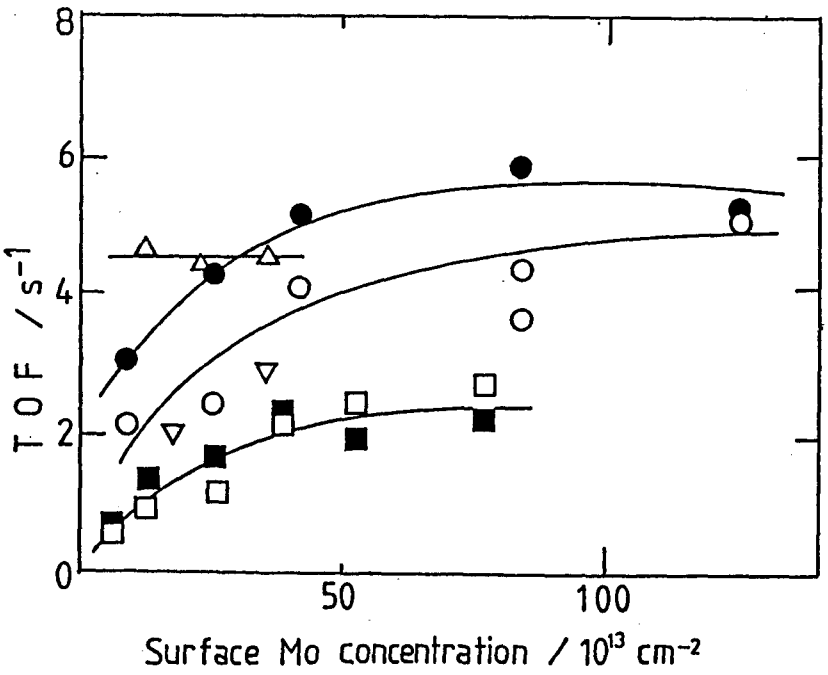

Figure 9 TOF of the supported-molybdenum sulfide catalysts for the HDS of thiophene against the surface Mo concentration, support, and pretreatment conditions.

■, Al_2O_3, H_2S/H_2 = 0; □, Al_2O_3, 0.1;
●, TiO_2, 0; ○, TiO_2, 0.1;
△, SiO_2, 0.1; ▽, Nb_2O_5, 0.1.

increased with the MoO_3 content almost irrespective of the sulfidation conditions. At H_2S/H_2 = 0, however, a plateau is seen above 15 wt% MoO_3. While, the TOF for the TiO_2-supported catalysts increases with the surface concentration of Mo and levels off around 40 x 10^{13} Mo cm^{-2} irrespective of the H_2S/H_2 ratio, as shown in Fig. 9. The TOF for the Nb_2O_5-supported catalyst is close to that for the TiO_2-supported catalysts. As for the SiO_2-supported catalysts, the TOF is very close to that for the TiO_2-supported catalysts at a very low content of Mo and at H_2S/H_2 = 0.1. It is obvious that the TOF of the Al_2O_3-supported catalysts is 2-3 times less than those of the catalysts supported on TiO_2, Nb_2O_5, and SiO_2, indicating that more active Mo sulfides are formed on the latter supports. It is considered that the dependence of TOF on the MoO_3 content result from the changes of the structure and dispersion of active molybdenum species.

In an analogy with the estimation of the dispersion degree of metal by using CO or H_2 adsorption for supported metal catalysts, it is proposed herein that the extent of dispersion of molybdenum sulfides (D_{Mo-S}) is evaluated from the amount of NO adsorption and the degree of sulfidation of molybdenum as in Equation (1).

$$D_{Mo-S} = \frac{\text{(Fraction of Mo which adsorbs } (NO)_2)}{\text{(Fraction of molybdenum sulfides)}} \quad (1)$$

On the basis of the XPS results of Hercules et al. [39], it is assumed here that the stoichiometry of sulfided molybdenum

species is two. The incomplete sulfiding of Mo in Figs. 4 and 5 indicates a partial transformation of Mo oxides to the sulfide species. The TOF of thiophene HDS reaction is depicted in Fig. 10 against the dispersion degree of molybdenum sulfides on Al_2O_3. When the catalyst was presulfided ($H_2S/H_2 > 0$), the TOF is evidently correlated well to the dispersion degree of molybdenum sulfides; the TOF increases, as the degree of MoS_2 dispersion decreases. The decreased dispersion degree is considered to correspond to an increased size of molybdenum sulfides, although no crystalline MoS_2 was detected by XRD except the catalyst with the lowest dispersion (30 wt% MoO_3). However, the TOF at $H_2S/H_2 = 0$ is higher than that for the presulfided catalysts and seems independent of the dispersion degree of molybdenum sulfides. It is suggested that the structure of sulfided molybdenum species formed at $H_2S/H_2 = 0$ are different from those produced by presulfiding with H_2S/H_2.

In order to characterize the molybdenum sulfides, LRS techniques were used. Typical spectra are shown in Fig. 11 for the MoO_3/Al_2O_3 catalysts. Regardless of the H_2S/H_2 ratio and loading levels, the peak at ca. 960 cm^{-1} in the oxidic state, which is characteristic to well-dispersed polymolybdate phases [40-42], completely disappeared after sulfidation. The LR spectra indicated that molybdenum oxides with Mo=O bonds were completely sulfided by H_2S/H_2 or the thiophene HDS reaction. When the catalyst was presulfided, a strong peak at 405 cm^{-1} accompanied by broad peaks at ca. 450 and 380 cm^{-1} was observed.

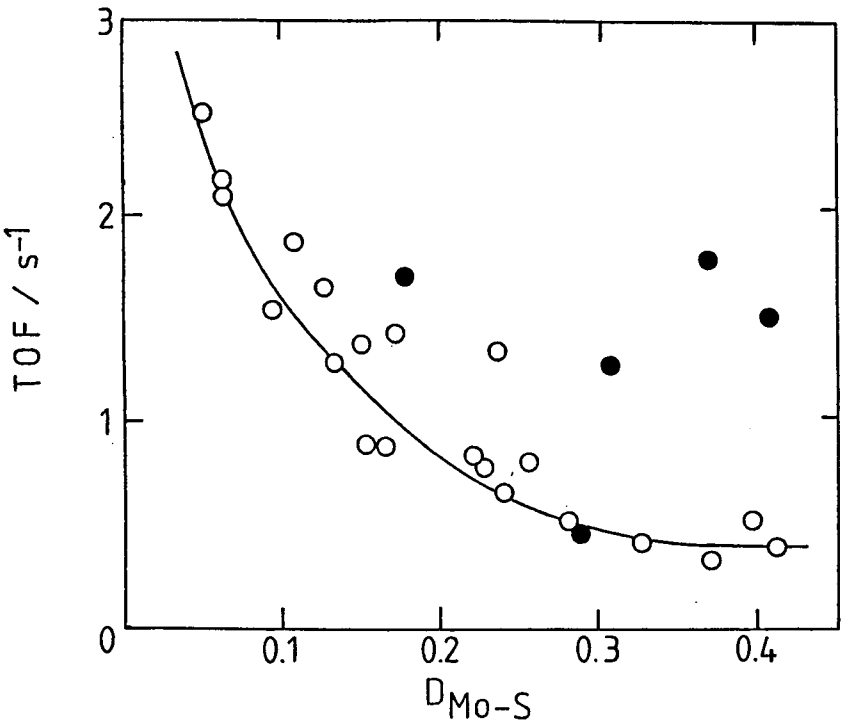

Figure 10 Dependence of the TOF of thiophene HDS reaction on the dispersion degree of molybdenum sulfide for the MoO_3/Al_2O_3 catalysts.

●, H_2S/H_2 = 0; O, > 0.1.

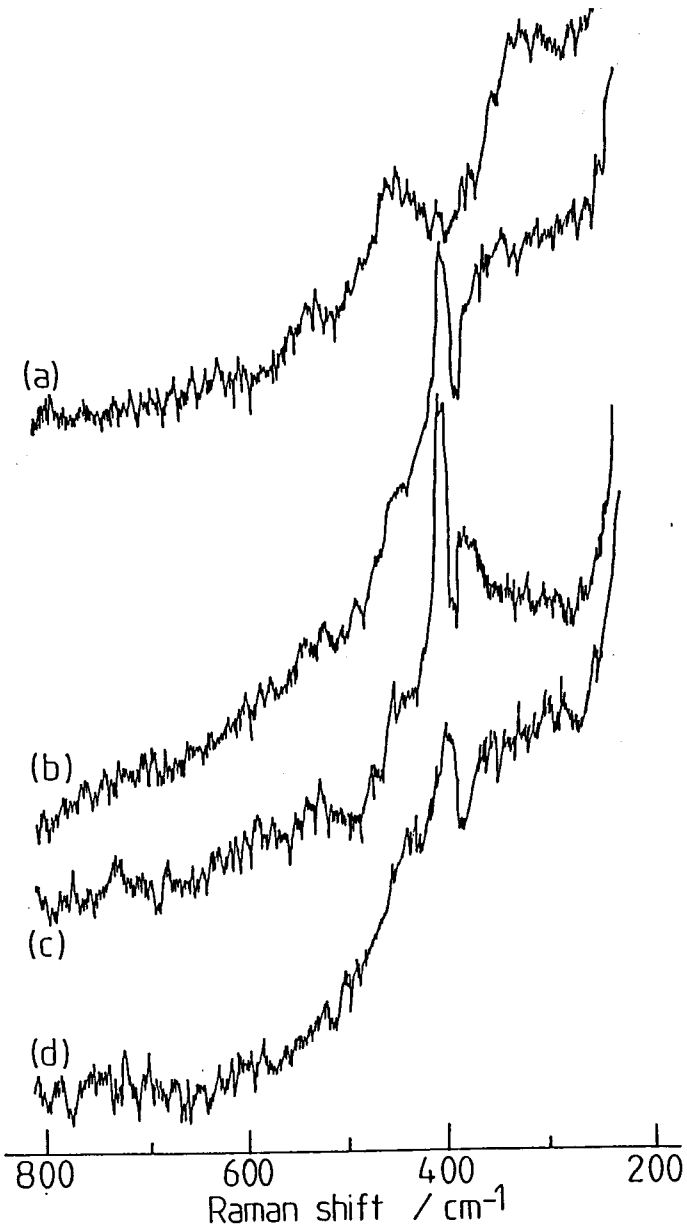

Figure 11 In situ laser Raman spectra for MoO_3/Al_2O_3 catalysts sulfided at 673 K in an atomospheric H_2S/H_2 stream, followed by the HDS of thiophene at the same temperature.
(a)15 wt%, H_2S/H_2 = 0; (b)15 wt%, 0.02;
(c)15 wt%, 0.1; (d)2.5 wt%,0.1.

These pair peaks are assigned to a MoS_2 phase [43]. The above findings indicate that the molybdenum sulfides formed on sulfided catalyst have a MoS_2-like structure. As for the TiO_2-supported catalysts at H_2S/H_2 = 0.1 a similar result was obtained by LRS measurements. Clausen et al. [16,17] and Huntly et al. [18] recently observed the presence of microcrystalline MoS_2 in sulfided catalysts by using EXAFS. On the other hand, when the catalyst was prereduced and subsequently sulfided during the reaction, the peaks at 380 and 405 cm^{-1} were not observed and only a broadened peak at 450 cm^{-1} due to a Mo-S stretching band [43] was detected as shown in Fig. 11. It is considered that the structure of the active molybdenum species is not a MoS_2-like structure, suggesting the formation of molybdenum oxysulfides or highly dispersed amorphous molybdenum sulfides.

The IR spectra of NO adsorbed on the sulfided catalysts are illustrated in Figs. 12 and 13 for sulfided MoO_3/Al_2O_3 and $/TiO_2$ catalysts, respectively. Irrespective of the pretreatment conditions and support, the spectra consist of two adsorption peaks at 1795 and 1715-1690 cm^{-1}. They are assigned to symmetric and asymmetric stretching bands of dinitrosyl species, respectively [44]. The band positions indicate that two NO molecules adsorb on sulfided Mo sites [22,25]. It is considered that even under the pretreatment conditions of H_2S/H_2 = 0, sulfided cus Mo sites are actually formed during the HDS reaction of thiophene. However, the spectroscopic features at H_2S/H_2 = 0 and those at 0.1 are significantly different; the symmetric/asymmetric

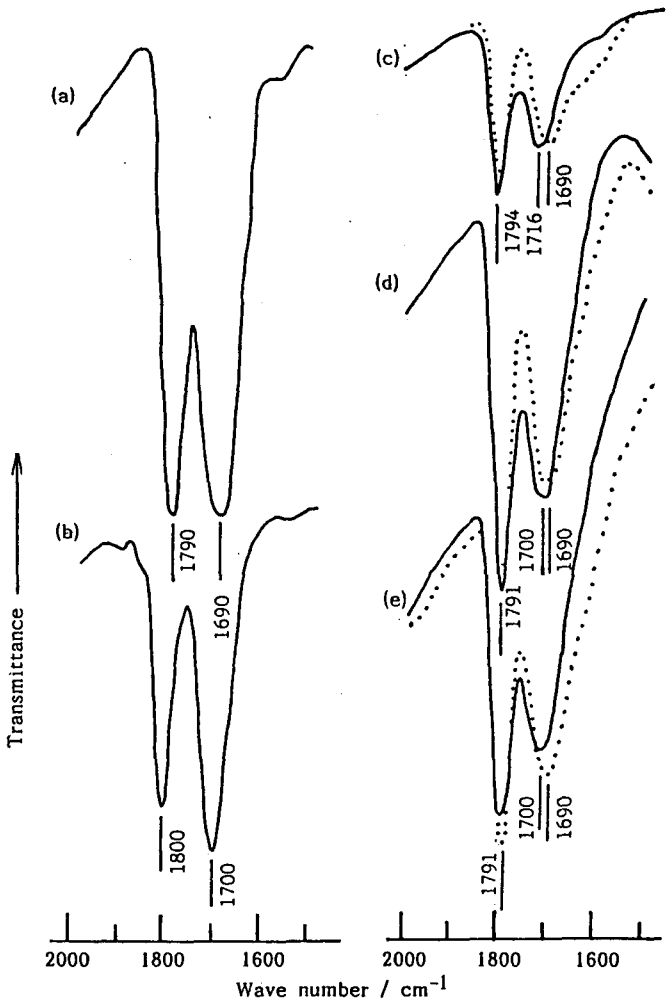

Figure 12 IR spectra of NO adsorbed on the MoO_3/Al_2O_3 catalysts reduced or sulfided at 673 K in an atmospheric H_2 or H_2S/H_2 stream, followed by the HDS of thiophene at the same temperature. (a)10 wt%, only reduced; (b)10 wt%, H_2S/H_2 = 0; (c)2.5 wt%, 0.1; (d)10 wt%, 0.1; (e)20 wt%, 0.1. The dotted line shows the change of the IR spectrum of preadsorbed NO when the sample was exposed to H_2S (5.3 kPa)and evacuated at room temperature for 30 min.

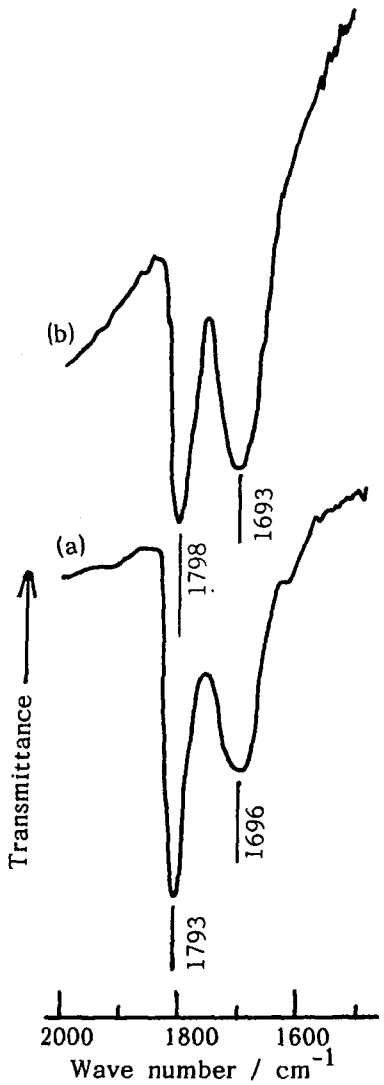

Figure 13 IR spectra of NO adsorbed on the TiO_2-supported molybdenum catalyst (3 wt% MoO_3) sulfided at H_2S/H_2 = 0.1 (a) and at H_2S/H_2 = 0 followed by the thiophene/H_2 reaction (b).

intensity ratios are 1.02 and 1.36 at H_2S/H_2 = 0 and 0.1 for the Al_2O_3-supported catalysts, respectively. The ON-Mo-NO angle (θ) is suggested to be different in these two sulfides and calculated to be 90 and 81°, when prereduced and presulfided, respectively, on the basis of a theoretical equation [44]; $I_{sym}/I_{asym} = \cot^2(\theta/2)$. In conjunction with the results of the LRS measurements, the IR spectrum observed at H_2S/H_2 = 0.1 is assigned to NO molecules adsorbed on a MoS_2-like structure, whereas the spectrum at H_2S/H_2 = 0 to dinitrosyls adsorbed on molybdenum oxysulfide or highly dispersed amorphous molybdenum sulfides. The IR spectroscopic features for NO adsorbed on the catalyst at H_2S/H_2 = 0 is very close to those for NO held on a reduced MoO_3/Al_2O_3 catalyst as shown in Fig. 12. A similar results can be obtained for the TiO_2-supported catalysts from the IR spectra in Fig. 13. This suggests that the structure of the sulfides formed under mild sulfidation conditions is similar to the structure of Mo oxide precursor phase.

The dependence of the TOF of thiophene HDS reaction on the dispersion degree of sulfided molybdenum in Fig. 10 suggests the presence of several kinds of molybdenum sites. In order to characterize further the NO adsorption sites, the TPD study of NO adsorbed on sulfided catalyst was conducted. The TPD profiles of NO (m/e = 30) are shown in Figs. 14 and 15 for the MoO_3/Al_2O_3 and TiO_2 catalysts, respectively. As for the Al_2O_3-supported catalysts, the main peak is observed at a desorption temperature of ca. 400 K, accompanying a weak shoulder at a higher

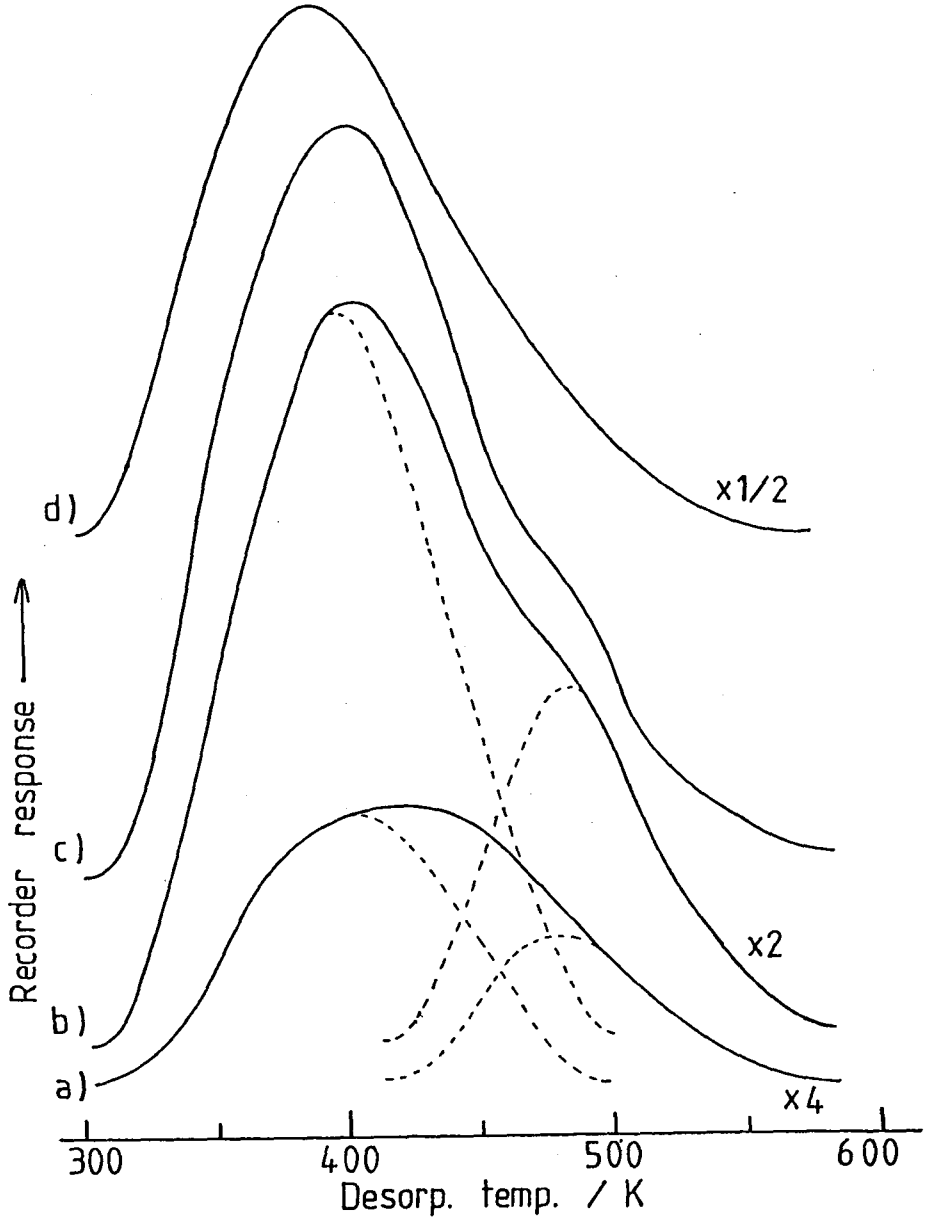

Figure 14 TPD profiles (m/e = 30) of NO adsorbed on the sulfided MoO_3/Al_2O_3 catalyst (H_2S/H_2 = 0.1). (a) 2.5 wt%, (b) 5 wt%, (c) 10 wt%, (d) 20 wt%. The broken lines show the resolved peaks.

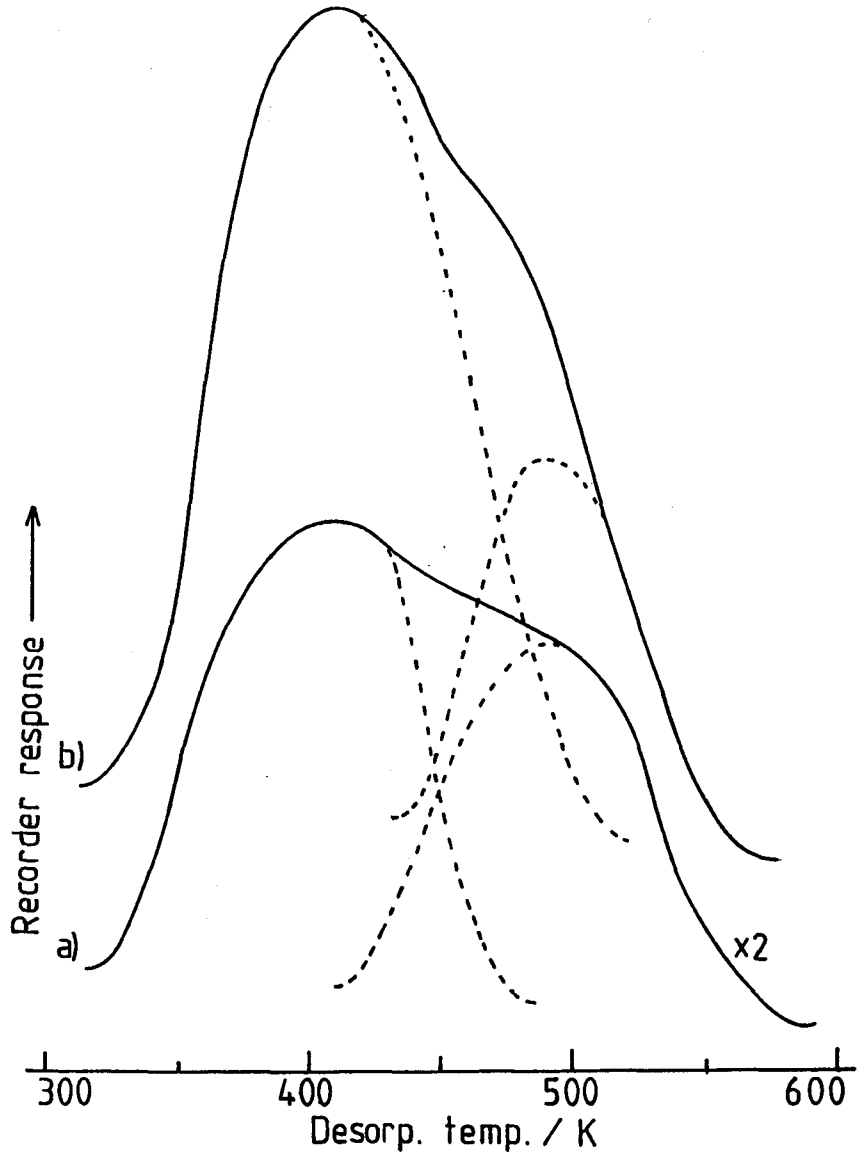

Figure 15 TPD profiles (m/e = 30) of NO adsorbed on the sulfided MoO_3/TiO_2 catalyst (H_2S/H_2 = 0.1).
(a) 3 wt%, (b) 10 wt%. The broken lines show the resolved peaks.

temperature side (ca. 480 K). On the other hand, the peak intensity of the shoulder at higher temperature for the TiO_2-supported catalyst (Fig. 15) is stronger than that for the Al_2O_3-supported catalyst at the same Mo surface concentration (40×10^{13} Mo cm^{-2}; 3 wt% for TiO_2 and 10 wt% for Al_2O_3). It seems that the relative intensity of the main peak at ca. 400 K increases with increasing the MoO_3 content in both catalyst systems. Accordingly, it is revealed that two kinds of NO adsorption sites are differentiated by the TPD techniques. According to the IR spectra of NO in Fig. 12, the TPD peaks are likely to be attributed to the signals due to distinctly different sulfided-Mo sites but not to composite peaks of sulfided and reduced Mo sites. Segawa et al. [45] have also reported two NO desorption peaks for reduced MoO_3/TiO_2 systems. The thermal desorption of NO accompanied a production of N_2O; the desorption temperature of N_2O was ca. 400 K and the peak area intensity ratio of N_2O/NO did not vary with MoO_3 content (0.8-1.0) for the Al_2O_3 catalysts.

In order to determine the configuration of the sulfided Mo sites, a coadsorption of NO and H_2S was examined. Figure 12 shows the changes in the IR spectra of NO when H_2S was introduced. No NO molecules were desorbed by the exposure of the sample to H_2S and by a subsequent evacuation at room temperature. On a contact of the NO-adsorption system with H_2S, the symmetric and asymmetric bands became considerably well separated, since the wave number of the latter peak was red-shifted by ca. 10 cm^{-1}.

Accordingly, the spectral changes are considered to result from the interactions between adsorbed NO and H_2S molecules. The TPD profiles of NO coadsorbed with H_2S are shown in Fig. 16 for the sulfided MoO_3/Al_2O_3 catalyst. The temperature of NO desorption at ca. 400 K raised by 30 K on the exposure of the sample to H_2S. The peak area intensity ratio of N_2O/NO significantly decreased by the H_2S adsorption (0.1-0.6). These findings also suggest the presence of interactions between adsorbed NO and H_2S molecules. On the basis of the IR and TPD results, we propose in Scheme 1 that sulfided Mo sites for NO adsorption consist of triply and doubly cus Mo species and that NO molecules adsorbed on the triply cus sites desorb at ca. 400 K and these on the doubly cus sites at ca. 480 K. Both NO species adsorb to form dinitrosyl or dimeric complex. Hydrogen sulfide molecule adsorbs on the triply cus Mo site preadsorbed with two NO molecules, affecting the IR and TPD of NO. The TPD peak at 430 K is assigned to the desorption of NO adsorbed on the triply cus Mo sites coadsorbed with H_2S or SH. It seems that the fraction of the doubly cus Mo sites in the TiO_2-supported catalyst is larger than that in the Al_2O_3-supported catalyst. With increasing the MoO_3 content in the molybdenum catalyst, the size of MoS_2 particles increases as deduced from the decrease in the NO/Mo ratio, accompanying an increase in the fraction of the triply cus Mo sites. This may be rationalized by a stabilization of multiply cus Mo sites by electronically compensating properties of semiconducting bulky MoS_2 phases.

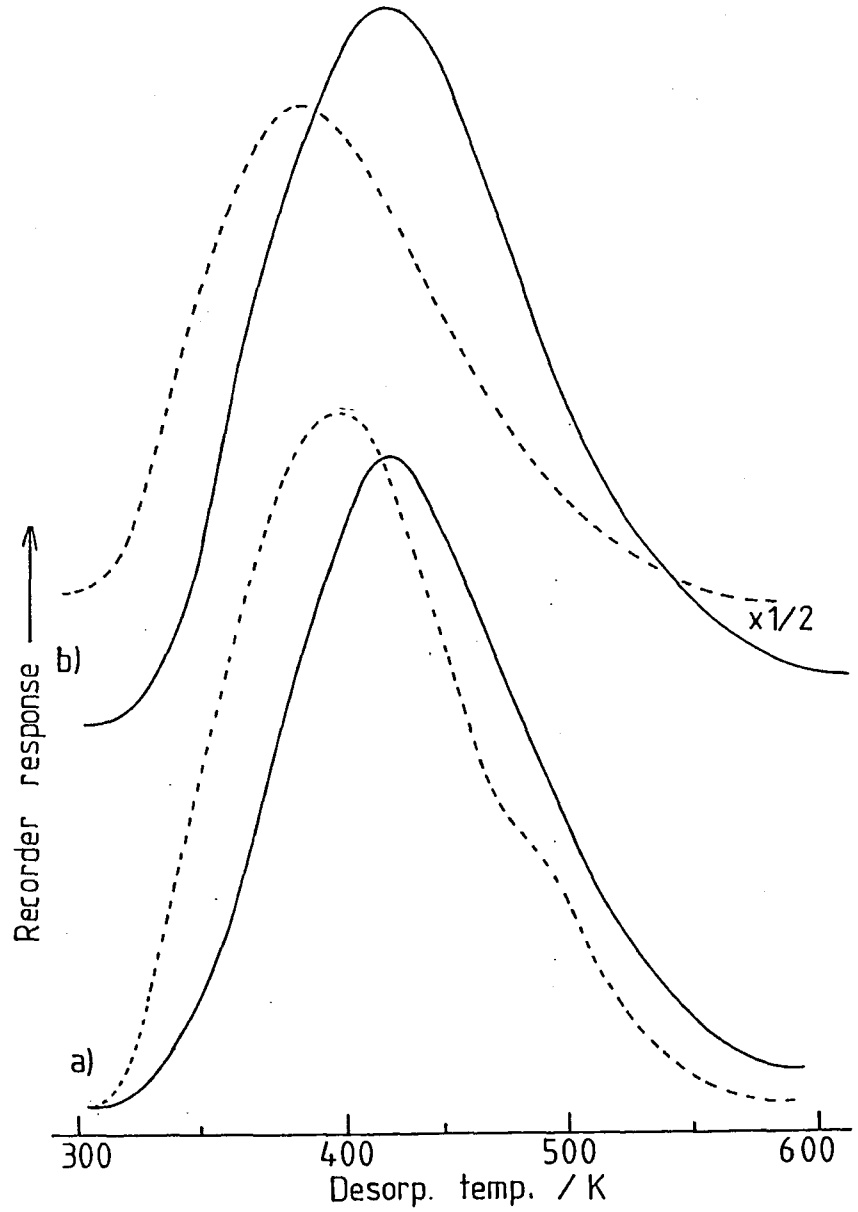

Figure 16 TPD profiles (m/e = 30) of NO on the sulfided MoO_3/Al_2O_3 catalyst (H_2S/H_2 = 0.1) coadsorbed with H_2S.

(a) 10 wt%, (b) 20 wt%. The broken line shows the TPD profile of adsorbed NO alone.

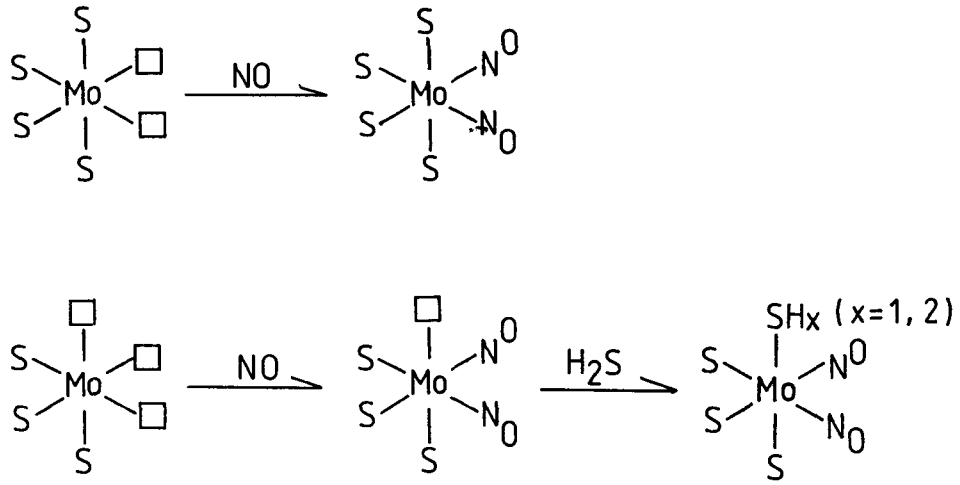

Scheme 1

In Fig. 17, the catalytic results on the hydrogenation of butadiene are shown for the MoO_3/Al_2O_3 and TiO_2 catalysts. It is apparent that the TOF increases with increasing the loading level of molybdenum. This is in line with the findings that the fraction of the triply cus Mo sulfide site increases with an increase in the Mo content, since it is well established that the hydrogenation proceeds only on triply cus Mo sites but not on doubly cus sites [46].

Combining the results on the TOF of sulfided molybdenum catalysts for the HDS reaction with the configuration of the NO adsorption sites, it is suggested that both the triply and doubly cus Mo species are active for the HDS of thiophene, probably the triply cus Mo sites showing higher activity. The activity of the sulfided catalyst is determined by two adverse factors; the number of active sites (NO adsorption sites) and the relative proportion of the triply and doubly cus Mo sites. These adverse factors are considered to cause a volcano type correlation between the intrinsic activity (activity/unit weight of Mo) and sulfidation degree of Mo (S/Mo) as observed previously [19].

Conclusions

On the basis of the results of XPS, LRS, and IR of NO adsorbed on the catalyst, it is revealed that the structure of Mo sulfides formed on the catalysts varies with the H_2S/H_2 ratio in the presulfiding atmosphere. It is demonstrated that MoS_2-like

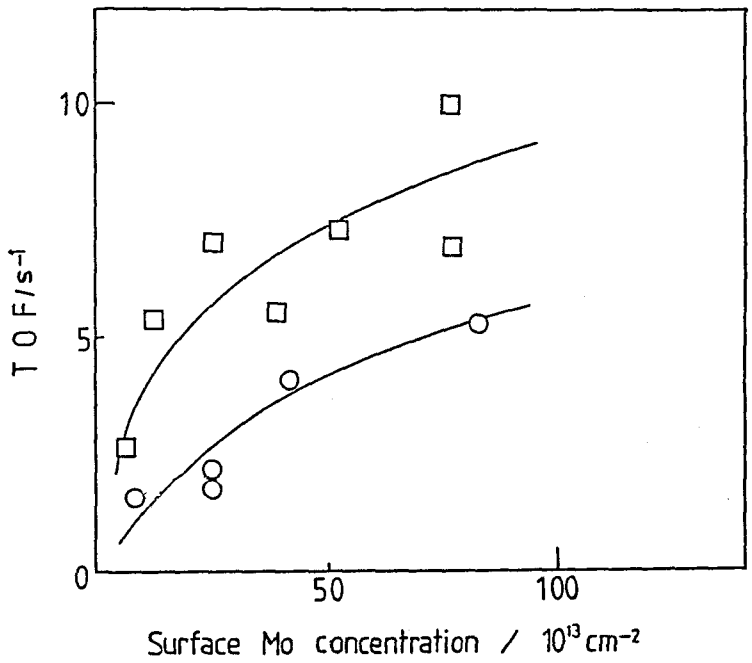

Figure 17 Dependence of the TOF of hydrogenation of 1,3-butadiene over the sulfided catalyst (H_2S/H_2 = 0.1) upon the surface Mo concentration.

□, Al_2O_3; ○, TiO_2;

structure is formed when presulfided (H_2S/H_2 > 0.02), while molybdenum oxysulfide or highly dispersed amorphous molybdenum sulfides are formed when prereduced (H_2S/H_2 = 0). The difference in the structure causes the difference in the thiophene HDS activity.

From the results of IR and TPD of NO adsorbed on sulfided catalysts, it is suggested that the NO adsorption sites consist of multiply cus Mo species, triply and doubly cus Mo sites. The fraction of the triply cus Mo sites increases with increasing the Mo content or with increasing the size of molybdenum sulfide clusters. Taking into account the thiophene HDS activity, it is considered that both sites are active for the reaction, the triply cus sulfided Mo species being more active than the doubly cus sulfided Mo species. The catalytic activity of the sulfide catalyst for the hydrogenation of butadiene is explained in terms of the presence of triply and doubly cus Mo sites and of their Mo-concentration dependence.

References

1) J.M.J.Lipsch and G.C.A.Schuit, J.Catal., 15, 179 (1969).

2) G.C.A.Schuit, P.Courty, and B.Delmon, AIChE J., 19, 417 (1973).

3) G.Hagenbach, P.Courty, and B.Delmon, J.Catal., 31, 264 (1973).

4) B.Delmon "Proc. Climax 3rd Int. Conf. Chemistry and Uses of Molybdenum" (H.F.Barry and P.C.H.Mitchell Eds.) Climax Molybdenum Co. Ann Arbor, Michigan 1979, p73.

5) R.J.H.Voorboeve and J.C.M.Stuiver, J.Catal., 23, 288, 243 (1971).

6) A.L.Farragher and P.Cosses, "Proc. 5th Int. Congr. Catal." (J.W.Hightower Ed.) 1973, p1301.

7) F.E.Massoth, Adv.Catal., 27, 265 (1978).

8) V.H.J.de Beer and G.C.A.Schuit "Preparation of Catalysts" (B.Delmon, P.A.Jacobs, and G.Poncelet, Eds.) Elsevier, Amsrerdam, 1976, p343.

9) P.Ratnasamy and S.Sivasanker, Catal.Rev.-Sci.Eng., 22, 401 (1980).

10) P.Grange, Catal.Rev.Sci.Eng., 21, 135, (1980).

11) P.C.H.Mitchell, "Catalysis" (C.Kemball and D.A.Dowden, Eds.) Specialist Periodic Report, Royal Society of Chemistry, London, vol.4, 175 (1980).

12) H.Topsøe and B.S.Clausen, Catal.Rev.-Sci.Eng., 26, 395 (1984).

13) H.Topsøe, B.S.Clausen, R.Candia, C.Wievel, and S.Mørup, J.Catal., 68, 433 (1981).

14) C.Wivel, R.Candia, B.S.Clausen, S.Mørup, and H.Topsøe, J.Catal., 68, 453 (1981).

15) Nan-Yu Topsøe and H.Topsøe, J.Catal., 84, 386 (1983).

16) B.S.Clausen, H.Topsøe, R.Candia, J.Villdsen, B.Lengeler, J.Als-Nielsen, and F.Christenen, J.Phys.Chem., 85, 3868, (1981).

17) R.Candia, B.S.Clausen, J.Bartholdy, Nan-Yu Topsøe, B.Lengeler, and H.Topsøe, "Proc. 8th Int. Congr. Catal." Verlag Chemie, Weinheim, 1984 vol.2 p375.

18) R.D.Huntley, T.J.Parham, R.P.Merrill, and M.J.Sienlco, Inorg.Chem., 22, 4144 (1983).

19) a) Y.Okamoto, H.Tomioka, Y.Katoh, T.Imanaka, and S.Teranishi, J.Phys.Chem., 84, 1833 (1980).

b) Y.Okamoto, H.Tomioka, T.Imanaka, and S.Teranishi, J.Catal., 66, 93, (1980).

20) a) Y.Okamoto, T.Imanaka, and S.Teranishi, J.Phys.Chem., 85, 3798 (1981).

b) H.Topsøe, B.S.Clausen, N.Burriesci, R.Candia, and S.Mørup, "Proc. Preparation of Catalysts II" (B.Delmon, P.A.Jacobs, and G.Poncelet, Eds.) Elsevier, Amsterdam, 1979, p479.

c) J.C.Dushet, E.M.van Oers, V.H.J.de Beer, and R.Prins, J.Catal., 80, 386 (1983).

d) G.MuraliDhar, F.E.Massoth, and J.Shabtai, J.Catal., 85, 44 (1984).

e) F.E.Massoth, G.Muralidhar, and J.Shabtai, J.Catal., 85, 53 (1984).

21) W.S.Millman and W.K.Hall, J.Phys.Chem., 83, 427 (1979).

22) J.Valyon and W.K.Hall, J.Catal., 84, 216 (1983).

23) J.B.Peri, Amer.Chem.Soc.Div.Petrol.Chem.Prepr., 23, 1281 (1978).

24) Nan-Yu Topsøe and H.Topsøe, J.Catal., 75, 354 (1982).

25) Y.Okamoto, Y.Katoh, Y.Mori, T.Imanaka, and S.Teranishi, J.Catal., 70, 445 (1981).

26) K.Segawa and W.K.Hall, J.Catal., 77, 221 (1982).

27) W.S.Millman and W.K.Hall, J.Catal., 59, 311 (1979).

28) S.J.Tauster, T.A.Pecoraro, and R.R.Chianelli, J.Catal., 63, 515 (1980).

29) S.J.Tauster and L.J.Riley, J.Catal., 67, 250 (1981); 70, 230 (1981).

30) B.S.Parekh and S.W.Weller, J.Catal., 47, 100 (1977); 55, 58 (1978).

31) C.H.Lui, L.Yuan, and S.W.Weller, J.Catal., 61, 282 (1980); 66, 65 (1980).

32) J.L.G.Fierro, S.Mendioroz, J.A.Pajares, and S.W.Weller, J.Catal., 65, 263 (1980).

33) M.I.Zaki, B.Vielhaber, and H.Knözinger, J.Phys.Chem., 90, 3176 (1986).

34) E.Delgado, G.A.Fuentes, C.Hermann, and H.Knözinger, Bull.Soc.Chim.Berg., 93, 735 (1984).

35) K.Segawa and W.K.Hall, J.Catal., 94, 133 (1982).

36) W.Suarez, J.A.Dumesic, and C.G.Hill, J.Catal., 94, 408 (1985).

37) Y.Murakami, "Preparation of Catalysts" (G.Poncelet, P.Grange and P.A.Jacobs, Eds) Elsevier, Amsterdam, 1983, vol.3 p775.

38) Y.Okamoto, M.Oh-Hara, A.Maezawa, T.Imanaka, and S.Teranishi, J.Phys.Chem., 90, 2396 (1986).

39) a) D.S.Zingg, L.E.Makovsky, R.E.Tischer, F.R.Brown, and D.M.Hercules, J.Phys.Chem., 84, 2898 (1980).
b) C.P.Li and D.M.Hercules, J.Phys.Chem., 88, 456 (1984).

40) C.P.Chang and G.L.Schrader, J.Catal., 60, 276 (1979).

41) F.R.Brown, L.E.Makovsky, and K.H.Rhee, J.Catal., 50, 162 (1977).

42) H.Jeziorowski and H.Knözinger, J.Phys.Chem., 83, 1166 (1979).

43) G.L.Schrader and C.P.Chang, J.Catal., 80, 369 (1983).

44) H.C.Yao and W.G.Rothschild, "Proc. 4th Int. Conf. Chemistry and Uses of Molybdenum" (H.F.Barry and P.C.H.Mitchell, Eds.) 1982, p31.

45) K.Segawa, D.S.Kim, and Y.Kurusu, "Proc. 8th Japan-USSR Catalysis Seminar" Tokyo, Japan, 1986, p131.

46) K.Tanaka and T.Okuhara, Catal.Rev.-Sci.Eng., 15, 249 (1977).

Chapter 3

Physicochemical Characterization of ZnO/Al_2O_3 and $ZnO-MoO_3/Al_2O_3$ catalysts

Abstract

The interaction modes of ZnO with Al_2O_3 and MoO_3/Al_2O_3 catalysts were investigated as a function of ZnO content (1-30 wt% with respect to Al_2O_3) and calcination temperature (673-1073 K) by using XPS, AES, and other physicochemical techniques. Particular attention was paid to the depth distribution of zinc ions in the surface layer of Al_2O_3 by using the $Zn\text{-}LMM/Zn2p_{3/2}$ intensity ratio coupled with Ar^+-sputtering techniques. Zinc ions are highly dispersed forming a "surface spinel" irrespective of the calcination temperature in ZnO/Al_2O_3 catalysts having low ZnO content (<10-15 wt%). With the ZnO/Al_2O_3 catalysts containing 1-2 wt% ZnO, it has been found that zinc ions are retained in the surface layer of the Al_2O_3 even when calcined at 1073 K. As for $ZnO/MoO_3/Al_2O_3$ catalysts, an enhanced segregation of zinc ions in a surface layer of Al_2O_3 was detected, suggesting the interactions with pre-existing molybdates on Al_2O_3, while no appreciable effects of ZnO on the distribution and reduction behavior of the molybdenum species were observed.

Introduction

Molybdena-alumina catalysts promoted by CoO are widely used as industrial hydrodesulfurization (HDS) catalysts. Addition of a small amount of a second promoter, such as ZnO, NiO, and MgO, is often claimed in patents to improve the HDS activity, selectivity, and stability of $CoO-MoO_3/Al_2O_3$ catalysts [1]. However, only a few fundamental investigations have been made to reveal the beneficial effects of the second promoter on the HDS catalysts [2-6]. It is considered that the second promoter modifies the interaction modes among molybdenum, cobalt, and Al_2O_3. Better understanding of such beneficial effects of the second promoter would be provided by revealing interaction modes between the second promoter such as ZnO and Al_2O_3.

The interaction between ZnO and Al_2O_3 receives little attention in spite of significant additive effects of ZnO in HDS catalysts [1] as well as the promoting effect of Al_2O_3 in $Cu-ZnO-Al_2O_3$ methanol synthesis catalysts [7-9], where $ZnO-Al_2O_3$ interaction would play important roles. Surface spectroscopic study of $ZnO-Al_2O_3$ systems is considered to be particularly required. Moreover, such information is valuable also for systematic understandings of the first transition metal-Al_2O_3 interaction modes.

XPS study of $ZnO-Al_2O_3$ system was undertaken by Vinek et al. [10] in connection with the acid and base strength and their catalytic properties. Recently, more detailed characterization

of ZnO/Al_2O_3 catalysts as a function of calcination temperature and loading level of ZnO was carried out by Strohmeier and Hercules [11], by using surface spectroscopic techniques. It has been found that at low ZnO loadings, an "aluminate type" phase (i.e. "surface spinel") is preferentially formed and that at higher loadings, bulk like ZnO segregates on the surface [11]. The latter fact was confirmed by the reactivity of Zn^{2+} towards H_2S or SO_2 [11].

In the present study, ZnO/Al_2O_3 and $ZnO-MoO_3/Al_2O_3$ catalysts were characterized by using X-ray photoelectron spectroscopy (XPS), Auger electron spectroscopy (AES), diffuse reflectance spectroscopy (DRS), X-ray diffraction (XRD), and temperature programmed reduction (TPR) techniques in order to obtain the information on the interaction modes of ZnO with Al_2O_3 and MoO_3/Al_2O_3 catalysts as a function of the loading level of ZnO and calcination temperature. Particularly, the depth distribution of the Zn^{2+} ions in Al_2O_3 was assessed by using an XPS-AES intensity analysis coupled with a sputtering technique. The interaction modes of ZnO with molybdates on Al_2O_3 were compared with those of CoO.

Experimental

Catalyst Preparation

Supported zinc oxide catalysts were prepared by a single or double dry impregnation method using γ-Al_2O_3 as a support,

which was provided by Catalysis Society of Japan as a reference catalyst (JRC-ALO-4) [12,13]. The BET surface area of the support was 163 $m^2\ g^{-1}$. The loading level of ZnO was adjusted to be 1 to 30 wt% with respect to the support.

ZnO/Al_2O_3 : An aqueous solution of the appropriate concentration of zinc nitrate (Wako Pure Chemicals Co.) was added to the Al_2O_3 (1.2 mL g-$Al_2O_3^{-1}$) and kneaded for 20 min at room temperature. Subsequently, the catalyst slurry was dried at 383 K for 18 h, followed by calcination in air at 823 K for 5 h.

$ZnO/MoO_3/Al_2O_3$: An aqueous solution of ammonium heptamolybdate (Nakarai Chemicals Co.) corresponding to 15 wt% MoO_3 with respect to the support was added to the Al_2O_3. The catalyst was dried at 383 K for 18 h and calcined at 823 K for 5 h to provide a MoO_3/Al_2O_3 catalyst. Subsequently, an aqueous solution of the appropriate concentration of zinc nitrate was added to the MoO_3/Al_2O_3 catalyst. The catalyst was dried at 383 K for 18 h, followed by a second calcination at 823 K for 5 h. $MoO_3/ZnO/Al_2O_3$ catalysts containing 15 wt% MoO_3 were also prepared as $ZnO/MoO_3/Al_2O_3$ catalysts with an inversed impregnation order of ZnO and MoO_3.

XRD Measurement

X-ray diffraction patterns of the catalysts were obtained at room temperature with a Shimazu VD-1 diffractometer using Cu $K\alpha_{1,2}$ radiation (0.154 nm) with a Ni filter. The diffraction patterns were compared with those in the ASTM powder diffraction

files for identification.

DRS Measurement

Diffuse reflectance spectra of the ZnO/Al_2O_3 catalysts were obtained with a Hitachi 200-20 spectrophotometer at room temperature in air. The measurements were made in the wavelength range of 450 to 200 nm. The spectra were referenced to an Al_2O_3 plate.

XPS and AES Measurements

XPS and AES spectra of the catalysts were obtained with a Hitachi 507 photoelectron spectrometer using Al $K\alpha_{1,2}$ radiation (1486.6 eV). The anode was operated at 9 kV and 50 mA. The catalyst sample was mounted on a sample holder made of copper metal using double-sided adhesive tape. The intensity ratios were determined by using the integrated areas of the Al2p, Mo3d, $Zn2p_{3/2}$, and Zn $L_3M_{4,5}M_{4,5}$ Auger spectra assuming linear back grounds. In sputtering experiments by using Ar^+ ions (pressure of Ar = 6.7 $x10^{-4}$ Pa, accelerating voltage; 1 kV), XPS spectra of the catalysts were obtained with a Shimazu ESCA 750 photoelectron spectrometer (Mg $K\alpha_{1,2}$ radiation; 1253.6 eV, 8 kV, 12 mA). The ZnO/Al_2O_3 catalyst was pressed into a thin plate (ca. 20 mg cm^{-2}) and mounted on a stainless steel sample holder by using electrically conductive paist.

TPR Measurement

The catalyst sample was reduced in a stream of a H_2/Ar mixture (5/95) at a constant flow rate by using an apparatus described elesewhere [14]. It was essentially identical with that reported by Cvetanovic and Amenomiya for a temperature programmed desorption study [15]. The reduction temperature was increased from room temperature to 823 K with a uniform heating rate of 5 K min^{-1}.

Results and Discussion

Bulk structures of the ZnO/Al_2O_3 catalysts were examined by XRD. The XRD spectra show only broad peaks attributable to γ-Al_2O_3 at a low loading level of ZnO (<10 wt%) irrespective of the calcination temperature (673-1073 K). With the catalyst calcined at 673 K, a set of weak XRD peaks due to ZnO was detectable at 15 wt% ZnO and increased in the intensities with increasing ZnO content. For the catalysts calcined at 823 K, the ZnO peaks were detected above 20 wt% ZnO. The average crystallite size of ZnO calculated from the XRD line broadening at 2θ=34.5° (ZnO(002)) by using a Scherrer equation (K = 0.9) was approximately 25 nm independent of the calcination temperature (673-823 K) and the loading level of ZnO (>20 wt%).

As regards the catalysts calcined at 1073 K, no peaks due to ZnO were observed in the XRD spectra up to the loading level of 30 wt% ZnO in contrast to the catalysts calcined at the lower

temperatures. Both γ-Al_2O_3 and $ZnAl_2O_4$ have spinel structures, so their XRD patterns are very close each other. However, as the loading level of ZnO increased, the intensities of the lines assinged to $ZnAl_2O_4$ (31.5, 37.2, and 60.0°) became stronger with respect to the peak due to γ-Al_2O_3 at 46.0°. Moreover, weak peaks at ca. 49 and 56° characteristic of $ZnAl_2O_4$ were observed to intensify with ZnO content. These results indicate a preferential formation of $ZnAl_2O_4$ at 1073 K rather than the crystallization of γ-Al_2O_3 or formation of high temperature forms of Al_2O_3.

Representative diffuse reflectance spectra of the ZnO/Al_2O_3 catalysts are illustrated in Fig. 1. Crystalline ZnO showed a characteristic absorption edge at ca. 370 nm, which was not observed for Al_2O_3. The dependences of the absorbance at 370 nm on ZnO content are shown in Fig. 2 for the ZnO/Al_2O_3 catalysts. With the catalysts calcined at 673 and 823 K, the absorption intensities increased abruptly at 15 and 20 wt% ZnO, respectively. This is in good agreement with the XRD results. The absorption intensities for the catalysts calcined at 673 and 823 K, however, were much weaker than the intensity for the mixture of γ-Al_2O_3 and ZnO, as shown in Fig. 2. As for the catalysts calcined at 1073 K, no absorption band was detected at 370 nm even at 30 wt% ZnO. The DRS and XRD results lead us to conclude that when the ZnO/Al_2O_3 catalysts are calcined at 673-823 K, small amounts of bulk-like ZnO are formed on the Al_2O_3 at >15-20 wt% ZnO, while $ZnAl_2O_4$ is produced when calcined at 1073 K.

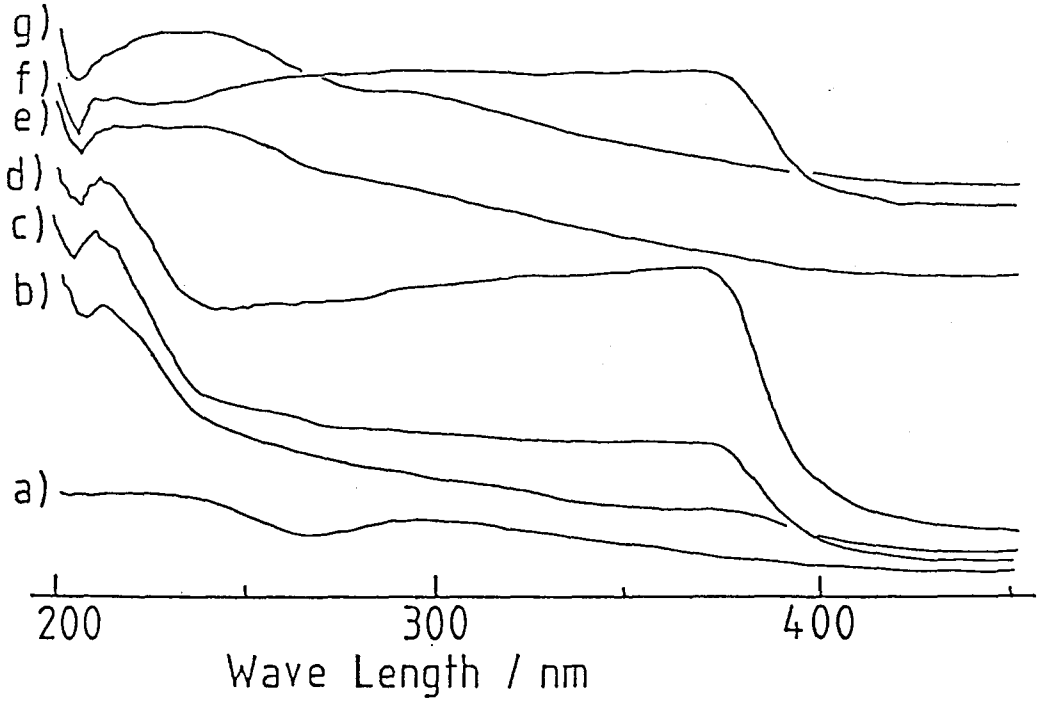

Fig. 1 Diffuse reflectance spectra of the ZnO/Al_2O_3 catalysts
a) γ-Al_2O_3; b) 673 K, 10 wt%; c) 673 K, 15 wt%
d) 673 K, 20 wt%; e) 823 K, 15 wt%
f) 823 K, 20 wt%; g) 1073 K, 20 wt%.

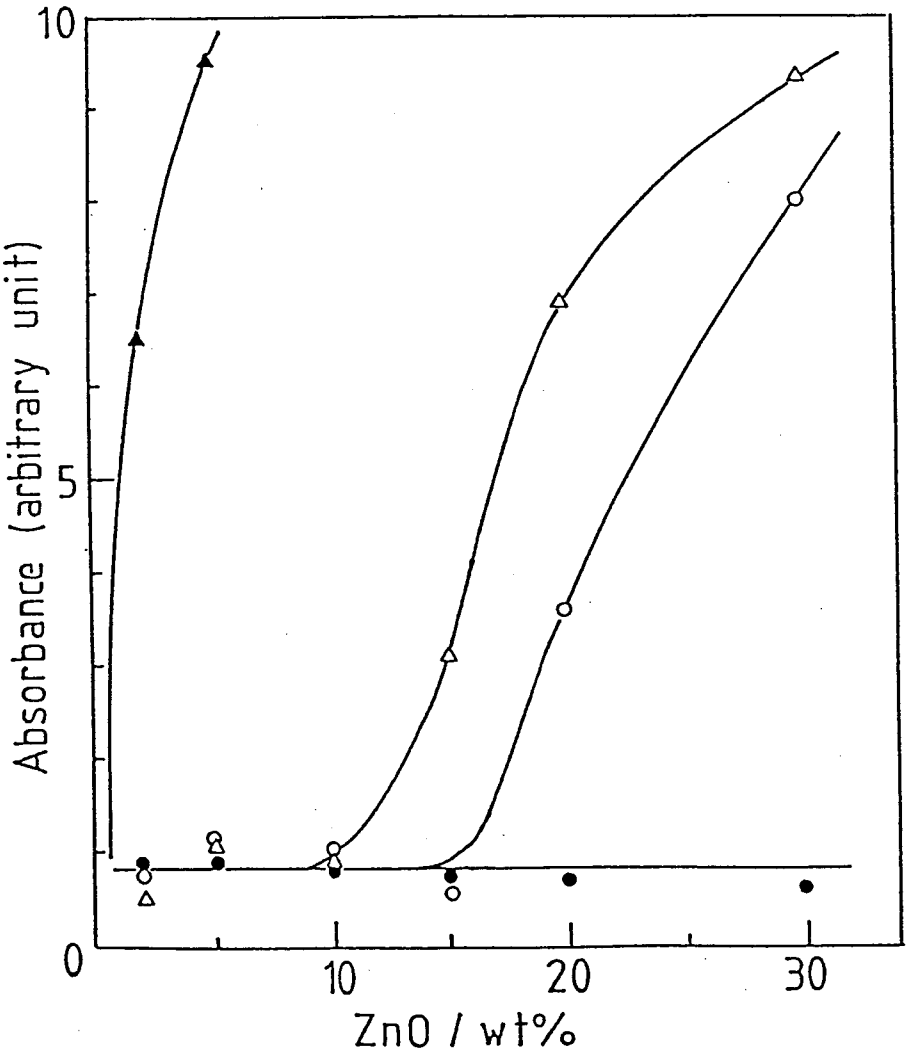

Fig. 2 Dependence of the absorbance at 370nm on ZnO content for ZnO/Al_2O_3 catalyst
calcination temperature; △:673 K, ○:823 K, ●:1073 K
physical mixture of ZnO and γ-Al_2O_3;▲

According to Strohmeier and Hercules [11], no crystalline ZnO was found by XRD for ZnO/Al_2O_3 catalysts containing less than 20 wt% Zn, which corresponds to 30 wt% ZnO with respect to Al_2O_3, although the calcination temperature was relatively low (673 and 600 K). The differences between their and present observations will be discussed below.

The chemical state of surface zinc species and the extent of distribution of zinc ions in the surface layer were examined by XPS and AES, coupled with Ar^+-sputtering techniques. The binding and kinetic energies were referenced to the Al2p level at 74.3 eV, which was originally determined by the C1s band at 285.0 eV due to adventitious carbon. The position of the bremmstrahlung Al KLL Auger level was invariant with the composition and calcination temperature and 1387.5 $\pm$ 0.2 eV. The XPS binding energy of the $Zn2p_{3/2}$ band and the AES kinetic energy of Zn $L_3M_{4,5}M_{4,5}$ level are listed in Table 1 for the ZnO/Al_2O_3 catalysts and reference compounds. The modified Auger parameter α' [16] was also evaluated; $\alpha' = KE_A+BE_p$, where KE_A and BE_p show the kinetic energy of Zn KLL Auger level and the binding energy of $Zn2p_{3/2}$ level, respectively. The chemical shift of the $Zn2p_{3/2}$ level between ZnO and $ZnAl_2O_4$ is 0.5 eV and considerably smaller than that of the Auger level (1.0 eV). The chemical shift in the Auger parameter is 0.5 eV between ZnO and $ZnAl_2O_4$. Similar results have been reported by Vinek et al. [10] and Strohmeier and Hercules [11]. Therefore, the Auger level was used to discriminate surface zinc species.

According to the results in Table 1, the LMM Auger kinetic energies are almost independent of both the loading level of ZnO and calcination temperature. They are close to the value for $ZnAl_2O_4$ rather than that for ZnO. This finding suggests the formation of a zinc "surface spinel", in which Zn^{2+} ions are incorporated into tetrahedral sites in a surface lattice of Al_2O_3 to form spinel-like structures. On the basis of their XPS-AES results, Strohmeier and Hercules [11] have reached the same conclusions. The DRS and XRD results showed the presence of small amount of ZnO in the catalyst calcined at 673-823 K and impregnated with >15-20 wt% ZnO. This might be suggested by slightly higher Auger kinetic energies for these catalysts. However, the XPS intensity analysis supports evidently the results of XRD and DRS as shown below.

In order to obtain information on the dispersion degree of Zn^{2+} ions, the $Zn2p_{3/2}$/Al2p XPS intensity ratios are plotted as a function of ZnO content in Fig. 3. With the catalysts calcined at 673 K, the $Zn2p_{3/2}$/Al2p ratio increased in proportion to ZnO content up to 20 wt%. Above 20 wt% ZnO, the slope of the $Zn2p_{3/2}$/Al2p ratio decreased and leveled off. As for the ZnO/Al_2O_3 catalyst calcined at 823 K, a similar linear dependency of the XPS intensity ratio on ZnO content was observed except for an additional change in the slope at 2 wt% ZnO. The change in the slope at a small loading level of ZnO was also observed for the catalyst calcined at 1073 K as shown in Fig. 3. The XPS intensity ratio decreased obviously with increasing the calcination

Table 1. XPS binding and AES Kinetic Energies[a] (eV) of $Zn2p_{3/2}$ and $L_3M_{4,5}L_{4,5}$ levels for ZnO/Al_2O_3 catalysts

ZnO /wt%	Calcination Temperature / K					
	673		823		1073	
	ZnLMM	$Zn2p_{3/2}$	ZnLMM	$Zn2p_{3/2}$	ZnLMM	$Zn2p_{3/2}$
1	987.5	1021.8	987.8	1021.7	987.8	1021.0
2	987.5	1021.8	987.6	1021.8	987.6	1021.8
3	987.3	1021.9	978.7	1021.7	987.4	1021.7
5	987.6	1021.7	987.6	1021.9	987.8	1021.7
10	987.8	1021.7	987.6	1021.9	987.4	1021.8
15	987.7	1021.6	987.6	1021.9	987.5	1022.1
20	987.7	1021.4	987.9	1021.8	987.5	1022.1
30	987.8	1021.4	987.8	1021.7	987.4	1021.7
Zn[b]	981.8	1021.6				
ZnO[b]	988.3	1021.7				
$ZnAl_2O_4$[c]	987.3	1022.2				

a) All values are referenced to Al2p=74.3eV

b) Referenced to C1s=285.0eV

c) Reported by Stromeier and Hercules [11] corrected for the present reference, Al2p=74.3eV

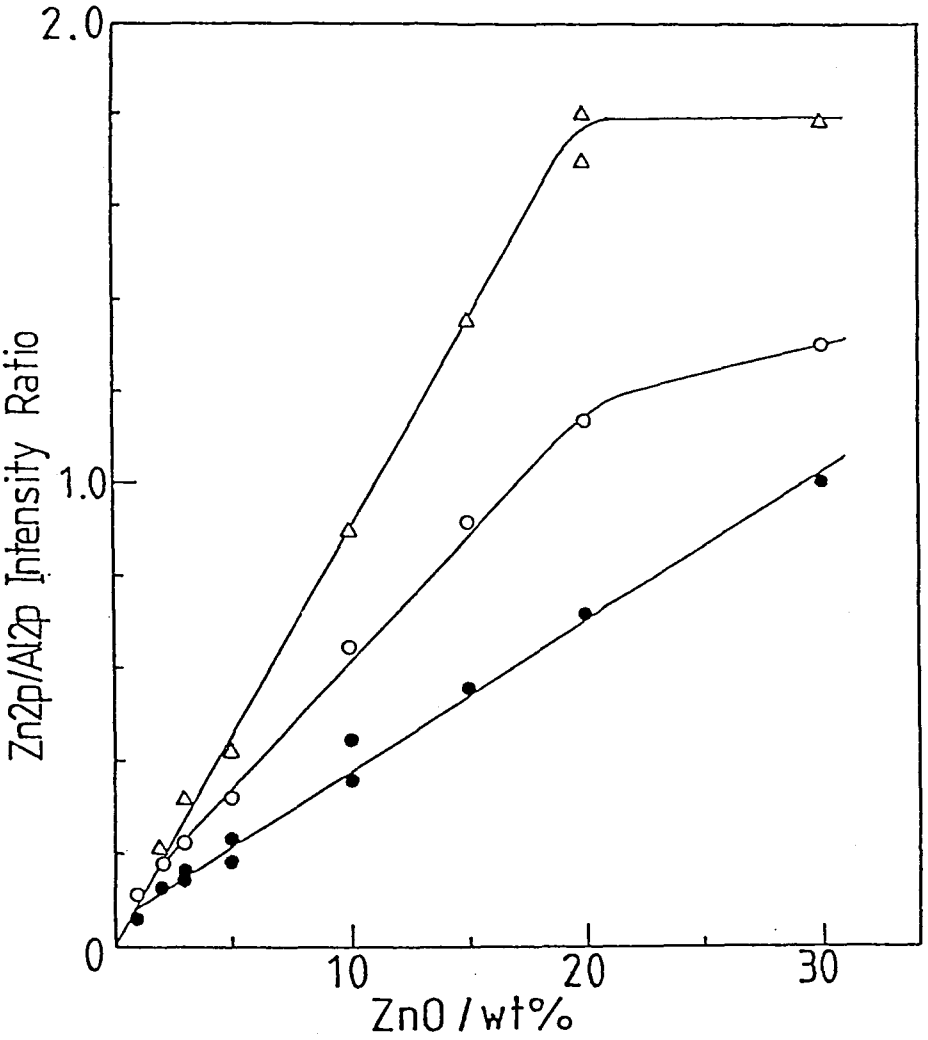

Fig. 3 $Zn2p_{3/2}$/Al2p XPS intensity ratio as a function of ZnO content for ZnO/Al_2O_3 catalyst calcination temperature; △:673 K, ○:823 K, ●:1073 K.

temperature except for the catalysts with 1-2 wt% ZnO.

The linear correlation in Fig. 3 for the ZnO/Al_2O_3 catalysts calcined at 673 K and containing < 20 wt% ZnO, indicates a high dispersion of zinc species over the Al_2O_3 surface [17-19]. The decreasing slopes at higher calcination temperatures are concluded to show an increasing extent of diffusion of zinc ions into a subsurface layer of Al_2O_3, taking into account the results from the XRD and DRS measurements. It is considered that the reductions in the slope of the intensity ratio at >20 wt% ZnO for the catalysts calcined at 673 or 823 K are attributable to a degradation of the dispersion degree of zinc ions [17-19], suggesting a formation of bulk like oxide phases. These conclusions are consistent with the XRD and DRS observations.

It is noteworthy, however, that up to the ZnO loading levels of 1 and 2 wt%, the $Zn2p_{3/2}$/Al2p intensity ratios for the catalysts calcined at 1073 or 823 K are identical with the ratios for the catalysts calcined at 673 K as shown in Fig. 3. It is conjectured that in the catalysts with such low ZnO content zinc ions are highly dispersed on the surface layer of the Al_2O_3 forming a "surface spinel" irrespective of the calcination temperature. The ZnO content of 1-2 wt% corresponds to $5\text{-}9\times10^{13}$ Zn^{2+} ions cm^{-2}. This is just the number of surface vacant cation sites, ca. 8×10^{13} cm^{-2}, expected for the (110) face of Al_2O_3 [20]. The thermal stability of the "surface spinel" observed here may be brought about by a significant decrease of surface free energy in the formation of the "surface spinel" from

ZnO and Al_2O_3 (cf. 90 and 650-925 erg cm^{-2} for ZnO and Al_2O_3, respectively [21]), thus suppressing the diffusion of zinc ions into a subsurface lattice of Al_2O_3.

The depth distribution of zinc ions was estimated by using the intensity ratio of the Zn $L_3M_{4,5}M_{4,5}$ Auger level to $Zn2p_{3/2}$ band, since these Auger- and photo-electrons have significantly different kinetic energies. It is well established that the escape depths of photo- and Auger-electrons depend mainly on their kinetic energies irrespective of an excitation method [22-24]. The kinetic energies of Zn Auger (LMM) and Zn2p bands are ca. 990 and 460 eV, so their escape depths are estimated to be ca. 1.4 and 0.8 nm, respectivety [24]. Accordingly, provided the Zn-LMM/Zn2p intensity ratio observed is smaller than that for a compound with a homogeneous depth distribution of zinc ions, e.g. ZnO, the concentration of zinc ions would become lower with increasing the depth (surface segregation of zinc ions) and vice versa. The surface structures of various Urushibara-Ni catalysts have been discussed on the basis of the Zn-LMM/$Zn2p_{3/2}$ intensity ratios [25].

The Zn-LMM/$Zn2p_{3/2}$ intensity ratio for the ZnO/Al_2O_3 catalysts are shown in Fig. 4. Regardless of the calcination temperature (673-1073 K), the Zn-LMM/$Zn2p_{3/2}$ ratios are remarkably smaller at 1-2 wt% ZnO than that for ZnO. This substantiates a strong surface segregation of zinc ions and therefore the suppressed diffusivity of zinc ions into the bulk, forming a very thin, probably, monomolecular "surface spinel".

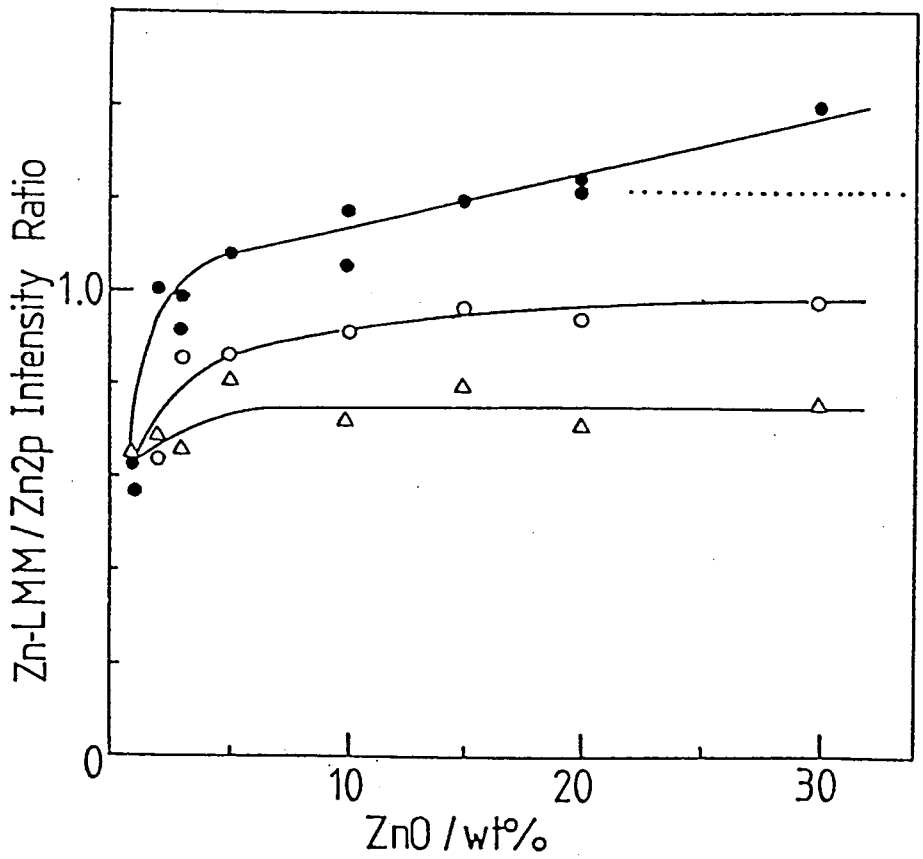

Fig. 4 Zn-LMM/$Zn2p_{3/2}$ intensity ratio as a function of ZnO content for ZnO/Al_2O_3 catalyst calcination temperature; △:673 K, ○:823 K, ●:1073 K. The intensity ratio for bulk ZnO is indicated by the dotted line.

The ratio greatly increased up to the loading level of 5 wt% ZnO and then became invariant or gradually increased, depending on the calcination temperature. A considerably low Zn-LMM/$Zn2p_{3/2}$ ratio for the ZnO/Al_2O_3 catalyst calcined at 673 K indicates the presence of a thin layer of the "surface spinel". Slightly increased values for the 823 K-calcined catalysts suggest a greater diffusion of zinc ions into an alumina subsurface. With the catalysts calcined at 1073 K, a much more extensive diffusion of zinc ions into a subsurface lattice of the Al_2O_3 is suggested at > 3 wt% ZnO by the Zn-LMM/$Zn2p_{3/2}$ ratios that are relatively high and even close to that for ZnO. Above 20 wt% ZnO, the ratio exceeds the value for ZnO, implying a higher concentration of zinc ions in a subsurface layer than that in a surface layer.

The depth profile suggested by the Zn-LMM/$Zn2p_{3/2}$ intensity ratio was confirmed by Ar^+-sputtering techniques. Several results for the representative ZnO/Al_2O_3 catalysts are shown in Fig. 5. The rate of sputtering depends on the number and energy of Ar^+ ions. However, it was very difficult to control the ion-current under the constant accelerating voltage of Ar^+ ions due to an insulating nature of the samples examined here. It should be noted, therefore, that the sputtering rate depends on the sample and that the depth profiles in Fig. 5 are semiquantitative.

With the catalysts calcined at 673 and 823 K, the $Zn2p_{3/2}$/Al2p XPS intensity ratios decreased, as the Ar^+-sputtering time increased. These findings suggest a higher concentration of Zn^{2+} in a thin surface layer than in a deeper

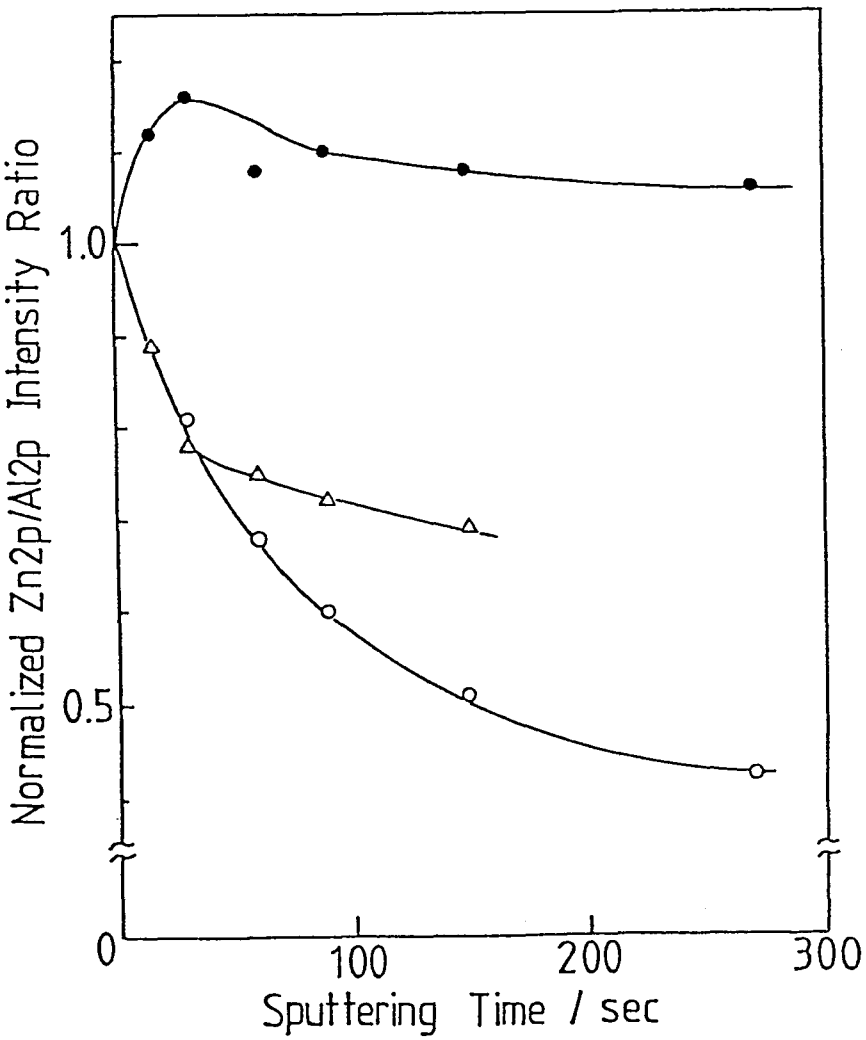

Fig. 5 Normalized $Zn2p_{3/2}$/Al2p intensity ratio vs. Ar^+-sputtering time

△ :15 wt%, 673 K, ○:20 wt%, 823 K

● :15 wt%, 1073 K.

subsurface layer. This is completely consistent with the conclusions drawn from the Zn-LMM/$Zn2p_{3/2}$ ratio. As for the catalysts calcined at 1073 K and containing 20 wt% ZnO, the $Zn2p_{3/2}$/Al2p intensity ratio showed a maximum for the sputtering time. This indicates that zinc ions exist more in the subsurface Al_2O_3 lattice rather than in the Al_2O_3 surface as suggested by the Zn-LMM/$Zn2p_{3/2}$ intensity analysis. Therefore, the depth profiles estimated by the Zn-LMM/$Zn2p_{3/2}$ intensity ratio are substantiated by the Ar^+-sputtering technique.

Significantly different XPS results have been reported by Stromeier and Hercules [11] for ZnO/Al_2O_3 catalysts calcined at 673 or 600 K in spite of major agreements. In contrast to the present saturation in the $Zn2p_{3/2}$/Al2p XPS intensity ratio at > 20 wt% ZnO (Fig. 3), an abrupt increase in the ratio was reported at > 20 wt% Zn (>30 wt% ZnO with respect to Al_2O_3). Additionally, no inflexion in the $Zn2p_{3/2}$/Al2p ratio at 1-2 wt% ZnO was observed by Stromeier and Hercules [11].

On the basis of the present results, it is concluded that in addition to the "surface spinel" a small amount of bulk-like oxide appears at >20 wt% ZnO, forming large islands of ZnO (ca. 25 nm by XRD). However, rather homogeneous overlayers of ZnO are considered to be formed on the ZnO/Al_2O_3 catalysts prepared by Stromeier and Hercules at >30 wt% ZnO, probably because of a better dispersion of zinc ions. These models are consistent with the XRD observations that bulk like ZnO appears at lower ZnO content in the present study than in their catalysts. With the

catalysts containing 1-2 wt% ZnO the present XPS-AES results suggest a suppressed diffusion of zinc ions into a subsurface of Al_2O_3. On the contrary, Stromeier and Hercules [11] indicated the absence of zinc ions on a top-most surface of the ZnO/Al_2O_3 catalysts by using ISS.

These differences in the $ZnO-Al_2O_3$ interaction modes may be resulted from the preparation method (wet [11] vs. dry impregnation), morphology (pore volume and diameter, particle size) and/or surface acid and base properties of the Al_2O_3 supports employed [26]. Impurity levels of Al_2O_3 would also affect the distribution and dispersion degrees of zinc ions in the Al_2O_3 surface as in CoO and NiO/Al_2O_3 systems [27]. With a homologue system, CoO/Al_2O_3, considerable differences have been similarly observed among workers [28-31]. More detailed investigations would be required to search the dominating factors determining the interaction modes between the first-transion metal oxide and Al_2O_3 surface.

The interaction of ZnO with the MoO_3/Al_2O_3 catalyst was examined in connection with that between CoO and MoO_3 supported on Al_2O_3. The interactions between CoO and MoO_3/Al_2O_3 are claimed to make CoO much more significantly dispersed over MoO_3/Al_2O_3 catalysts than Al_2O_3 [28,29]. The $MoO_3/ZnO/Al_2O_3$ and $ZnO/MoO_3/Al_2O_3$ catalysts showed the identical binding and kinetic energies of the $Zn2p_{3/2}$ and Zn $L_3M_{4.5}M_{4,5}$ levels with those for the ZnO/Al_2O_3 catalysts within the accuracy ($\pm$ 0.2 eV). The $Mo3d_{5/2}$ binding energy was 232.8 eV.

When MoO_3 is supported on the ZnO/Al_2O_3 catalysts, the intensity ratios of the $Zn2p_{3/2}$/Al2p and Zn-LMM/$Zn2p_{3/2}$ were not alterd in spite of the second calcination at 823 K, indicating no change in the dispersion and depth distribution of zinc ions. On the other hand, when ZnO was added to the MoO_3/Al_2O_3 catalyst containing 15 wt% MoO_3, the $Zn2p_{3/2}$/Al2p ratio became considerably larger than that for the ZnO/Al_2O_3 catalyst at >2 wt% ZnO, while no appreciable change in the Zn-LMM/$Zn2p_{3/2}$ ratio was detected as shown in Fig. 6. The addition of MoO_3 induced no XRD peaks due to ZnO. As discussed above, the reduced $Zn2p_{3/2}$/Al2p XPS intensity ratio for the ZnO/Al_2O_3 (823 K) catalysts at >2 wt% ZnO is ascribable to the diffusion of zinc ions into the subsurface layer of Al_2O_3 on the basis of the XPS-AES analysis and Ar^+ sputtering technique. Consequently, the increase in the $Zn2p_{3/2}$/Al2p intensity ratio is considered to be attributed to an enhanced segregation of zinc ions in a surface layer of Al_2O_3 by the interactions between zinc ions and molybdate phases attached to the alumina surface. It is suggested that a considerable amount of Zn^{2+} ions is present between well dispersed molybdate layer and Al_2O_3 surface. The Zn-LMM/$Zn2p_{3/2}$ ratio may be compensated by the segregation of Zn^{2+} ions in an Al_2O_3 surface layer and by the overlayer of molybdate phase.

With $CoO/MoO_3/Al_2O_3$ catalysts, similar interactions between CoO and MoO_3/Al_2O_3 are proposed [30-32]. ISS revealed the incorporation of Ni^{2+} within molybdate phases for $NiO/MoO_3/Al_2O_3$ catalysts at the expense of Ni^{2+} in Al_2O_3 subsurface [33]. The

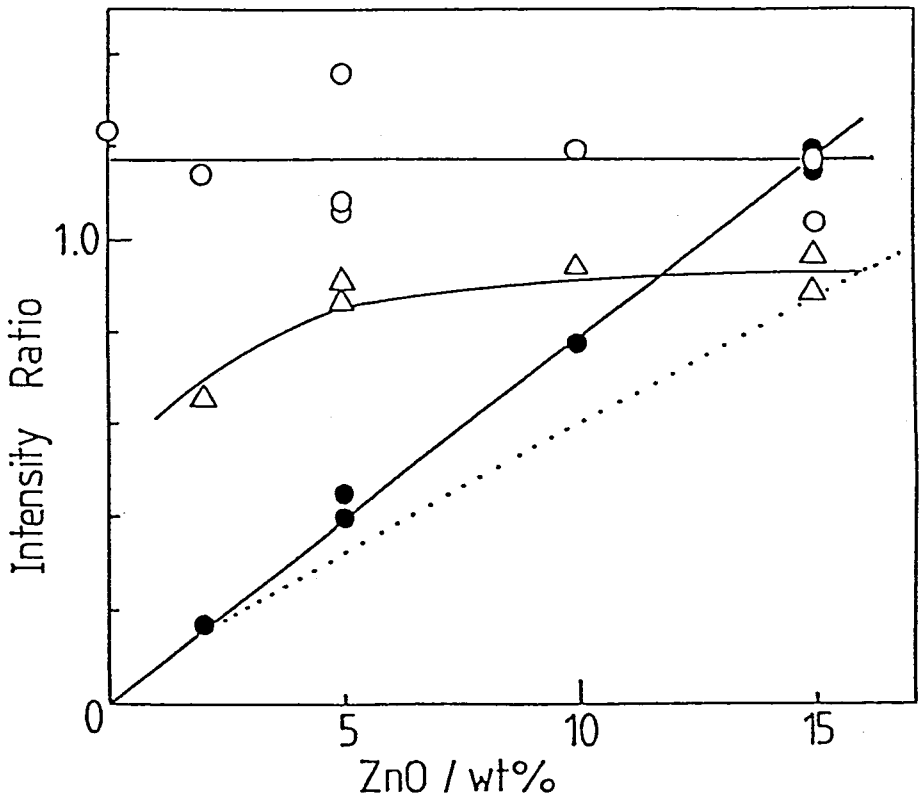

Fig. 6 Intensity ratio as a function of ZnO content for $ZnO/MoO_3/Al_2O_3$ catalyst
O:Mo3d/Al2p, ●:$Zn2p_{3/2}$/Al2p,
△:Zn-LMM/$Zn2p_{3/2}$.

present study suggests that a series of first transition metal, Co^{2+}, Ni^{2+}, and Zn^{2+}, shows analogous interactions with pre-existing molybdate phases on Al_2O_3.

The Mo3d/Al2p intensity ratios for the $ZnO-MoO_3/Al_2O_3$ catalysts are identical to that for the MoO_3/Al_2O_3 catalyst. In addition, the TPR spectra for the $ZnO/MoO_3/Al_2O_3$ and $MoO_3/ZnO/Al_2O_3$ catalysts were very close to that for the MoO_3/Al_2O_3 catalyst in the reduction temperature and amount of H_2 consumed. The XPS and AES measurements of the reduced $ZnO-MoO_3/Al_2O_3$ catalysts showed exclusively the reduction of molybdenum. These findings indicate that the doping of ZnO has no appreciable influence on the dispersion degree and reduction behavior of molybdenum species.

From the above facts, it is suggested that ZnO added to $CoO-MoO_3/Al_2O_3$ catalysts as a second promoter would modify the distribution of cobalt species rather than that of molybdenum species. In fact, Chin and Hercules [34] have reported that for the CoO/Al_2O_3 catalysts at low CoO content (<8 wt%), the addition of ZnO enhances the formation of tetrahedral cobalt species (i.e. a cobalt "surface spinel"). Similar results have been obtained from the TPR studies of CoO/Al_2O_3 catalysts [35]. The distribution of Ni^{2+} ions are also strongly affected by the addition of ZnO into NiO/γ-and η-Al_2O_3 [36].

References

1) "Molybdena Catalyst Bibliography", Climax Molybdenum Company of Michigan, No. 1-8, 1964-1981.

2) C.L.Kibby and H.E.Swift, J.Catal., 45, 231 (1976).

3) J.F.Patzer, W.L.Kehl, and H.E.Swift, J.Catal., 62,211 (1980).

4) N.P.Martinez and P.C.H.Mitchell, "Proceeding of the Climax Third International Conference on the Chemistry and Uses of Molybdenum" H.F.Barry and P.C.H.Mitchell, Eds., Climax Molybdenum Company, Ann Arbor, Michigan, (1979) p.105.

5) F.J.Gil Llambias, J.L.G.Fierro, J.M.D.Tascon, and A.Lopez Agudo, "Proceeding of the Climax Fourth International Conference on the Chemistry and Uses of Molybdenum" H.F.Barry and P.C.H.Mitchell, Eds., Climax Molybdenum Company, Ann Arbor, Michigan, (1982) p.361.

6) J.G.L.Fierro, A.Lopez Agudo, P.Grange, and B.Delmon, "Proceedings of the 8th International Congress on Catalysis", Berlin, (1984) 2, p.363.

7) R.G.Herman, G.W.Simmons, and K.Klier, "Proceedings of the 7th International Congress on Catalysis", T.Seiyama and K.Tanabe, Eds., Kodansha, Tokyo, (1981) p.475.

8) G.Petrini and F.Garbassi, J.Catal.,90, 133 (1984).

9) K.Shimomura, K.Ogawa, M.Oba, and Y.Kotera, J.Catal.,52, 191, (1978).

10) H.Vinek, H.Noller, M.Ebel, and K.Schwarz, J.Chem.Soc.,Faraday Trans. 1, 73, 734 (1977).

11) B.R.Stromeier and D.M.Hercules, J.Catal., 86, 266 (1984).

12) Y.Murakami, "Preparation of Catalysts, III", G.Poncelet, P.Grange, and P.A.Jacobs, Eds., Elsevier, Amsterdam, (1983) p.775.

13) Y.Okamoto, M.Oh-hara, A.Maezawa, T.Imanaka, and S.Teranishi, J.Phys.Chem., 90, 2396 (1986)

14) Y.Okamoto, Y.Konishi, K.Fukino, T.Imanaka, and S.Teranishi, "Proceedings of the 8th International Congress on Catalysis", Berlin, 5, (1984) p.159.

15) R.J.Cvetanovic and Y.Amenomiya, Adv. Catal., 17, 103 (1967).

16) C.D.Wagner, L.H.Gale, and R.H.Raymond, Anal.Chem., 51, 466 (1979)

17) P.J.Angevine, W.N.Delgass, and J.C.Varturi, "Proceedings of the 6th International Congress on Catalysis", (1977) p.611.

18) F.P.J.M.Kerkhof and J.A.Moulijin, J.Phys.Chem., 83, 1612 (1979).

19) Y.Okamoto, H.Tomioka, Y.Katoh, T.Imanaka, and S.Teranishi, J.Phys.Chem., 84, 1833, (1980).

20) H.Knozinger and P.Ratnasamy, Catal.Rev.-Sci.Eng., 17, 31 (1978).

21) S.H.Overbury, P.A.Bertrand, and G.A.Somorjai, Chem.Rev., 75, 547 (1975).

22) T.A.Carlson, "Photoelectron and Auger Spectroscopy", Plenum, New York, (1975).

23) W.N.Delgass, G.L.Haller, R.Kellerman, and J.H.Lusford, "Spectroscopy in Heterogeneous Catalysis", Academic Press, New York, (1979) p.267.

24) C.R.Brundle, J.Vac.Sci.Techol., 11, 212 (1974).

25) Y.Okamoto, Y.Nitta, T.Imanaka, and S.Teranishi, J.Chem.Soc.,Faraday Trans. 1, 76, 998 (1980).

26) K.Foger, "Catalysis, Science and Technology", J.R.Anderson and M.Boudart, Eds., Springer-Verlag, New York, Vol.4,(1984) p.227.

27) a) M.Houalla, J.Lemaitre, and B.Delmon, J.Chem.Soc.,Faraday Trans. 1, 78, 1389 (1982), b) A.Lycourghiotis, C.Defosse, F.Delannay, J.Lemaitre, and B.Delmon, Ibid., 76, 1677 (1980), c) G.Muralidhar, F.E.Massoth, and J.Shabtai, J.Catal., 85, 44 (1984).

28) F.E.Massoth, Adv.Catal., 27, 265 (1978).

29) Y.Okamoto, T.Imanaka, and S.Teranishi, J.Catal, 65, 488 (1980).

30) R.L.Chin and D.M.Hercules, J.Phys.Chem., 86, 3079 (1982).

31) K.S.Chung and F.E.Massoth, J.Catal., 64, 320, 322 (1980).

32) C.Wivel, B.C.Clausen, R.candia, S.Mørup, and H.Topsøe, J.Catal., 87, 497 (1984).

33) H.Knozinger,H.Jeziorowski, and E.Taglauer, "Proceeding of the 7th International Congress on Catalysis", T.Seiyama and K.Tanabe, Eds., Kodansha, Tokyo, (1981) p.604.

34) R.L.Chin and D.M.Hercules, J.Catal., 74, 121 (1982).

35) A.Maezawa, T.Adachi, Y.Okamoto, and T.Imanaka, unpublished results.

36) A.Cimino, M.Lo Jacono, and M.Schiavello, J.Phys.Chem., 79, 243 (1975).

Part II

Preparation of
Highly Dispersed Molybdenum Sulfides

Chapter 4

Thermal Stabilities of Molybdenum Carbonyls Encaged in Zeolites

Abstract

Decompositions of $Mo(CO)_6$ and the resulting subcarbonyl species adsorbed on Y- and X-type zeolites were investigated utilizing IR, temperature programmed decomposition, and XPS techniques. It was found that the thermal stabilities of $Mo(CO)_6$ encapsulated in zeolite depended on the Si/Al ratio and cation involved (X < Y, H < Li < Na < K < Cs), while intermediate subcarbonyl species, $Mo(CO)_{3\ ads}$, showed a completely reversed thermal stability. The drastic difference in the stabilizing properties between zeolites is proposed to reside in a difference in the basic strength of zeolite framework oxygen. The structure of $Mo(CO)_{3\ ads}$ is proposed on the basis of the IR spectra. The XPS results suggest that the adsorbed $Mo(CO)_3$ species is decomposed to Mo-metal aggregates at 473 K.

Introduction

Transition-metal carbonyls supported on organic or inorganic matrices show prominent catalytic properties. Various types of

interaction modes between metal carbonyls and (surface) functional groups have been proposed and recently reviewed [1,2]. Among inorganic materials having high specific surface areas, zeolites would provide potential media for producing well-defined catalytically active metal species, because of their well characterized structures [3]. Low-valent molybdenum catalysts prepared from $Mo(CO)_6$ encapsulated in zeolites are involved in such systems. Interesting catalytic features of $Mo(CO)_6$ supported on decationized Y zeolites (HY) have been reported by Yashima et al.[4] for polymerization and hydrogenation of ethylene and metathesis of propylene. Their results suggest great potential for a precise control of catalytic reactions by employing zeolites as supporting matrices.

Infrared studies of adsorption and decomposition of $Mo(CO)_6$ on NaY and HY zeolites have been conducted by Gallezot et al. [5] and Howe et al. [6,7] to elucidate interaction modes between the carbonyls and the zeolites and to reveal intermediate subcarbonyl species. With NaY zeolite, it is suggested that $Mo(CO)_6$ is thermally decomposed to molybdenum metal [6,7] in contrast to $Mo(CO)_6$ encaged in HY zeolite [4-6], where Mo is shown to be oxidized by the reaction with surface hydroxyl groups in the zeolite. The subcarbonyl species $Mo(CO)_{4\ ads}$ has been suggested to be thermally stable in HY [5] and NaY [7] zeolites. On the other hand, $Mo(CO)_{3\ ads}$ has been proposed as a stable intermediate subcarbonyl species on Al_2O_3 [8-10] and ZnO [11]. The difference in the stable subcarbonyl species between these

matrices seems to be important to the understanding of the chemistry of anchoring metal carbonyls. Thermal properties of metal carbonyls adsorbed on supporting materials provide fundamental knowledge about the interaction modes between the carbonyls and the surface functional groups and about optimization of catalyst preparation.

In the present study, decompositions of $Mo(CO)_6$ and the resulting subcarbonyls encapsulated in alkali metal exchanged zeolites were investigated by utilizing IR, temperature programmed decomposition, and XPS as a function of zeolite compositional Si/Al ratio (NaY and NaX). It is found herein that decomposition temperatures of the carbonyl species depended strongly on the zeolite composition and cation involved.

Experimental

Two kinds of NaY zeolites having different compositions (Si/Al = 2.43; SK-40, Nikka Seiko Co. and = 2.78; JRC-Z-Y5.6, Catalysis Society of Japan [12]) and a NaX zeolite (Si/Al = 1.23; 13X, Gasukuro Kogyo Co.) were utilized in the present study. Molybdenum hexacarbonyl was supplied by Strem Chemicals and used as received. HY zeolite (Si/Al = 2.78) were supplied by Catalysis of Japan as reference catalysts (JRC-Z-HY5.6). The NaY zeolite (JRC-Z-Y5.6) was ion-exchanged with a series of alkali-metal cations to produce MY zeolites (M; Li, K, or Cs). The degree of ion-exchange is summarized in Table 1.

Table 1 Degree of Ion-exchange of Zeolite

Zeolite	Degree of ion exchange[a] / %
HY	91, 76
LiY	45
KY	51
CsY	58
KX	68
CsX	50

a) Obtained from the XPS intensity of the Na KLL Auger band.

Powdered zeolites were pressed into self-supporting wafers (thickness, ca. 10 mg cm^{-2}) for IR studies. The samples were pretreated in a vacuum (< 1 x 10^{-3} Pa) at 673 K for 1-2 h in an in situ IR cell. After having recorded a background spectrum, the zeolite wafers were exposed to $Mo(CO)_6$ vapor (ca. 8 Pa [13]) at room temperature (ca. 295 K) for a selected period. The IR spectra were recorded at room temperature in a transmittance mode on a Hitachi double beam spectrophotometer (EPI-G). The resolution was 2.5 cm^{-1} at wavenumber 3000 cm^{-1}.

In TPDE (temperature programmed decomposition) studies of $Mo(CO)_6$ encaged in zeolites, zeolite samples were used in powdered forms. After having been evacuated at 673 K for 1-2 h, the zeolites were exposed to $Mo(CO)_6$ vapor at room temperature for 12 h. The decomposition of $Mo(CO)_6$ adsorbed on the zeolites was conducted in a dynamic vacuum and evolved gases were continuously and repeatedly analyzed by a mass filter (ULVAC, MSQ-150A) over a mass range of m/e = 1-51 (1 cycle; 130 s). The decomposition temperature was increased at a rate of 1.8 K min^{-1} from room temperature to ca. 600 K. In the present zeolite systems CO (m/e = 12 and 28) was the only major desorption product, accompanying a negligible amount of H_2 (m/e = 2). No formation of CH_4 (m/e = 15) and CO_2 (m/e = 44) was detected during the decomposition of $Mo(CO)_6$/zeolites in vacuum.

The XP (X-ray photoelectron) spectra of the zeolites were measured at room temperature on a Hitachi 507 photoelectron spectrometer using an Al K_α radiation (1486.6 eV; 9 kV, 50 mA). The

zeolite samples were mounted on a double-sided adhesive tape and evacuated at room temperature in a pretreatment chamber (< 1 x 10^{-3} Pa) prior to the XPS measurements. The binding energies were referenced to the C 1s band at 285.0 eV due to adventitious carbon. $Mo(CO)_6$/NaY samples that were prepared and activated at elevated temperatures in a conventional vacuum line were transferred to the pretreatment chamber by using a nitrogen-filled glove box. In these samples, the binding energy of the Si2p level from the NaY zeolite predetermined above was utilized for establishing the charging correction.

Results and Discussion

The IR spectra of $Mo(CO)_6$ adsorbed on NaY (JRC-Z-Y5.6) are depicted in Fig. 1. It is evident that on room temperature-adsorption, the structure of $Mo(CO)_6$ is retained almost intact with some distortions in the symmetry of the molecule. The lowering of the molecular symmetry is evidenced by the appearance of the normally infrared inactive ν_1 bands around 2120 cm^{-1} (Fig. 1-b). The wavenumbers of the fundamental vibrations of $Mo(CO)_6$ encapsulated in the NaY and NaX zeolites were calculated from the various combination bands at 2500-1900 cm^{-1}. They are summarized in Table 2 and compared with the literature values [14-16] for $Mo(CO)_6$ in various phases. Our results are in excellent agreement with those calculated from the data reported by Yon-Sing and Howe [7] except for the additional ν_1 band at

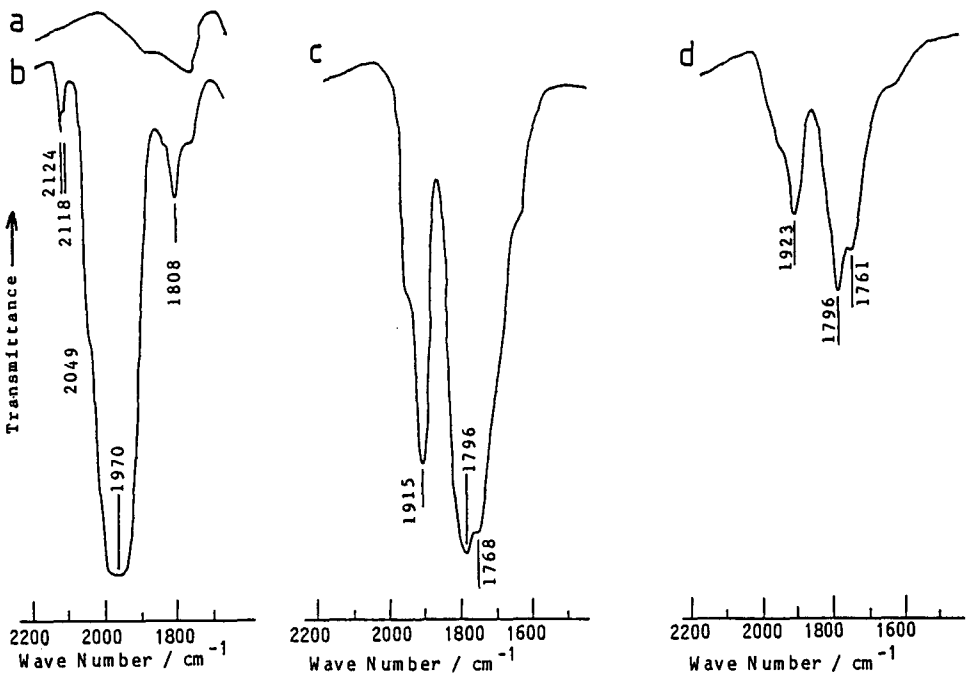

Figure 1 Infrared spectra of adsorption and decomposition of $Mo(CO)_6$ on NaY (JRC-Z-Y5.6) zeolite. a) background (evacuated at 673 K for 1 h), b) exposed to $Mo(CO)_6$ vapor for 1 min, followed by an evacuation for 10 min at room temperature, c) evacuated at 373 K for 20 min, and subsequently d) evacuated at 423 K for 20 min.

Table 2 Fundamental Frequencies of $Mo(CO)_6$ Encaged in NaY and NaX Zeolites

Approximate Mode	Normal[a]	Spectral Activity[a]	NaY		NaX	Vapor[c]	Solutions		Solid[a]
			this work	Howe[b]			$CHCl_3$[d]	CH_2Cl_2[a]	
ν_1	ν(CO)	R[e]	2123	2127-2123	2123	2124	2115	2117	2112
			2117				2110		
ν_2	ν(MC)	R	415	418		392			401
ν_3	ν(CO)	R	2016	2014		2027	2021	2019	2003
ν_4	ν(MC)	R				344		394	389
ν_5	δ(MCO)	IA				481			555
ν_6	ν(CO)	IR	1973	1975	1955	2004	1983		1990
ν_7	δ(MCO)	IR				593			593
ν_8	ν(MC)	IR	357	357		368			370
ν_9	δ(CMC)	IR	81	84		81			
ν_{10}	δ(MCO)	R				506		448	468
ν_{11}	δ(CMC)	R	110	109		81		91	100
ν_{12}	δ(MCO)	IA				512			478
ν_{13}	δ(CMC)	IA				62			

a) Reference 14 , b) Calculated from the data of reference 7, c) Reference 16
d) Reference 15 , e) R; Raman IR; Infrared, and IA; inactive

2117 ± 2 cm^{-1} in the present study. The fundamental frequencies of $Mo(CO)_6$ encaged in the NaY seem to be rather close to those for vapor or for solutions, implying weak adsorptive interaction of $Mo(CO)_6$ in the zeolite supercage.

Concerning the doubled ν_1 band in Fig. 1-b, equivalent pair peaks were also observed for SK-40 (SK-40). The spectral intensities of these two ν_1 bands were found to grow simultaneously with increasing adsorption of the carbonyl up to saturation. However, the 2117 cm^{-1} band seemed to be removed more easily on evacuation of sample at room temperature than the band at 2123 ± 2 cm^{-1}, resulting in the formation of subcarbonyl species (e. g. 1808 cm^{-1}). Accordingly, the double peak may suggest the existence of two kinds of $Mo(CO)_6$ with slightly different configurations as a result of different interaction modes with the zeolite framework. A similar double ν_1 peak has also been noted for $Mo(CO)_6$ dissolved in $CHCl_3$ [15] as quoted in Table 2. This was reconfirmed in the present study.

On evacuation at room temperature, three new bands appeared at 1835, 1808, and 1790 cm^{-1} as shown in Fig. 1-b and gradually grew with increasing evacuation time, accompanyed by a color change from white to light yellow. The yellow color may indicate the formation of $Mo(CO)_5$ species. These observations show a gradual decomposition of $Mo(CO)_6$ to produce subcarbonyls.

The IR spectrum changed drastically on evacuation at 373 K, showing the formation of a new fairly stable subcarbonyl species (Fig. 1-c). Some of this species remained anchored even at 423 K

(Fig. 1-d) and disappeared completely on further evacuation at 473 K. This subcarbonyl species is characterized by major absorption bands at 1915, 1796, and 1768 cm^{-1}. These spectral features for the NaY zeolite are quite consistent with the results reported by Howe and coworkers. [6,7].

In the present study, more detailed decomposition steps were investigated by increasing stepwise the evacuation temperature up to 370 K. Figure 2 depicts such IR spectra for SK-40 zeolite. NaY showed essentially the identical characteristics. However, it was recognized that SK-40 decomposed $Mo(CO)_6$ more readily at room temperature than NaY, resulting in stronger bands at 1835, 1810, and 1788 cm^{-1} in a similar treatment sequence (Fig. 1-b vs. 2-a). After a prolonged evacuation at room temperature, the 1789 cm^{-1} band became the most intensified (Fig. 2-b). At slightly elevated temperatures (313-318 K), several new bands appeared as shown in Fig. 2-c together with the intensified band around 1790 cm^{-1}. On further evacuation at 317-331 K (Fig. 2-d,e), the 2123 cm^{-1} band due to $Mo(CO)_6$ was completely removed and the 2045 and 1953 cm^{-1} signals were reduced in the intensity. However, the absorption bands at 2020 and 1918 cm^{-1} showed maximum intensity at 317-320 K (Fig. 2-d). At temperatures higher than 333 K (Fig. 2-f), the stable carbonyl species was observed as in the case of NaY zeolite (Fig. 1-c) which remained intact even after a prolonged evacuation at 383 K (Fig. 2-g). These decomposition steps were completely reversible with regard to evacuations and CO introduction. Treatment at 423 K in vacuo reduced appreciably the

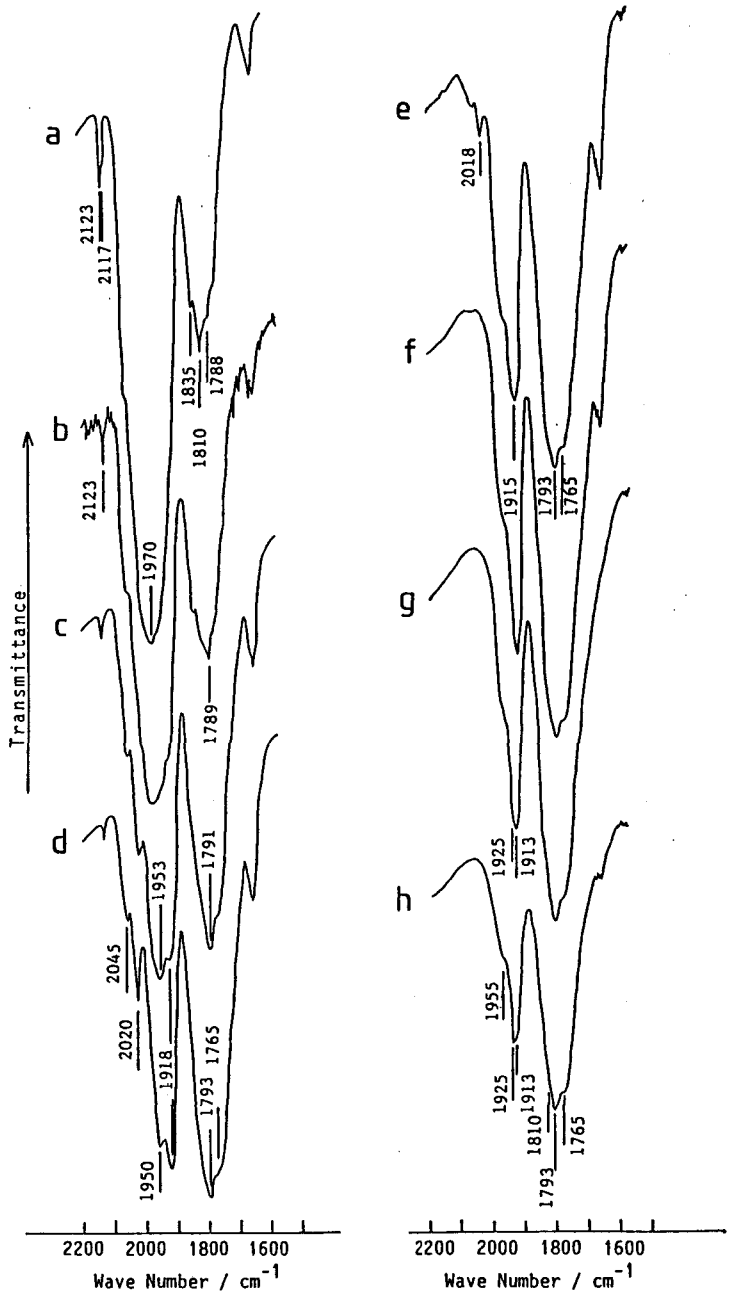

Figure 2 Infrared spectra of decomposition of $Mo(CO)_6$ adsorbed on NaY (SK-40) zeolite pre-evacuated at 673 K for 1 h. a) exposed to $Mo(CO)_6$ vapor for 30 s, followed by a 10 min-evacuation at 293 K, b) additional evacuation for 60 min at 295 K, c) evacuated at 313-318 K for 10 min, d) at 317-320 K for 10 min, e) at 322-331 K for 10 min, f) at 333-341 K for 20 min, g) at 383 K for 6.5 h, and h) at 415-423 K for 10 min, successively.

Table 3 CO Stretching Frequencies of Molybdenum Carbonyls Encaged in NaY and NaX Zeolites

Zeolite	Carbonyl Species	Ir Bands[a] observed (cm^{-1})	Assignments
NaY	$Mo(CO)_6$	2123,[w] 2117,[w] 2048,[sh] 1970,[vs]	$Mo(CO)_6$
	I	1810	$Mo_2(CO)_{10}$
	II	2046, 1953, 1835	$Mo(CO)_5$ ads
	III	2020, 1918, 1789	$Mo(CO)_4$ ads
	IV	1955,[sh] 1925,[sh] 1913,[s] 1810,[w,sh] 1793,[s] 1765[sh]	$Mo(CO)_3$ ads
NaX	$Mo(CO)_6$	2123,[w] 1955[s]	$Mo(CO)_6$
	II'	2047, 1828	$Mo(CO)_5$ ads
	III'	1910, 1782	$Mo(CO)_4$ ads
	IV'	1916,[s] 1896,[s] 1763[vs]	$Mo(CO)_3$ ads

a) Only resolved bands are shown here.
vs; very strong, s; strong, w; weak, and sh; shoulder peak

whole spectral intensity (Fig. 2-h), whereas thermal treatment at 450 K almost eliminated the carbonyl bands. The intensities of the bands at 1913 and 1925 cm^{-1} were reversed at 423 K. A similar observation was made with NaY (Fig. 1-c vs. 1-d). These findings imply that a few stabilized subcarbonyl species with slightly different configurations exist as a consequence of different adsorption sites in a supercage (e.g. S_{II} and S_{III}).

It is apparent from the IR studies that $Mo(CO)_6$ encaged in the NaY zeolite is decomposed to the stable subcarbonyl species through several intermediate subcarbonyls. On the basis of the spectral changes, subcarbonyl species I-IV are tentatively proposed and summarized in Table 3. It seems that $Mo(CO)_6$ is thermally decomposed stepwise from I and/or II through IV. Comparing NaY and SK-40 zeolites, it is revealed that the thermal stabilities of $Mo(CO)_6$ and intermediate subcarbonyl species (I -III) are greater in NaY (Si/Al = 2.78) than in SK-40 (2.43), while the stability of species IV is entirely reversed in these NaY zeolites.

The oxidation state of molybdenum species in the NaY zeolite was examined utilizing XPS. Figure 3 shows the XP spectra of the Mo3d level for the $Mo(CO)_6$/NaY evacuated at elevated temperatures (A) and subsequently exposed to air at room temperature for controlled periods (B). The binding energies of the Mo3d levels are summarized in Table 4 and compared with those for several molybdenum compounds relevant to this system [17,18]. The $Mo3d_{5/2}$ energies for the $Mo(CO)_6$/NaY activated at various

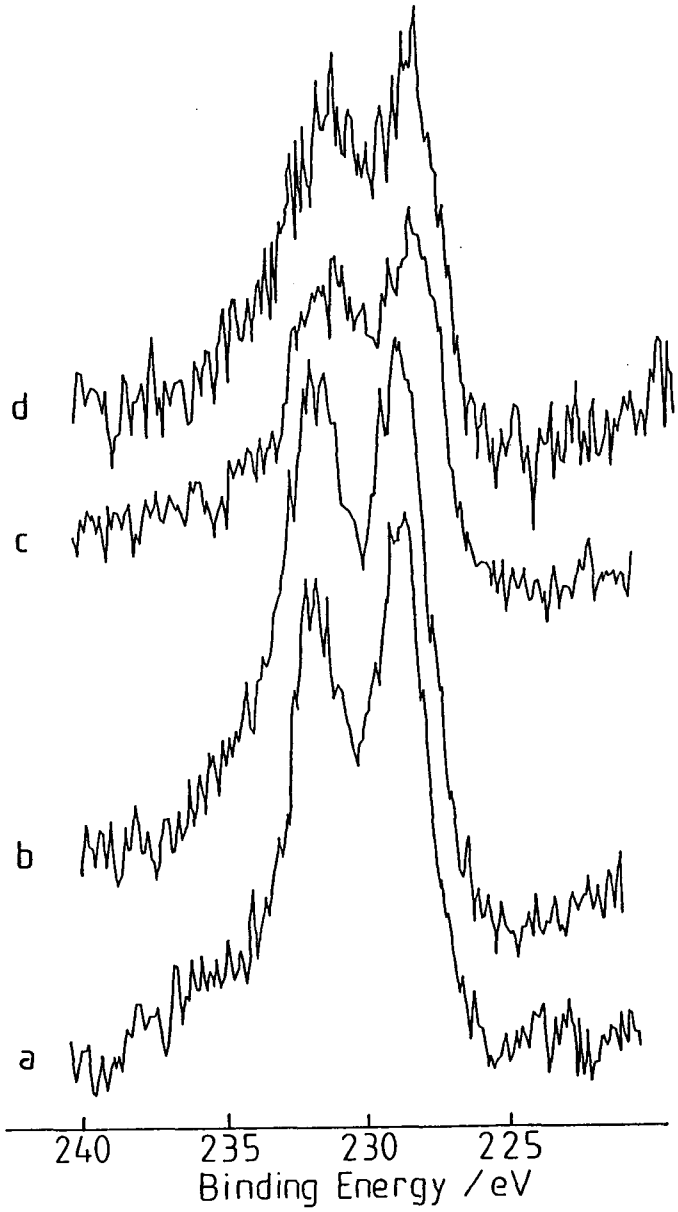

Figure 3-A X-Ray photoelectron spectra of $Mo(CO)_6$/NaY (JRC-Z-5.6) zeolite. a) $Mo(CO)_6$ adsorbed on NaY at room temperature, b) evacuated at 373 K for 20 min, c) evacuated at 473 K for 20 min, and d) evacuated up to 633 K in a temperature programmed decomposition experiment at a rate of 1.8 K min^{-1}.

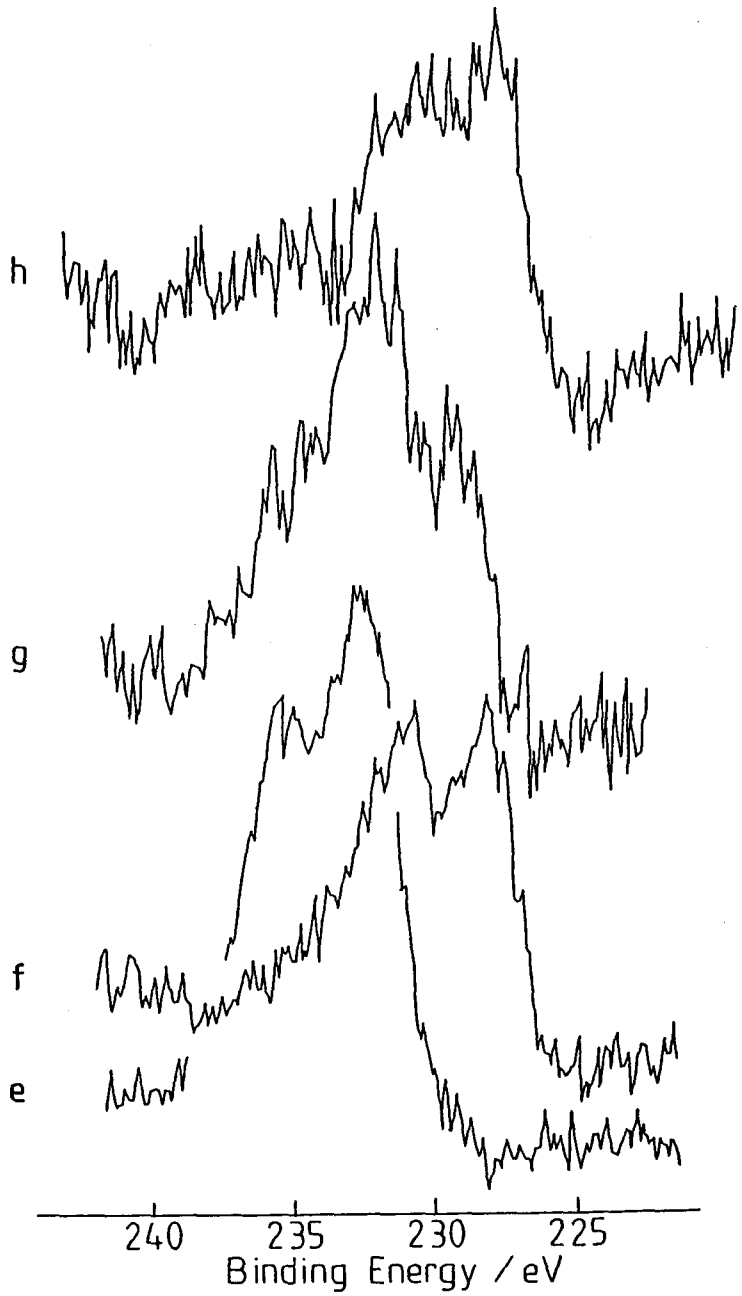

Figure 3-B X-Ray photoelectron spectra of $Mo(CO)_6$/NaY (JRC-Z-5.6) zeolite. e) exposure of sample-b to air for 50 s at room temperature, f) exposure of sample-c to air for 50 s, g) subsequent exposure of sample-f to air for 24 h, and h) exposure of sample-d to air for 130 s.

Table 4 X-Ray Photoelectron Spectroscopy Results on $Mo(CO)_6$/NaY Zeolite Treated at Elevated Temperatures in vacuo and Reference Compounds

Treatment Temperature (K)	Binding Energy (eV)[a] Mo $3d_{5/2}$	Mo $3d_{3/2}$	Reference
ca. 290	228.5	231.8	this work
373	228.6	231.6	
	233.0[b]	235.6[b]	
473	228.2	231.2	
	228.4[b]	231.1[b]	
	229.9, 232.6[c]		
633	228.4	231.0	
	228.4[d]	231.0[d]	
MoO_3	233.1		17[e]
Mo(V)	231.9		
MoO_2	229.9		
Mo metal	228.4		18[f]
$[(\eta^5\text{-}C_5H_5)Mo(CO)_3]_2$	227.8		
$Mo(\eta^5\text{-}C_5H_5)(CO)_3Cl$	229.2		
$(CH_3)_3SnMo(CO)_3(\eta^5\text{-}C_5H_5)$	228.9		
$Cl(CH_3)_2SnMo(CO)_3(\eta^5\text{-}C_5H_5)$	228.4		

a) Referenced to the Si 2p level at 102.5 eV.

b) Exposed to air at room tenperature for 50 s.

c) for 24 h.

d) for 135 s.

e) Referenced to C 1s = 285.0 ev.

f) The binding energies are shifted by +1.4 eV to adjust the Mo 3d binding energy for MoO_3 to that of reference 17.

conditions are very close to those for molybdenum metal and molybdenum carbonyl complexes within the accuracy of the XPS measurements (± 0.2 eV). Slightly broadened Mo3d spectra observed at high evacuation temperatures (> 470 K) are ascribable to the molybdenum species oxidized to some extent during the heat-treatments perhaps by adsorbed (residual) water. Accordingly, it is concluded that molybdenum is retained essentially in a zero-valent state during the thermal treatments of $Mo(CO)_6$ encaged in the NaY zeolites with formation of zero-valent subcarbonyl species at 370 K and final decomposition to molybdenum metal (> 470 K).

With the molybdenum/NaY zeolites, the reactivity of molybdenum species to air was examined by XPS. As depicted in Fig. 3-B, the molybdenum species (subcarbonyl IV in Table 3) produced by evacuation at 373 K was completely oxidized to Mo^{6+} species, when exposed to air at room temperature for 50 s. This was also inferred by the instantaneous color change from brown to white observed. On the other hand, the XP spectra for the Mo species activated at > 473 K were slightly broadened by relatively short oxidation-treatments (50 or 130 s) at room temperature, suggesting that only a small part of metallic species is oxidized to higher-valent species. A prolonged exposure to air produced high oxidation states of molybdenum; Mo^{4+} and Mo^{6+} as deduced from the XPS binding energies. These findings indicate that molybdenum metal aggregates are formed rather than atomically dispersed metal particles, even at 470 K. The aggregation of Mo-

metal is suggested to occur at 673 K from the pore volume measurements of $Mo(CO)_6$/NaY [7].

Figure 4 depicts the IR spectra of $Mo(CO)_6$ encapsulated in the NaX zeolite following progressive evacuation at ambient and elevated temperatures. In sharp contrast to the NaY zeolites, the NaX zeolite is shown to drastically decompose $Mo(CO)_6$ even at room temperature, producing stepwise several subcarbonyl species. Upon mere contact of $Mo(CO)_6$ with the NaX, the IR spectrum appeared to be quite different from that for $Mo(CO)_6$ adsorbed on the NaY (Fig. 4-b). The sample turned orange in color. The bands due to subcarbonyls prevailed over the signals attributable to $Mo(CO)_6$ (ν_1; 2123 and ν_6; 1955 cm^{-1} in Table 1). With increasing evacuation time (Fig. 4-c), the bands at 1782 cm^{-1} increased in intensity, while the signal intensities at 1828, 1910, and 2047 cm^{-1} decreased simultaneously, perhaps after initial slight enhancement. The appearance of a shoulder peak at 1763 cm^{-1} on a prolonged evacuation (100 min; Fig. 4-e) may explain the somewhat complicated behavior of the bands around 1910 cm^{-1}, since the 1763 cm^{-1} band accompanies two strong bands at 1916 and 1896 cm^{-1}, as shown in Fig. 4-f. No band due to subcarbonyl I (1810 cm^{-1}) in the NaY zeolites was detected with the NaX zeolite.

On evacuation at elevated temperatures, a stable subcarbonyl species, characterized by three bands, was formed (Fig. 4-f) and retained even at 473 K in spite of a slight decrease in the relative intensity of the 1896 cm^{-1} band (Fig. 4-g), as observed

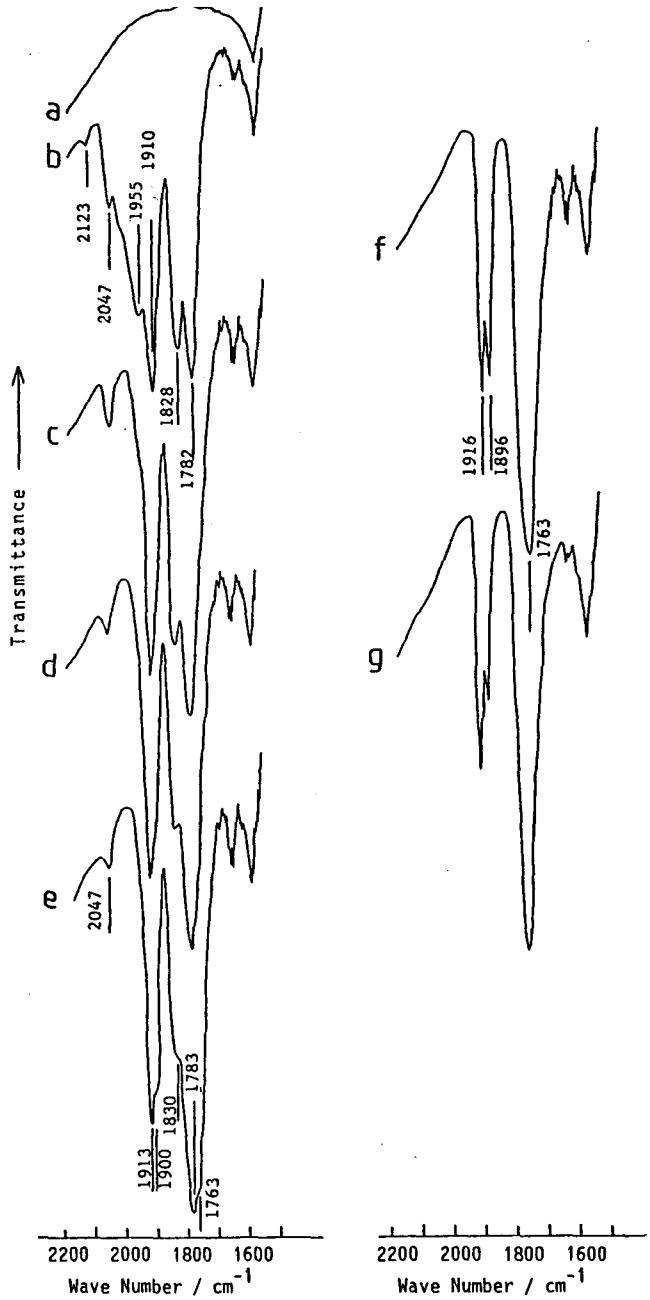

Figure 4 Infrared spectra of adsorption and decomposition of $Mo(CO)_6$ on NaX zeolite. a) background (evacuated at 673 K for 1 h), b) exposed to $Mo(CO)_6$ vapor for 1 min, followed by an evacuation for 10 min at room temperature, c) evacuated for 40 min, d) for 70 min, e) for 100 min at room temperature, f) for 20 min at 473 K, and g) for 20 min at 573 K.

with the corresponding absorption bands for the NaY zeolites (Fig. 1-d and 2-h). The carbonyl bands vanished at 573 K. Introduction of CO (3.3×10^3 Pa) at room temperature into the subcarbonyl/NaX system activated at 473 K readily restored the original spectrum. However, after the sample had been treated at 573 K under vacuum, no carbonyl absorption bands were restored on exposure of the sample to CO (3.5×10^3 Pa) at room temperature. These findings indicate that the decomposition of $Mo(CO)_6$ to the subcarbonyl species is reversible in the NaX zeolite, while the subcarbonyl species are irreversibly decomposed to molybdenum metal. Similar observations were made for the NaY zeolites.

The IR bands observed during the decomposition of $Mo(CO)_6$ in the NaX are tentatively attributed to the species II'-IV' in Table 3 on the basis of the spectral features on the thermal activations in Fig. 4. $Mo(CO)_6$ is decomposed stepwise to subcarbonyls II', III', IV', and finally to Mo metal. The subcarbonyl species (IV') encaged in the NaX zeolite is considerably more stable than the corresponding species IV in the NaY zeolites, whereas $Mo(CO)_6$ and the intermediate subcarbonyls show completely reversed thermal stabilities in these matrices.

TPDE experiments were conducted in a dynamic vacuum to confirm the aforementioned IR results. Figure 5 depicts the TPDE spectra for $Mo(CO)_6$ encapsulated in the Y-zeolites. It is clearly demonstrated that $Mo(CO)_6$ decomposes in two main steps in these zeolites. This decomposition feature substantiates the existence of thermally stable subcarbonyl species on the zeolites. In the

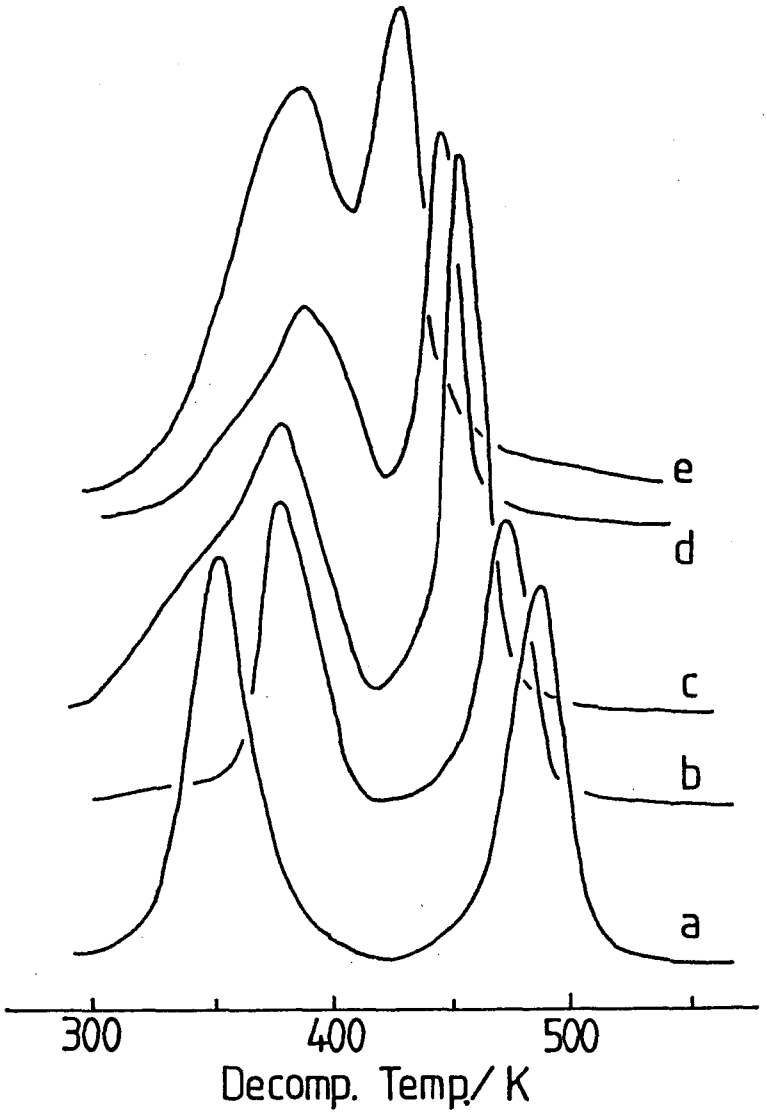

Figure 5 TPDE profiles of CO (m/e = 28) for $Mo(CO)_6$ encaged in the zeolites. a) CsY, b) KY, c) NaY, d) LiY and e) HY.

vapor phase, $Mo(CO)_6$ is known to decompose thermally to Mo-metal at 423 K [19]. Accordingly, it is evident that in the zeolite matrices the decomposition of $Mo(CO)_6$ is initiated at considerably lower temperature, whereas the final decomposition of the subcarbonyl species is markedly suppressed.

The decomposition temperatures T_L and T_H are summarized in Table 5. It is revealed that T_L and T_H depend both on the cation involved in the zeolite and on the Si/Al ratio. T_L decreases and, on the contrary, T_H increases with decreasing the Si/Al ratio and the electronegativity of the cation. Comparing these thermal stabilities of hexa- and sub-carbonyl species with those observed in the aforementioned IR results, it is concluded that the T_L peak corresponds to the formation of the subcarbonyl species IV and IV' by the successive decomposition of $Mo(CO)_6$ and intermediate subcarbonyls, whereas the T_H peaks arise from the thermal decomposition of species IV and IV' to Mo metal.

Figure 6 depicts T_L and T_H as a function of the O 1s BE of the zeolite. It is apparently demonstrated that the effects of the cation and composition of the zeolite upon the thermal decomposition behaviors of $Mo(CO)_6$ and the subcarbonyls are correlated to the O1s BE, that is, to the basic strength of the zeolite framework oxygen. At a higher O1s BE, T_L and T_H seem to merge into the decomposition temperature (410-420 K) of $Mo(CO)_6$ in a vapor phase [19]. Accordingly, it is concluded that the partial decomposition of $Mo(CO)_6$ to the subcarbonyl species is promoted by the basic nature of the framework oxygen, whereas the thermal

Table 5. XPS, TPDE, and IR results on $Mo(CO)_6$ encaged in a zeolite

Zeolite[a)]	O1s BE /eV	Decomposition Temperature/K T_L	T_H	Peak Intensity Ratio; T_L/T_H	ν(CO) Bands[b)] /cm^{-1}
HY (91)	532.6	396	430		A[c)]; 2048, 1965, 1820, 1670
HY (76)	532.5	386	427	1.23	B[c)]; 1927, 1793
LiY (45)	532.2	387	445	1.48	1924, 1796, 1760
NaY	532.0	378	454	1.37	1915, 1796, 1770
KY (51)	531.9	378	475	1.29	
SK-40	531.8	366	459	1.27	1913, 1793, 1765
CsY (58)	531.5	351	489	1.25	1912, 1756
NaX	531.1	308	508	1.00	1917, 1895, 1770
KX (68)	531.3	331	516	1.39	1913, 1783, 1734
CsX (50)	530.9	310	513	0.96	1905, 1775, 1744, 1725

a) Number in parentheses; the degree of ion-exchange estimated from the Na KLL X-ray-induced Auger intensity.

b) Main bands due to subcarbonyl species formed at 373 K.

c) Both A and B are observed for the H-type zeolites. Species C (2072, 2019, 1994 cm^{-1}) predominated at 423 K for HY (91) zeolite.

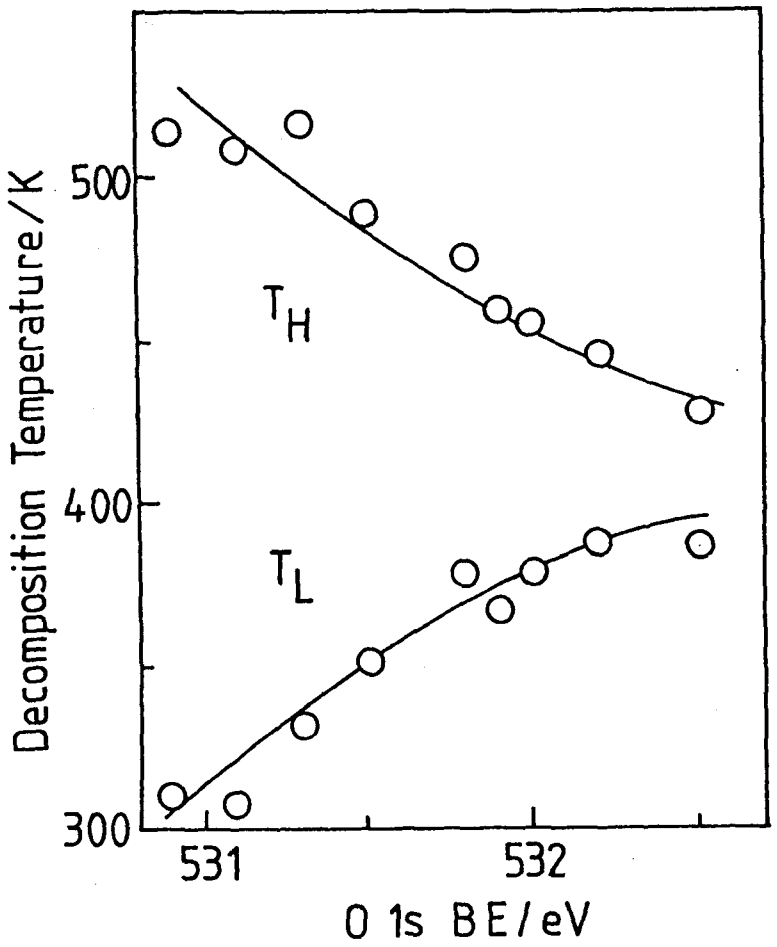

Figure 6 Dependencies of the decomposition temperatures T_L and T_H upon the O1s binding energy for the zeolite.

stability of the subcarbonyl species is enhanced also by the basic sites. It is conjectured that $OC\text{-}O^{2-}(Z)$ interactions induce the decompositions of $Mo(CO)_x$ species (x = 6-4). On the other hand, the subcarbonyl species, is stabilized by the framework oxygen through coordinations of oxygen lone pairs; $Mo \rightarrow O^{2-}(Z)$. The interactions of $OC\text{-}O^{2-}(L)$ is proposed for $Mo(CO)_6$ adsorbed on MgO on the basis of IR studies [22]. With $Mo(CO)_6/Al_2O_3$, the subcarbonyl species, $Mo(CO)_3$, is speculated to be adsorbed on a triad of oxygen anions constituting surface hydroxyl groups and/or lattice [9].

The stoichiometries, CO/Mo ratio, of subcarbonyl species IV and IV' can be estimated from the TPDE spectra. The amount of evolved CO is considered to be propotional to the spectral area. The peak area ratios of the T_L and T_H peaks were 1.5-0.9 for all zeolites (Table 5). These are close to unity. Furthermore, it is considered that the total peak area corresponds to the stoichiometry of CO/Mo = 6, since no formation of CH_4 and CO_2 were detected in the present systems. Therefore, it is concluded that the major subcarbonyl species stable at ca. 370 K are $Mo(CO)_{3\ ads}$ rather than $Mo(CO)_{4\ ads}$ [5,7] or $Mo(CO)_{2\ ads}$.

However, these TPDE procedures might involve some ambiguities for the determinations of an exact composition of the subcarbonyl species; some part of $Mo(CO)_6$ might be decomposed directly to molybdenum metal (NaY) [7,20] or to partially oxidized molybdenum species (HY) [4a,5,20] at T_L or T_H and/or undetected carbon containing products might be formed at the expense of CO.

$Mo(CO)_6$ and subcarbonyl species might sublime from the zeolite cage during the TPDE experiments. In order to remove these ambiguities in the above TPDE experiments, a ^{13}CO isotopic laveling technique was applied by utilizing a fact that the subcarbonyl species is reversibly converted to original $Mo(CO)_6$ at room temperature [5,7].

After evacuation at 373 K until no evolution of CO was detected, ^{13}CO (MSD, 99.3 %) was introduced stepwise to the subcarbonyl species in the zeolites at 300-330 K to reproduce $Mo(CO)_6$. The formation of $Mo(CO)_6$ was confirmed by a color change of the sample (from brown to white). After measurement of the amounts of ^{12}CO and ^{13}CO in the gas phase, TPDE profiles were obtained for ^{12}CO (m/e = 28 and 12) and ^{13}CO (29 and 13).

$$Mo(^{12}CO)_6 \xrightarrow[\Delta]{} Mo(^{12}CO)_x \xrightarrow{^{13}CO} Mo(^{12}CO)_x(^{13}CO)_{6-x}$$

Figure 7 shows the profiles thus obtained for the NaY zeolite. The $^{12}CO/^{13}CO$ ratio was invariant all over the decomposition and close to unity (1.1). Taking into consideration the amounts of ^{12}CO and ^{13}CO in the gas phase and the amount of adsorbed Mo, the composition of $Mo(CO)_{3.2}$ was obtained for the subcarbonyl species encapsulated in the NaY zeolite. Duplicated experiments confirmed the results. In the case of the HY zeolite, the stoichiometry of the stable subcarbonyl species was calculated to be $Mo(CO)_{2.9}$. These results unambiguously substantiate the stoichiometry of $Mo(CO)_3$ for the subcarbonyl species encapsulated in the NaY and HY zeolites. The existence of stable

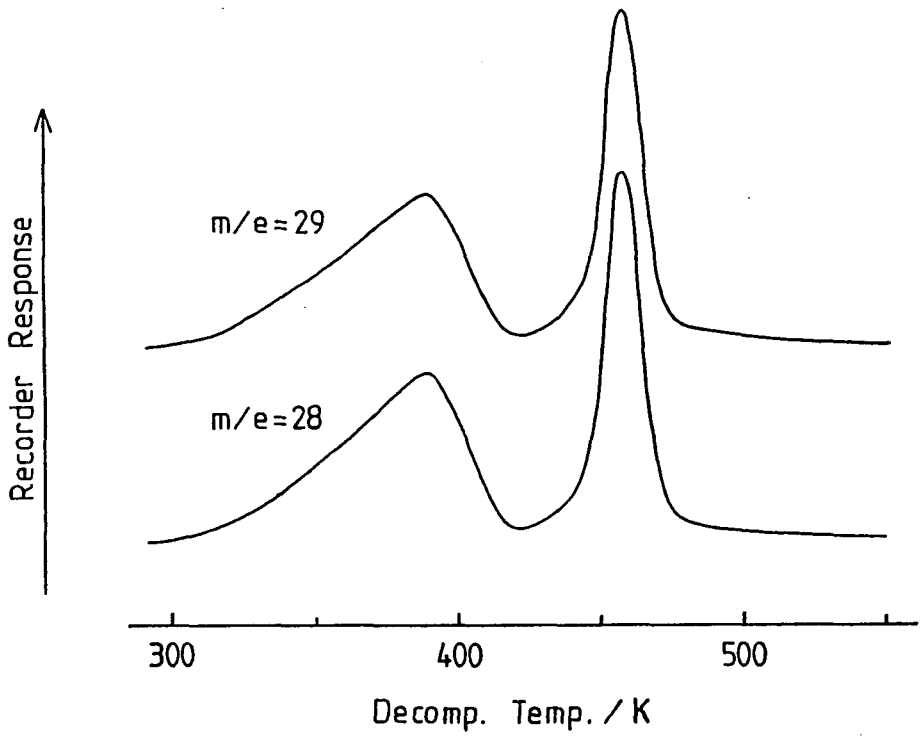

Figure 7 Temperature programmed decomposition profiles of ^{12}CO (m/e = 28) and ^{13}CO (29) for $Mo(CO)_6$ reproducted by a ^{13}CO introduction to the subcarbonyl species encaged in the NaY zeolite (JRC-Z-Y5.6) (0.6 $Mo(CO)_6$/supercage).

$Mo(CO)_{3\ ads}$ species has also been proposed for some oxide supports, Al_2O_3 [8-10] and ZnO [11], while Howe et al. [7] have claimed the formation of stable $Mo(CO)_{4\ ads}$ on NaY zeolite. The cause of the difference in the stoichiometry between the present and Howe's studies is not clear at present. However, the IR a spectra for species IV and IV', which have been regarded as evidence of $Mo(CO)_{4\ ads}$ [7], do not seem to be in conflict with the $Mo(CO)_{3\ ads}$ species as discussed below.

As shown in the IR studies, $Mo(CO)_6$ is decomposed stepwise to species IV or IV'. Taking into account the stoichiometries of the stable subcarbonyls, the subcarbonyl species differentiated by the IR bands are tentatively assigned in the Table 3. The proposed decomposition steps are given in Scheme 1. In the NaX zeolite, the IR peak assigned here to $Mo_2(CO)_{10}$ was not observed. This may be due to a higher reactivity of the NaX than the NaY zeolites toward the rather unstable species. The existence of stable intermediate species, such as $Mo(CO)_2$, was not suggested by the IR studies during the decomposition of $Mo(CO)_{3\ ads}$ to Mo-metal. This may also be evidenced by a sharpened TPDE peaks at T_H relative to the peaks at T_L. Further studies might be required for a decisive conclusion.

The IR spectrum due to the species IV in Fig. 1-c or 2-h-f consists of mainly three bands. $Mo(CO)_3$ compounds in C_{3v} symmetries should show only two bands, as observed in many organometallic compounds. However, when the structure of $Mo(CO)_3$ is distorted to a lower symmetry, more than two bands are antici-

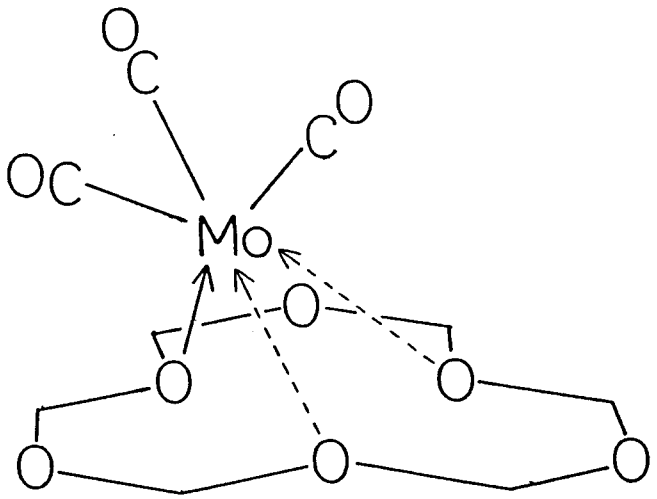

Figure 8 Proposed model for $Mo(CO)_{3\ ads}$ on NaY zeolites.

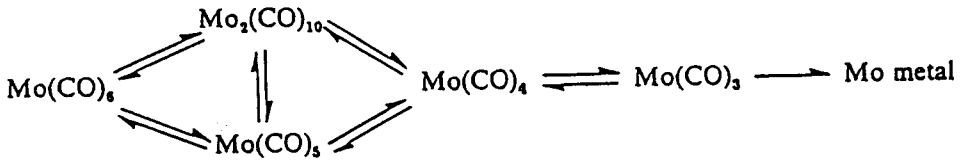

Scheme 1

pated. Very recently, Kirlin et al. [21] have reported the IR spectra of the surface species prepared from the reaction of $H_3Re_3(CO)_{12}$ with Al_2O_3 or MgO. Their spectral features are very close to those for species IV. They have assigned the surface species to $Re(CO)_3(O\text{-}M)(HO\text{-}M)_2$ (M = Mg or Al) on the basis of the IR, electron tunneling, and UV spectra. Therefore, it seems reasonable to assign the IR spectra of species IV to a $Mo(CO)_3$ moiety adsorbed on an oxygen triad with a significantly distorted octahedral symmetry. The structure is proposed in Fig. 8.

The $Mo(CO)_3$ moiety is considered to be greatly stabilized by forming three dative bonds with zeolite oxygens. From considerations analogous to those of Kirlin et al. [21], it is proposed that two Mo$\rightarrow$O bonds are weaker than the remaining one in NaY and the reversed structure in NaX. The coordinations of oxygen loan pair electrons to the $Mo(CO)_3$ moiety are readily broaken to restore Mo-CO bonds upon an exposure to CO. Stabilization of surface $M(CO)_x$ (M = metal) species by dative bonds from surface hydroxy groups and/or lattice oxygens are also proposed for $Mo(CO)_x$ on Al_2O_3 [9] and $Re(CO)_3$ on MgO and Al_2O_3 [21]. The other small shoulder peaks may suggest the presence of more than one $Mo(CO)_{3\ ads}$ species with slightly different structures (e. g. on Site II or Site III) and/or possible small perturbations of M(CO) by Na^+ cations (Lewis acid)-carbonyl interactions.

The contribution of basic sites to the carbonyl-zeolite interactions is reflected on the observed band positions in Table

5. The bands of the carbonyls in the zeolites are considerably red-shifted, compared with those of corresponding organometallic compounds as noted by Howe et al. [6,7]. This is interpretable in terms of the dative interactions with zeolite framework oxygen, resulting in the increased electron density on the molybdenum atom and subsequent red-shifts of the ν(CO) bands. In addition, the carbonyl species in the NaX zeolite always exhibit lower wavenumbers than the corresponding species in the NaY zeolites, as shown in Table 3. This is apparently due to a stronger electron donation of the NaX zeolite compared with the NaY zeolites. The stronger electron donation induces stronger Mo-C bonds, resulting in the higher thermal stability of $Mo(CO)_{3\ ads}$.

Conclusions

The decompositions of $Mo(CO)_6$ encapsulated in zeolites were investigated to examine the effect of zeolite composition using IR, temperature programmed decomposition, and XPS techniques. The salient findings and conclusions in this study are as follows.

i) $Mo(CO)_6$ is decomposed stepwise in a vacuum through intermediate carbonyl species into a thermally stable subcarbonyl species, $Mo(CO)_{3\ ads}$, and finally to molybdenum metal aggregates.

ii) The order of the thermal stabilities of $Mo(CO)_6$ and of the intermediate subcarbonyl species are Y-zeolite > X-zeolite and Cs > K > Na > Li > H, while the stability of $Mo(CO)_{3\ ads}$ is completely reversed among these zeolites.

iii) The marked differences in the thermal stabilities of the molybdenum carbonyl species among the NaX and NaY zeolites are understandable in terms of the difference in the basic strength of framework oxygen in the zeolite.

iv) The structure of $Mo(CO)_{3\ ads}$ is proposed on the basis of the IR and XPS spectra.

References

1) D.C.Bailey and S.H.Langer, Chem.Rev., 81, 109 (1981).

2) J.Phillips and J.A.Dumesic, Appl.Catal., 9, 1 (1984).

3) J.M.Thomas, "Chemistry and Physics of Solid Surfaces VI" (R.Vanselow and R.Howe, Eds.) Springer Verlag, Berlin, 1986, p107.

4) a) T.Yashima, T.Komatsu, and S.Namba, Chem.Express, 1, 701 (1986) and references therein.
b) T.Yashima, T.Komatsu, and S.Namba, Proc. Climax Fourth Intern. Conf. Chemistry and Uses of Molybdenum" (H.F.Barry and P.C.H.Mitchell, Eds.) Climax Molybdenum Comp. Ann Arbor, Michigan, 1982, p274.

5) P.Gallezot, G.Coudurier, M.Primet, and B.Imelik, "Molecular Sieves II" (J.R.Katzer, Ed.) ACS Symp. Ser. Vol.40, 1977, p144.

6) S.Abdo and R.F.Howe, J.Phys.Chem., 87, 1713 (1983).

7) Y.Yon-Sing and R.F.Howe, J.Chem.Soc.,Faraday Trans.1, 82, 2887 (1986).

8) A.Brenner and R.L.Burwell, J.Amer.Chem.Soc., 97, 2565 (1975).

9) A.Brenner and R.L.Burwell, J.Catal., 52, 353 (1978).

10) A.Kazusaka and R.F.Howe, J.Mol.Catal., 9, 183 (1980).

11) K.Tanaka, Y.Zhai, and K.Aomura, "Proc. Climax Intern. Conf. Chemistry and Uses of Molybdenum" (H.F.Barry and P.C.H.Mitchell, Eds.) Climax Molybdenum Comp. Ann Arbor,

Michigan, 1982, p278.

12) T.Hattori, H.Matsumoto, and Y.Murakami, Fourth Intern. Symp. Preparation of Heterogeneous Catalysts, Louvain-la-neuve, 1986.

13) R.R.Monchamp and F.A.Cotton, J.Chem.Soc., 1438 (1960).

14) R.L.Amster, R.B.Hannan, and M.C.Tobin, Spectrochim. Acta, 19, 1489 (1963).

15) L.H.Jones, J.Chem.Phys., 36, 2375 (1962).

16) L.H.Jones, Spectrochim. Acta, 19, 329 (1963).

17) Y.Okamoto, K.Oh-Hiraki, T.Imanaka, and S.Teranishi, J.Catal., 71, 99 (1981).

18) S.O.Grim and L.J.Matienzo, Inorg.Chem., 14, 1014 (1975).

19) E.M.Fednova and J.V.K.Krykova, Russ.J.Inorg.Chem., 11, 141 (1966).

20) T.Komatsu, S.Namba, T.Yashima, K.Domen, and T.Onishi, J.Mol.Catal., 33, 345, (1985).

21) P.S.Kirlin, F.A.DeThomas, J.W.Bailey, H.S.Gold, C.Dybowski, and B.C.Gates, J.Phys.Chem., 90, 4882 (1986).

22) E.Guglielminotti and A.Zecchina, J.Chim.Phys., 78, 891 (1981).

Chapter 5

Hydrogenation Activity of Molybdenum Subcarbonyl Species Encaged in Zeolites

Abstract

Molybdenum subcarbonyl species encaged in a zeolite, particularly in LiY, was found to show a high activity for the selective hydrogenation of 1,3-butadiene to cis-2-butene (> 96 %), this providing the first example of a hydrogenation activity of molybdenum subcarbonyl species immobilized on inorganic matrices.

Introduction

Molybdenum hexacarbonyl supported on inorganic matrices is a potential precursor to produce well-dispersed low valent molybdenum species [1]. Burwell et al. [2,3] have investigated various catalytic reactions over $Mo(CO)_6$ activated under various conditions. The catalytically active species comprised Mo-subcarbonyls, Mo-metal, and partially oxidized species. $Mo(CO)_6$ encaged in HY zeolite also for hydrogenation and metathesis of propylene and polymerization of ethylene [4]. In this system,

$Mo(CO)_6$ was completely decarbonylated during activations.

The catalytic properties of molybdenum subcarbonyls stabilized on oxide surface have rarely been reported up to now. With $Mo(CO)_6/Al_2O_3$ catalysts, Brenner and Burwell [2] have demonstrated that a subcarbonyl species, $Mo(CO)_3$, formed at 373 K shows the catalytic activity for the metathesis of propylene at 326 K in spite of 20-30 times lower activity than that of partially oxidized Mo-species produced by higher temperature activations. O'Neill and Rooney [5] and Brenner et al. [6] have made similar observations. However, no further catalytic properties of molybdenum subcarbonyls immobilized on inorganic materials have been explored yet.

In this present study, it has been demonstrated for the first time that molybdenum subcarbonyl species encaged in Y-zeolites show a stable activity for a highly selective hydrogenation of 1,3-butadiene to cis-2-butene.

Experimental

A NaY zeolite (Si/Al = 2.78) and its alkali-metal cation exchanged forms (M^+-Y; M^+ = Li, K, and Cs) were employed for the encapsulation of $Mo(CO)_6$. A decationized zeolite (HY), TiO_2 (Degussa, P-25), and γ-Al_2O_3 were also examined. The zeolite was exposed to a vapor of $Mo(CO)_6$ at room temperature for 12 h after an evacuation at 673 K for 1-2 h. The amount of $Mo(CO)_6$ encaged in the zeolite was about two molecules/supercage irrespective of

the cation involved. The hydrogenation of 1,3-butadiene was conducted over molybdenum species at 19.3 ± 0.7 kPa (H_2/butadiene = 2) and 423 or 273 K using a closed circulation system (200 cm^3). The amount of zeolite used in the reaction was 50 mg. The reaction gas was analyzed by GLC.

Results and Discussion

The compositional change of the reaction gas is depicted in Fig. 1 for the hydrogenation of butadiene over a freshly prepared $Mo(CO)_6$/LiY catalyst at 423 K as a function of the reaction time. It is demonstrated in Fig. 1 that butadiene is preferentially hydrogenated to cis-2-butene (> 96 %) at a significantly high rate, while the hydrogenation of cis-2-butene is not promoted at all and a slow isomerization is observed only after the complete consumption of butadiene. Carbon monoxide was evolved by a partial decomposition of $Mo(CO)_6$ and its pressure amounted to ca. 1.3 kPa during the reaction. This was also observed with the other freshly prepared $Mo(CO)_6$ catalyst systems. It was found that the catalyst could be reused in spite of a gradual activity loss, so long as CO was present during the reaction. When completely decarbonylated at 473 K, the molybdenum catalyst exhibited a significantly reduced activity and a different product distribution. The selectivity was not altered by the presence of CO.

These catalytic results for the $Mo(CO)_6$/LiY catalyst are

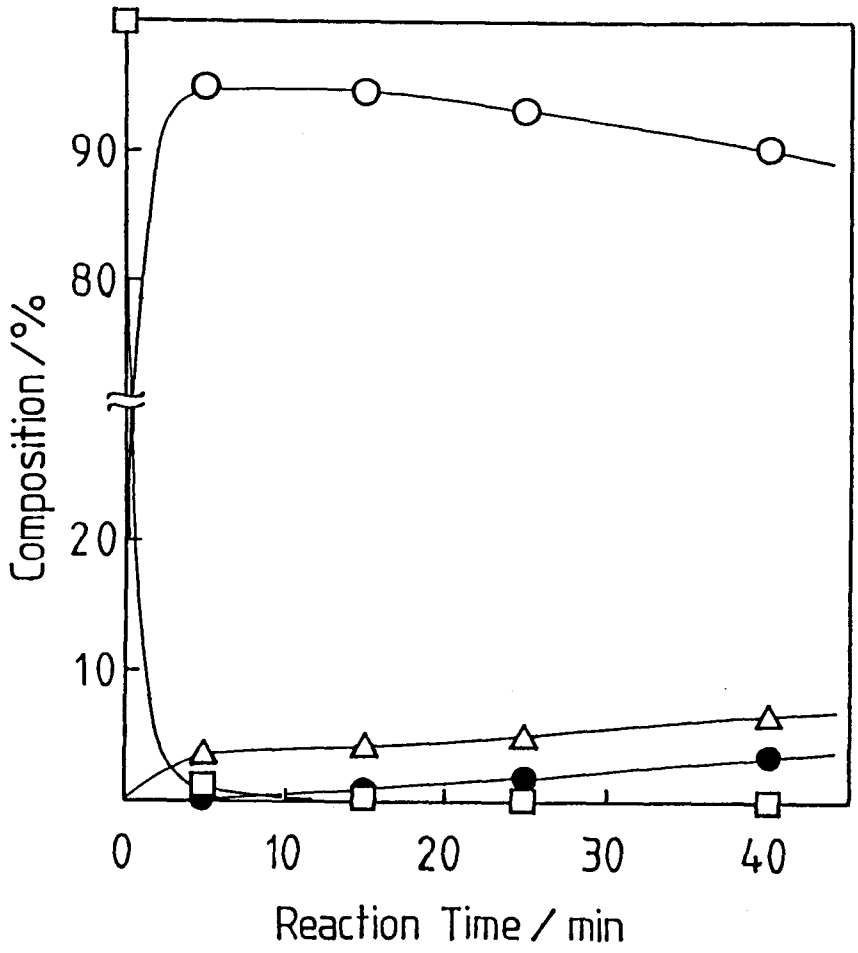

Figure 1 Composition of the reaction gas as a function of the reaction time for the hydrogenation of 1,3-butadiene over a $Mo(CO)_6$/LiY zeolite catalyst at 423 K.
○; cis-2-butene, △; 1-butene,
●; trans-2-butene, □; butadiene.

summarized in Table 1 as well as those for the other $Mo(CO)_6$ catalysts. It is worthy noting in Table 1 that M^+-Y zeolites show excellent selectivities to cis-2-butene in the hydrogenation of butadiene. However, the activity decreases in the order of LiY > NaY >> KY > CsY. On the other hand, the HY zeolite and other non-zeolitic materials exhibited non-selective hydrogenations under the present activation and reaction conditions.

It is well established that Mo-subcarbonyl species thermally stable at ca. 420 K are reversibly formed in the supercages of M^+-Y [7,8] and HY [9] zeolites during the decomposition of $Mo(CO)_6$. The composition of the subcarbonyl species was revealed to be $Mo(CO)_3$ on the basis of IR [8], temperature programmed decomposition [8] and ^{13}CO-isotopic laveling techniques [10]. Mo carbonyls, $Mo(CO)_x$ (x = 6-4), were found to be unstable at the reaction temperature in the zeolite cages [7-9]. On evacuation at 473 K, $Mo(CO)_3$ was irreversibly decomposed to Mo-metal for M^+-Y zeolites [4,7,8] or to partially oxidized Mo species for HY [4,9], Al_2O_3 [11], and, probably, TiO_2. Accordingly, it is concluded that molybdenum subcarbonyl species encaged in M^+-Y zeolites are responsible for the highly selective hydrogenation of 1,3-butadiene to cis-2-butene, whereas Mo-metal and partially oxidized Mo species for the non-selective hydrogenation.

The activity and selectivity of the molybdenum subcarbonyl species encaged in the zeolite are summarized in Table 2 for the hydrogenation of butadiene at 273 K as well as those of Mo metal (partially oxidized for the HY zeolite as evidenced by XPS). The

Table 1. Hydrogenation of 1,3-butadiene over $Mo(CO)_6$ encaged in a zeolite at 423 K

Zeolite[a]	Activation[b] Mode	Conversion at 5 min/%	Selectivity/%[c] n-b	1-b	t-2-b	c-2-b
LiY (45)	F	97.2	0.0	3.7	0.3	96.0
	473 K	6.6	5.3	42.2	11.2	41.3
	373 K[d]	6.0[d]	0.0	1.6	0.0	98.4
NaY	F	79.2	0.1	3.2	0.2	96.5
	373 K[d]	2.7[d]	0.0	0.3	0.0	99.7
KY (51)	F	12.9	0.0	3.2	0.3	96.5
CsY (58)	F	7.6	0.0	3.2	0.0	96.8
HY (76)	F	1.7	4.9	13.6	51.8	29.7
	473 K	14.2	10.4	34.1	14.9	40.6
TiO_2 (3.1)[e]	F	4.5	3.2	55.4	12.5	28.9
Al_2O_3 (2.0)[e]	F	3.1	2.1	53.3	12.2	32.4

a) Number in parentheses ; the degree of ion exchange. b) F; non-treatment where $Mo(CO)_6$ was used as prepared. After the reaction, the catalyst was evacuated at 473 K. c) n-b; n-butane, 1-b; 1-butene, t-2-b and c-2-b; trans- and cis-2-butene, respectively. d) Reaction temperature; 273 K and Conversion; at 1 h/%. e) Loading level of Mo (wt%).

Table 2 Hydrogenation of Butadiene at 273 K over Molybdenum Species Encaged in a Zeolite

Zeolite	Subcarbonyl[a]					Metal[b]				
	TOF[c] /h^{-1}	Selectivity[d]/%				TOF[c] /h^{-1}	Selectivity[d]/%			
		b	1-b	t-2-b	c-2-b		b	1-b	t-2-b	c-2-b
LiY	0.55	0	1.6	0	98.4	2.12	10.5	72.1	9.9	7.5
NaY	0.25	0	0.3	0	99.7	1.88	5.3	74.2	14.7	5.8
CsY	0.09	0	0	0	100	<0.01				
HY	0.06	2.4	23.9	10.4	63.3	0.58	10.6	53.6	9.8	26.0

a) Prepared by an evacuation at 373 K for 30 min.

b) Prepared by an evacuation at 473 K for 30 min.

c) Turnover frequency measured at the reaction time of 1 h.

d) b;butene, 1-b;1-butene, t-2-b;trans-2-butene, and c-2-b;cis-2-butene.

subcarbonyl species and Mo metal species were prepared by the evacuation at 373 and 473 K, respectively, for 30 min. The formations of the subcarbonyl species were confirmed by IR techniques in separate experiments. No further evolution of CO was detected during the hydrogenation at 273 K. A selective formation (>98%) of cis-2-butene was found over the subcarbonyl species in the Li, Na, and CsY zeolites. No productions of trans-2-butene and butane were detected. The product distributions were not altered with the reaction time. The diversified products for the subcarbonyl species in the HY zeolite are probably due to a sequential isomerization of the primary product. The formation of butane suggests the presence of Mo metal or partially oxidized species. The products of the butadiene hydrogenation over Mo metal are completely different from those over the subcarbonyl species, substantiating that cis-2-butene is selectively formed over the subcarbonyl species. A plausible reaction path is shown in Fig. 2.

The catalytic activity of the subcarbonyl species decreases in a order of LiY > NaY >CsY. This is inversely correlated to the order of the thermal stability of the subcarbonyl species or the strength of the interactions between the subcarbonyl species and zeolite framework oxygens. However, it is not ruled out that the size effects of cation control the apparent rate of the catalytic reaction. The low activity of the HY zeolite may be ascribed to the acidic sites in the zeolite.

Extremely high activities for the hydrogenation of propylene

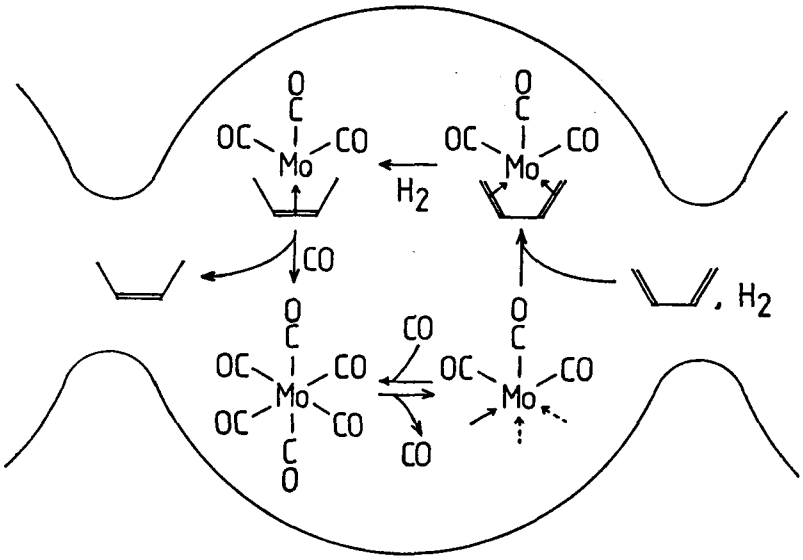

Figure 2 Plausible reaction path.

reported by Brenner [12] over $Mo(CO)_6/Al_2O_3$ catalysts at 423-473 K in a flow reaction system are ascribable to highly dispersed Mo-metal and/or partially oxidized Mo species, since the subcarbonyls show no olefin-hydrogenation activities as deduced from Table 1. This was confirmed by separate experiments.

In the case of photo-assisted hydrogenation of diene over $Mo(CO)_6$, $Mo(CO)_3$ is supporsed to be catalytically active species, although isomerization reactions of resultant olefins are important and various isomers are produced [13]. $Mo(CO)_6$ encaged in the zeolite seems to provide much more selective and active catalysts for the hydrogenation of diene to cis-olefins.

Therefore, it is concluded that the thermal stability and catalytic properties of the molybdenum subcarbonyl species are regulated by the cation and composion of the zeolite. This provides a promising clue to the preparation of well-defined molybdenum catalysts.

References

1) D.C.Bailey and S.H.Langer, Chem.Rev., 81, 109 (1981).

2) A.Brenner and R.L.Burwell, J.Catal., 52, 364 (1978).

3) a) R.Nakamura, D.Pioch, R.G.Bowmann, and R.L.burwell, J.Catal., 93, 388 (1985).

b) R.Nakamura and R.L.Burwell, J.Catal., 93, 399 (1985).

4) T.Yashima, K.Komatsu, and S.Namba, Chem.Express, 1, 701 (1986).

5) P.P.O'Neill and J.J.Rooney, J.Am.Chem.Soc., 94, 4383 (1972).

6) A.Brenner, D.A.Hucul, and S.J.Hardwick, Inorg.Chem., 18, 1478 (1979).

7) Y.Yong-Sing and R.F.Howe, J.Chem.Soc.,Faraday Trans.1, 82, 2887 (1986).

8) Y.Okamoto, A.Maezawa, H.Kane, I.Mitsushima, and T.Imanaka, J.Chem.Soc.,Faraday Trans.1, in the press.

9) P.Gallezot, G.Coudurier, M.Primet, and B.Imelik, "Molecular Sieves, II" (J.R.Katzer, Ed.) ACS Symp.Ser. Vol.40, 1977, p.144.

10) Y.Okamoto, A Maezawa, H.Kane, and T.Imanaka, J.Catal., under submission.

11) A.Brenner and R.L.Burwell, J.Catal., 52, 353 (1978).

12) A.Brenner, J.Mol.Catal., 5, 157 (1979).

13) M.Wrighton, D.S.Ginley, M.A.Schroeder, and D.L.Morse, Pure Appl.Chem., 41, 671 (1975).

Chapter 6

Preparation of Highly Dispersed Molybdenum Sulfide Catalysts from Molybdenum Hexacarbonyl

1. Molybdenum Sulfide/Alumina System

Abstract

Sulfided molybdenum catalysts prepared from $Mo(CO)_6$ were found to show higher catalytic activities than conventional MoO_3/Al_2O_3 catalysts for the hydrogenation of 1,3-butadiene and hydrodesulfurization of thiophene. Sulfiding process of the subcarbonyl species on Al_2O_3 and NO adsorption were studied by IR techniques.

Introduction

Sulfided molybdenum/alumina catalysts are widely used as hydrotreating catalysts. These catalysts are usually prepared by impregnation methods, followed by activation or presulfidation. The catalysts with low MoO_3 contents obtained in this way show only low catalytic activities. This is attributed to low reducibility of Mo species due to strong interactions with the

support [1,2]. Low valent molybdenum species are potential candidates for the preparation of sulfided molybdenum catalysts with high activities at low molybdenum contents.

Burwell et al. [3] prepared molybdenum species with low oxidation states supported on alumina by using $Mo(CO)_6$. These catalysts are very active for the hydrogenations of propylene [4,5] CO and CO_2 [6,7] and hydrogenolysis of cyclopropane [5]. Yashima et al. have shown similar results for $Mo(CO)_6$ encaged in HY zeolites [8]. These catalysts are composed of metallic or low-valent molybdenum oxides.

In this study, $Mo(CO)_6$ was examined to prepare catalytically active Mo sulfides with low Mo contents for the hydrogenation of 1,3-butadiene and hydrodesulfurization (HDS) of thiophene. The activities were compared with those of conventional sulfide catalysts.

Experimental

γ-Al_2O_3 was provided by the Catalysis Society of Japan as a reference catalyst (JRC-ALO-4, BET surface area; 163 m^2g^{-1}) [9]. Powdered Al_2O_3 was evacuated at 473-873 K for 1 h, followed by an exposure to a $Mo(CO)_6$ vapor (ca. 8 Pa) for 5 min and a subsequent evacuation for 10 min at room temperature. Such exposure-evacuation cycles were repeated 8 times. The loading level of Mo, thus prepared, was ca. 2 wt% as MoO_3. The sample was

evacuated at 373 or 673 K for 1 h and sulfided at 373 or 673 K for 1 h using a H_2/H_2S gas (H_2/H_2S = 2, ca. 2 kPa) and a closed circulation system. After a subsequent evacuation at 673 K for 40 min, the hydrogenation of 1,3-butadiene was carried out at 273 K and ca. 1 kPa (H_2/butadiene = 2). With the HDS of thiophene, the sample was evacuated at 673 K for 1 h and sulfided at the same temperature for 1.5 h using an atmospheric H_2S/H_2 (0.1) stream. Subsequently, the HDS of thiophene was conducted for 1 h at 673 K and an atmospheric pressure of thiophene/H_2 (1.6% thiophene, 1.0 L STP min^{-1}), followed by the measurements of the activity. Both reaction gases were analyzed by glc. A MoO_3/Al_2O_3 catalyst (2.5 wt% MoO_3) was prepared by a pore volume impregnation method using an aqueous solution of ammonium paramolybdate.

Results and Disussion

Figure 1 depicts the intrinsic hydrogenation activity (conversion per unit weight of MoO_3 at the reaction time of 10 min) as a function of the sulfidation degree of Mo estimated from the S2p/Mo3d XPS intensity ratio. It is likely that the hydrogenation activity of sulfided Mo/Al_2O_3 catalyst prepared from $Mo(CO)_6$ decreased and subsequently leveled off with increasing the extent of sulfidation irrespective of the pretreatment and sulfidation conditions. It is evident from Fig. 1 that the activity of the catalyst prepared from $Mo(CO)_6$ is

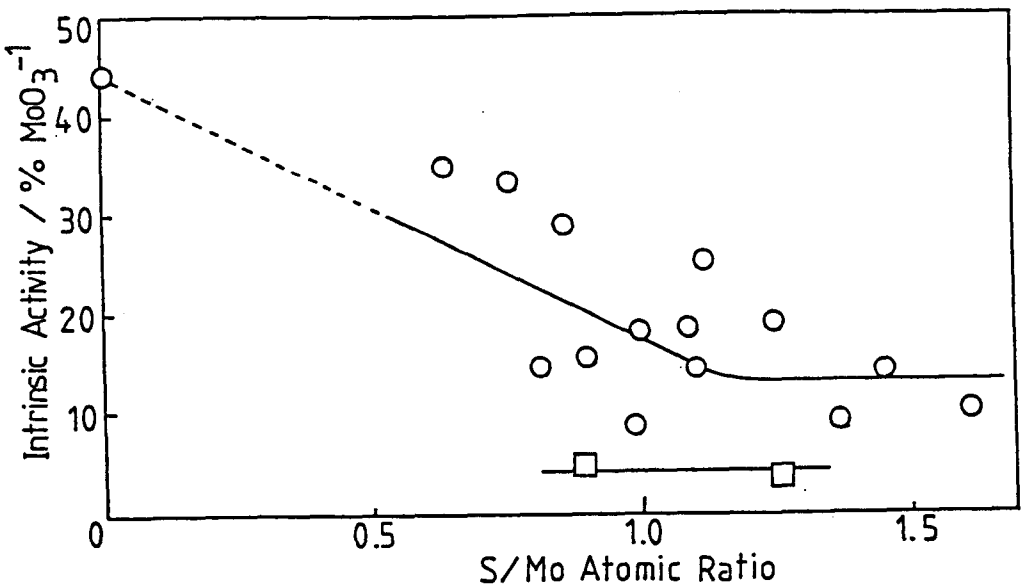

Figure 1 Dependencies of the hydrogenation activity of sulfided Mo/Al_2O_3 catalysts on the extent of sulfidation of Mo. Prepared from $Mo(CO)_6$ (○) and by the impregnation (□).

2-3 times higher than that of the sulfided MoO_3/Al_2O_3 catalyst with a similar level of Mo-loading (2.5 wt% MoO_3). As for the HDS of thiophene, it was also found that the sulfided catalyst prepared from $Mo(CO)_6$ showed 1.5 times higher activities than the corresponding conventional catalyst. It is demonstrated that the sulfided Mo catalysts prepared from $Mo(CO)_6$ show higher catalytic activities than the conventional catalysts for the hydrogenation of 1,3-butadiene and the HDS of thiophene.

In order to obtain some insights into a sulfiding process, IR spectra were measured with $Mo(CO)_6$ adsorbed on the Al_2O_3. As shown in Fig. 2, adsorbed subcarbonyl species, $Mo_2(CO)_6$ (2003, 1880, and 1570 cm^{-1}) and $Mo_2(CO)_8$ (2030, 1950, and 1640 cm^{-1}) [10], are mainly observed after evacuation at 373 K. An introduction of H_2S at room temperature (ca. 3.3 kPa) was found to remove these subcarbonyl species immediately and to provide bands at 2030 and 1940 cm^{-1} with weak shoulder peaks at around 1980 and 1810 cm^{-1}. A subsequent adsorption of NO showed doublet bands (1790 and 1685 cm^{-1}) characteristic to NO adsorbed on sulfided molybdenum species [11]. The doublet bands were observed at 1813 and 1706 cm^{-1} when NO was introduced to a $Mo(CO)_6/Al_2O_3$ catalyst evacuated at 673 K. They are assigned to NO adsorbed on Mo-oxide sites. Although the exact structures of the molybdenum species are currently under study, it is apparent that subcarbonyl species react immediately with H_2S to produce coordinatively unsaturated molybdenum sulfides at room temperature.

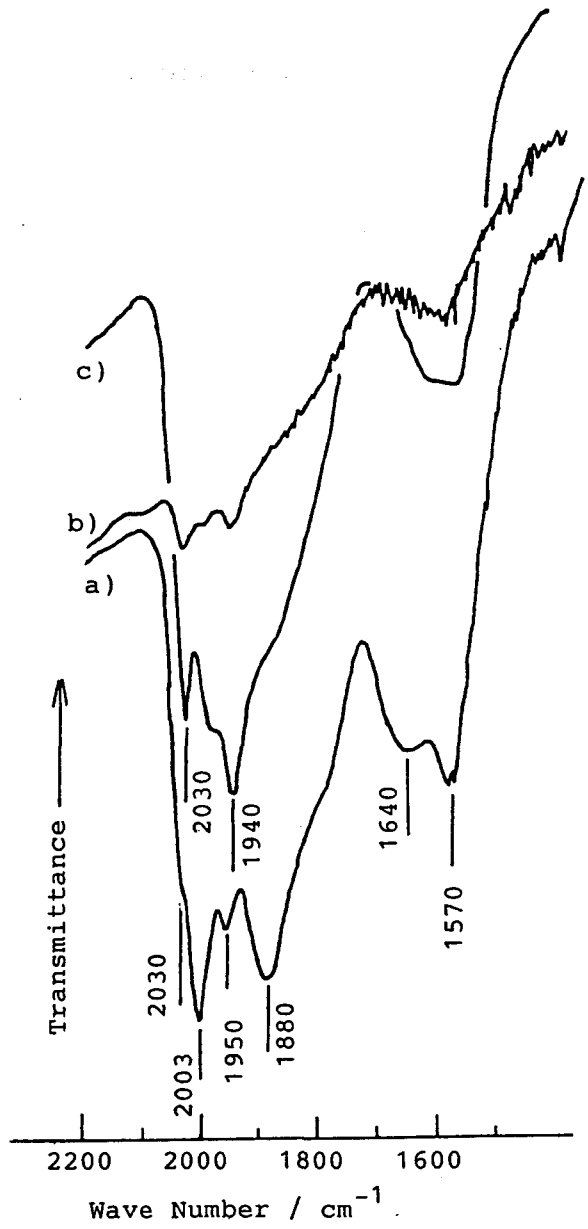

Figure 2 IR spectra of molybdenum subcarbonyl/ Al_2O_3 catalyst. (a) exposed to $Mo(CO)_6$ vapor for 10min, followed by an 1h-evacuation at 373 K, (b) sample a was exposed to H_2S (10 kPa) at 373 K, and (c) sample a was exposed to H_2S (ca. 3.3 kPa) at room temperature.

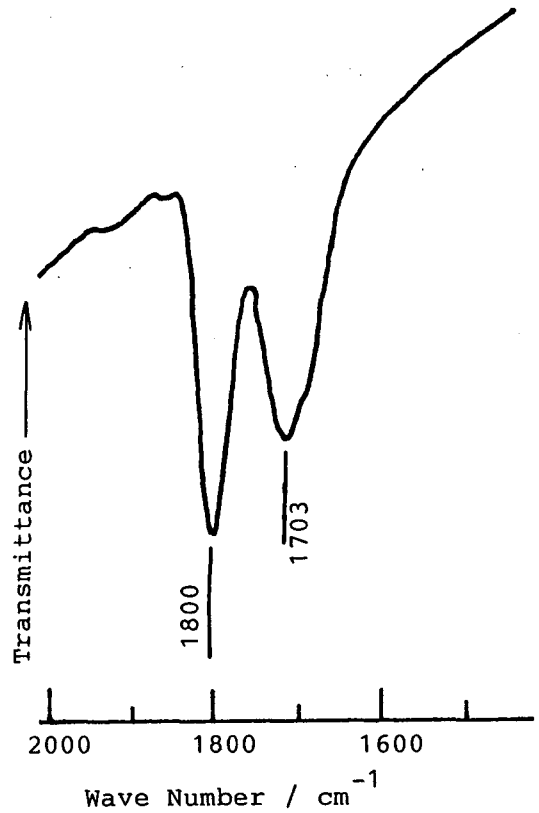

Figure 3 IR spectra of chemisorbed NO on the sulfided Mo/γ-Al_2O_3 catalyst prepared from $Mo(CO)_6$.

When a Mo-subcarbonyl/Al_2O_3 system prepared at 373 K was exposed to H_2S at the same temperature, the carbonyl stretching bands were almost completely removed (Fig. 2). As shown in Fig. 3, a subsequent NO adsorption at room temperature showed typical doublets at 1800 and 1703 cm^{-1} that were very close to those observed for sulfided MoO_3/Al_2O_3 (2.5 wt%) catalyst (1797 and 1716 cm^{-1}) [12]. Therefore, the active Mo sites on the sulfided catalysts in Fig. 1 are considered to consist mainly of sulfided Mo species. The angles of ON-Mo-NO oscillators estimated from the IR band intensity ratio of symmetric/asymmetric bands [13] were 96 and 85° for the $Mo(CO)_6$ catalysts evacuated at 673 K and sulfided at 373 K, respectively. The latter value was very close to the sulfided MoO_3/Al_2O_3 catalyst (84°) [12]. Accordingly, it seems that the increased catalytic activities of sulfided Mo/Al_2O_3 catalysts prepared from $Mo(CO)_6$ are attributed to the increase in the amount of active Mo sites rather than the change in the configuration of active Mo sites.

References

1) D.S.Zingg, L.E.Makowsky, R.E.Tischer, F.R.Brown, and D.M.Hercules, J.Phys.Chem., 84, 2898 (1980).

2) C.P.Li and D.M.Hercules, J.Phys.Chem., 88, 456 (1984).

3) A.Brenner and R.L.Burwell, J.Am.Chem.Soc., 97, 2565 (1975).

4) R.L.Burwell, J.Catal., 86, 301 (1984).

5) R.G.Bowman and R.L.Burwell, J.Catal., 88, 388 (1984).

6) R.G.Bowman and R.L.Burwell, J.Catal., 63, 463 (1980).

7) C.B.Murchison, "Proc.4th.Inter.Conf.Chem. and Uses of Molybdenum" (H.F.Barry and P.C.H.Mitchell, Eds.), p197, Climax Molybdenum Company, Ann Arbor, Michigan, 1982.

8) T.Yashima, T.Komatsu, and S.Namba, Chem.Express, 1, 701 (1986) and references therein.

9) a) Y.Murakami, "Preparation of Catalysis" (G.Ponecelet, P.Grange, and P.A.Jacobs, Eds.) vol.III, p775, Elsevier Amsterdam, 1983.

   b) see Chapter 1.

10) A.Kazusaka and R.F.Howe, J.Mol.Catal., 9, 183 (1980).

11) J.Valyon and W.K.Hall, J.Catal., 84, 216, (1983).

12) see Chapter 2.

13) H.C.Yao and W.G.Rothschild, "Proc. 4th Int. Conf. Chemistry and Uses of Molybdenum" (H.F.Barry and P.C.H.Mitchell, Eds.) 1982, p31.

2. Molybdenum Sulfide/Zeolite System

Abstract

It is found that molybdenuum subcarbonyl species, $Mo(CO)_3$, in the HY and NaY zeolite react with H_2S to produce carbonyl species coordinated with SH, $Mo(CO)_3(SH)$. The sulfided Mo/zeolite catalysts prepared from $Mo(CO)_6$ was demonstrated to show higher activity for the hydrodesulfurization of thiophene than conventional MoO_3/Al_2O_3 catalysts. This is ascribed to an extremely high dispersion of molybdenum sulfides in zeolites on the basis of the NO adsorption.

Introduction

Molybdenum sulfide catalysts are widely used in industry for hydrodesulfurization (HDS). As for MoO_3/Al_2O_3 catalysts with low MoO_3 contents prepared by a impregnation method, low reducibility of Mo species due to strong interactions with the support [1,2] cause low catalytic activities. Low valent molybdenum species such as $Mo(CO)_6$ are potential candidates for the preparation of sulfided molybdenum catalysts with high activities even at low molybdenum contents.

Metal or metal oxide catalysts prepared from transition-metal carbonyls immobilized on inorganic matrices show prominent catalytic properties [3-5]. In particular, zeolites are expected

to provide potential media for producing well-characterized species owing to their well-defined electronic and geometric structures. Low-valent molybdenum species prepared from $Mo(CO)_6$ encaged in zeolites are included in such systems [6-10]. With $Mo(CO)_6$ encaged in HY zeolites, Yashima et al. [11] have shown that molybdenum is oxidized by the reaction with surface hydroxyl groups and that the average oxidation number of molybdenum increases with increasing the concentration of hydroxyl groups and the decomposition temperature of the carbonyl. The oxidation of molybdenum by hydroxyl groups was also demonstrated by XPS measurement [12]. Under their activation conditions, $Mo(CO)_6$ is completely decarbonylated. Detailed properties of molybdenum carbonyl species encaged in zeolites have been described in Chapters 4 and 5.

In this present study, a high reactivity of the subcarbonyl species toward H_2S was examined for preparation of highly dispersed molybdenum sulfide catalysts for the HDS reaction of thiophene.

Experimental

NaY and HY zeolites were supplied by Catalysis Society of Japan as reference catalysts (JRC-Z-Y5.6 and -HY5.6, Si/Al = 2.78 for both zeolites). Another kind of NaY zeolite (NaY(4.8)) was also provided by Catalysis Society of Japan as a reference catalyst (JRC-Z-Y4.8; Si/Al = 2.38). The NaY zeolite was ion-

exchanged with a series of alkali-metal cations to produce MY zeolites (M; Li, K, Rb, and Cs) as described previously [13]. The degree of ion-exchange is summarized in Table 1 in Capter 4 except for RbY(4.8). The degree of ion-exchange of the RbY(4.8) zeolite was 64%.

After an evacuation at 673 K for 1.5 h, the powdered zeolite was exposed to a $Mo(CO)_6$ vapor (ca. 8 Pa) [14] at room temperature for 16 h. The sample was evacuated at 473 K for 1.5-2 h, followed by an exposure to H_2S (ca. 6.5 kPa) at the same temperature for 30 min. Sebsequently, the catalyst was evacuated at 473 K for 30 min and then at 673 K for 30 min. The HDS reaction of thiophene was conducted for 1 h at 673 K and an atmospheric pressure of thiophene/H_2 (1.6 % thiophene, 1 L STP min^{-1}), followed by a measurement of the activity at a reaction time of 1 h. The reaction gas was analyzed by GLC. Subsequently, the catalyst was treated with an atmospheric pressure of a deoxygenated and dehydrated H_2-stream at 673 K for 1 h and evacuated at the same temperature. After being cooling to room temperature under a dynamic vacuum, the amount of NO chemisorption was measured at room temperature (exposed to NO for 0.5 h and evacuated for 1 h, accompanied by NO physisorption experiments). After that, the XP spectra of the catalyst was measured without exposing the catalyst to air. The XPS measurements were made on a Hitachi 507 photoelectron spectrometer at 9 kV and 50 mA. Assuming linear backgrounds, the intensity ratio were determined by using the integrated areas of

the Mo3d, S2p, S2s, and Si2s levels. The binding energies were referenced to the Si2s level.

Results and discussion

The decomposition of $Mo(CO)_6$ encaged in the zeolite gives the formation of molybdenum subcarbonyl species which is assigned to $Mo(CO)_3$ (see Capter 4). In order to prepare highly dispersed molybdenum sulfides, the reaction between $Mo(CO)_3$ encaged in the zeolite and H_2S was examined. Figure 1 shows the IR spectra of the $Mo(CO)_3$ encaged in the NaY and HY zeolites exposed to H_2S (5 kPa) at room temperature. The spectra changed rapidly at first and then gradually on an exposure to H_2S. On a prolonged exposure time (16 h), the spectra exhibited characteristic ν(CO) band at 2018, 1980, and 1940 cm^{-1} and did not change with an evacuation at room temperature. As for the HY zeolite, a broad band at 1980 cm^{-1} predominated after a 16 h-exposure to H_2S at ambient temperature as shown in Fig. 1. The ν(S-H) bands were observed at 2530 cm^{-1} for both the zeolite systems. The sulfur content (S/Mo atomic ratio estimated by S2p/Mo3d XPS intensity ratio) of the subcarbonyl species in the NaY zeolite was calculated to be 1.2. The TPDE experiments of a $H_2S/Mo(CO)_3$/NaY system showed that the complex was decomposed at 350 K, accompanying a significant amount of hydrogen evolution. In addition, the amount of CO evolved during the TPDE corresponded to that for $Mo(CO)_3$. These findings suggest that $Mo(CO)_3$ in the HY and NaY zeolites react

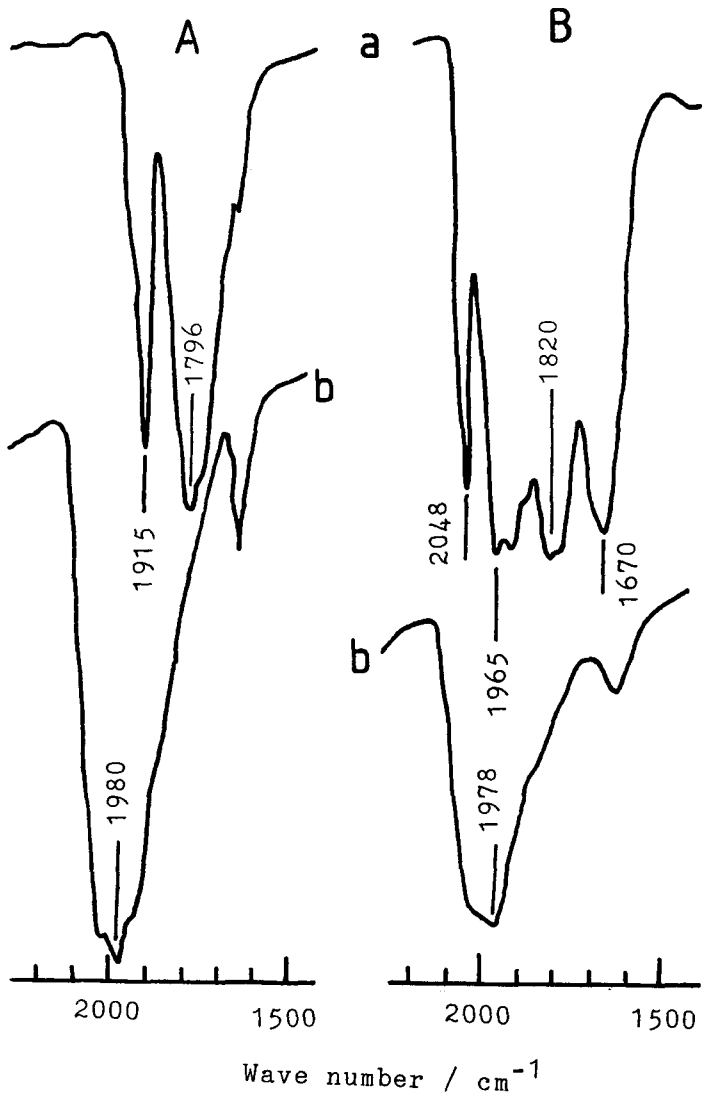

Figure 1 IR spectra of the subcarbnyl species encaged in NaY (A) and HY (B) zeolites.
(a) $Mo(CO)_3$ formed at 373 K and (b) $Mo(CO)_3$ exposed to H_2S (5 kPa) at ca. 300 K.

with H_2S to produce carbonyl species coordinated with SH, $Mo(CO)_3(SH)_{ads}$. A similar complex, $(\eta^5\text{-}C_5H_5)Mo(CO)_3(SH)$, is known to be prepared from $(\eta^5\text{-}C_5H_5)Mo(CO)_3H$ and elemental sulfur [15].

On the other hand, no carbonyl bands were observed when $Mo(CO)_3$/NaY was exposed to H_2S (5 kPa) at 373 K and the S/Mo atomic ratio was estimated to be 2.1 from a XPS measurement.

The thiophene HDS activity of the $Mo(CO)_3$/zeolite catalysts exposed to H_2S at 373 K and subsequently evacuated at 673 K are summarized in Table 1. The HDS activity (% $g\text{-}cat^{-1}$) of the sulfided catalysts prepared from $Mo(CO)_6$ except for the HY zeolite are 4-5 times larger than that of the MoO_3/Al_2O_3 catalyst sulfided at H_2S/H_2 = 0.1 and 673 K.

Among the sulfided catalysts prepared from $Mo(CO)_6$, the HDS activity of the NaY or KY zeolite shows a maximum as shown in Fig. 2. The HY zeolite-supported catalyst is as active as the Al_2O_3-supported catalyst prepared by a conventional impregnation method.

The XPS spectra of the Mo3d band are shown in Fig. 3. As for the HY zeolite-supported catalyst, the Mo3d binding energy (BE) is higher than that of the other zeolite-supported catalyst as shown in Table 1. It is indicated that Mo species on the HY zeolite is slightly oxidized by hydroxyl groups during the formation of $Mo(CO)_3$ [11]. Therefore, it is considered that the valence state of Mo sulfides on HY zeolite differs from those on the other zeolites. The $Mo3d_{5/2}$ BE of crystalline MoS_2 was 229.6 eV, which is very close to that of the sulfided Mo/HY

Table 1. HDS reaction and XPS results on sulfided Mo/zeolite catalyst.

Zeolite	O1s BE / eV	Activity /% g-cat^{-1}	TOF[a] /s^{-1}	Fraction of cus Mo	Mo3d$_{5/2}$ BE / eV	Mo3d/Si2s XPS intensity ratio
HY	532.6	3.5	1.9	0.16	229.7	0.14
LiY	532.2	13.5	4.9	0.25	229.2	0.32
NaY	532.0	18.7	5.2	0.31	229.2	0.42
KY	531.9	18.8	3.9	0.41	229.4	0.35
RbY	531.5	13.5	3.5	0.32	228.9	0.39
CsY	531.5	12.6	2.9	0.36	229.1	0.44
Al_2O_3 (10wt% MoO_3)		3.8	0.9	0.13		

a) estimated from the amount of NO chemisorption.

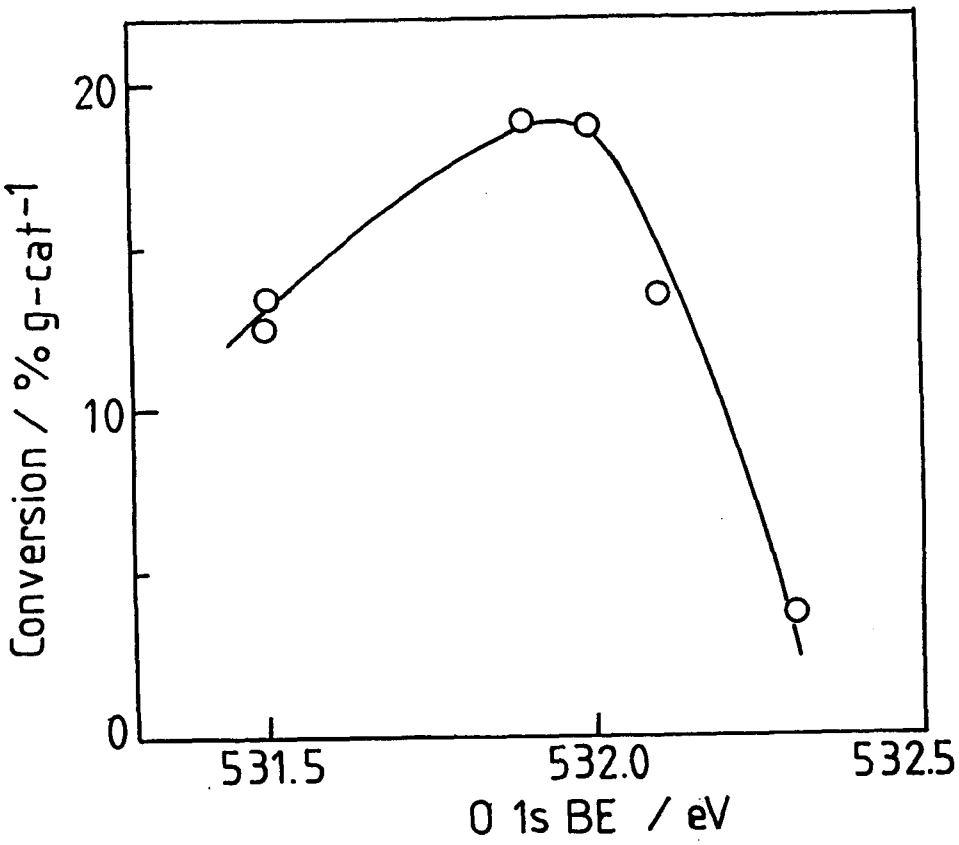

Figure 2 Dependency of the thiophene HDS activity of the sulfided Mo/zeolite catalysts upon the O1s binding energy.

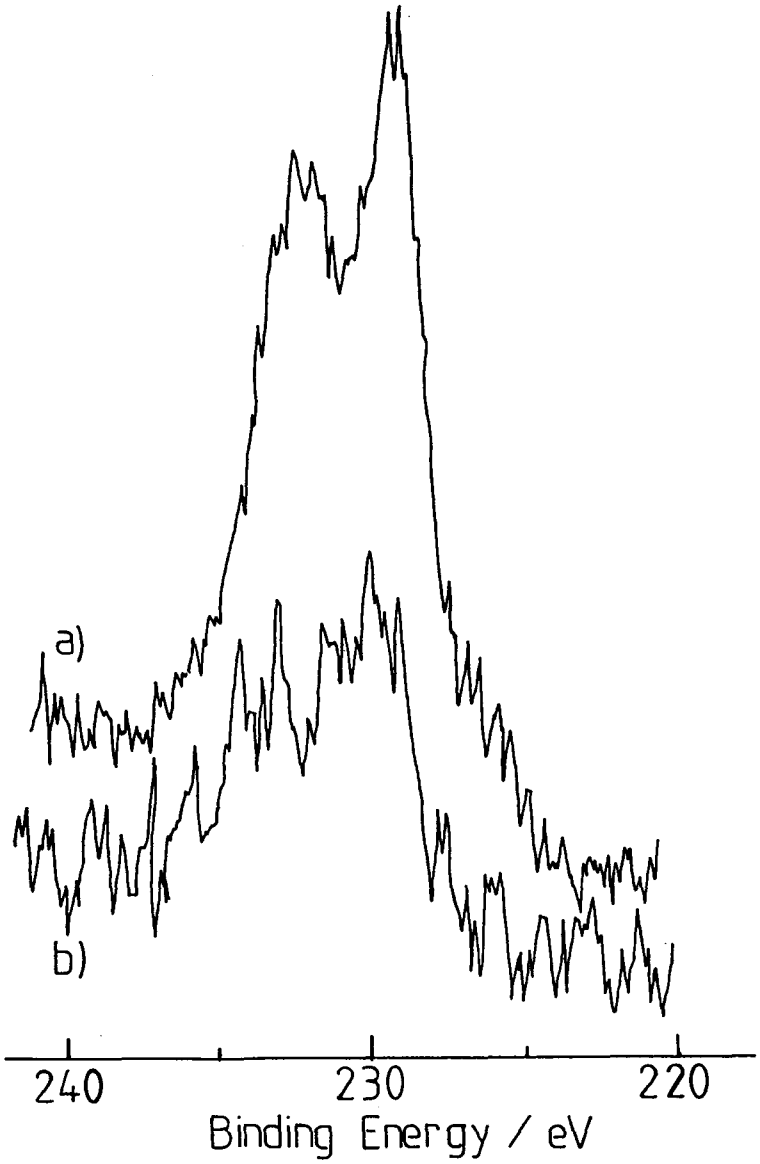

Figure 3 X-ray phtoelectron spectra of molybdenum sulfide/zeolite. (a) NaY and (b) HY zeolites.

catalyst. It is concluded that the oxidation number of Mo on HY zeolite is ca. 4 and that of the molybdenum sulfide species on the other zeolites are lower than 4.

The turn-over frequency (TOF) of the thiophene HDS reaction over the sulfided Mo/zeolite catalysts prepared from $Mo(CO)_6$ are also summarized in Table 1 and depicted in Fig. 4 as a function of the O1s BE. Except for the HY zeolite, the TOF decreases with decreasing the O1s BE. This indicates that the interaction strengths between $Mo(CO)_3$ and, probably, resulting sulfides and zeolite framework oxygen affect the TOF of the thiophene HDS reaction. It is considered that the lower TOF of HY zeolite is attributed to the oxidation of Mo sulfide on the basis of the XPS results in Fig. 3.

The dispersion degree of sulfided molybdenum was assessed by the amount of NO chemisorption at ca. 300 K [16]. The fraction of coordinatively unsaturated (cus) Mo thus obtained is summarized in Table 1 and shown in Fig. 5 as a function of the O1s BE. The fraction of cus Mo on the sulfided Mo/zeolite catalysts prepared from $Mo(CO)_6$ were 2-3 times higher than that in the sulfided MoO_3/Al_2O_3 catalyst except for the HY zeolite. It is concluded that highly dispersed Mo sulfides are prepared by using $Mo(CO)_6$ encaged in zeolites. As for the HY zeolite, it is suggested that Mo species aggregate during the formation of $Mo(CO)_3$ or the sulfidation from the Mo3d/Si2s XPS intensity ratio as listed in Table 1.

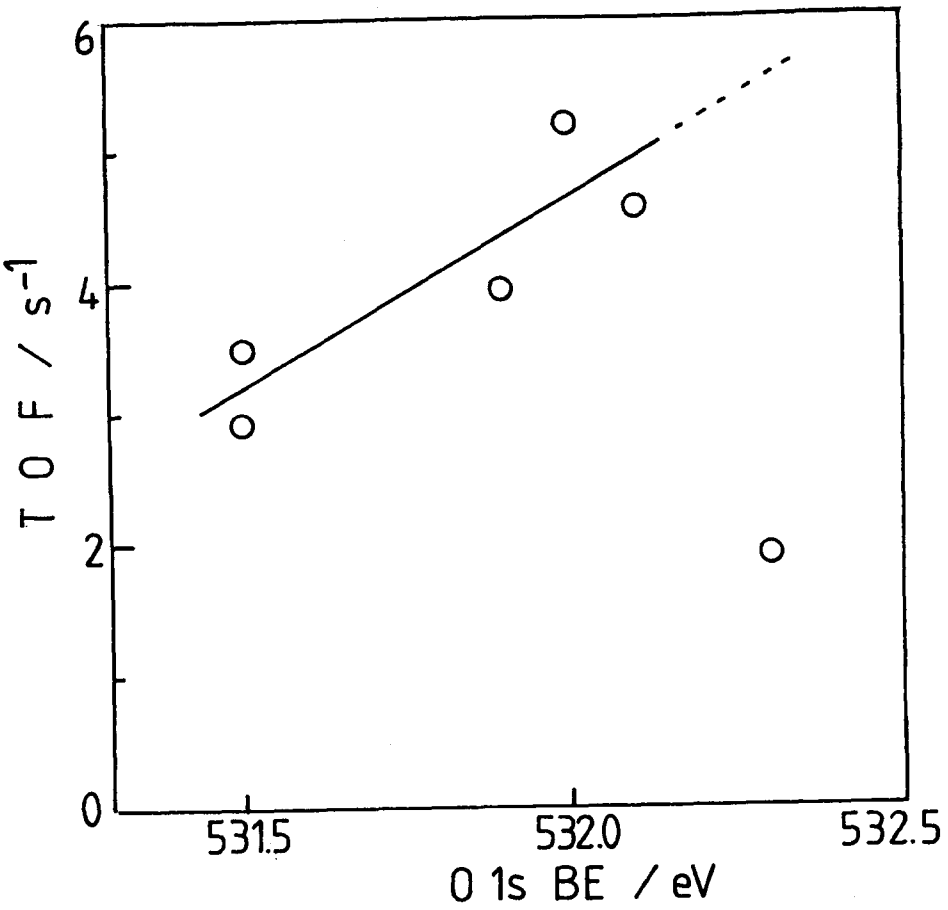

Figure 4 Turn-over frequency of the thiophene HDS reaction over the sulfided Mo/zeolite catalysts as a function of the O1s binding energy.

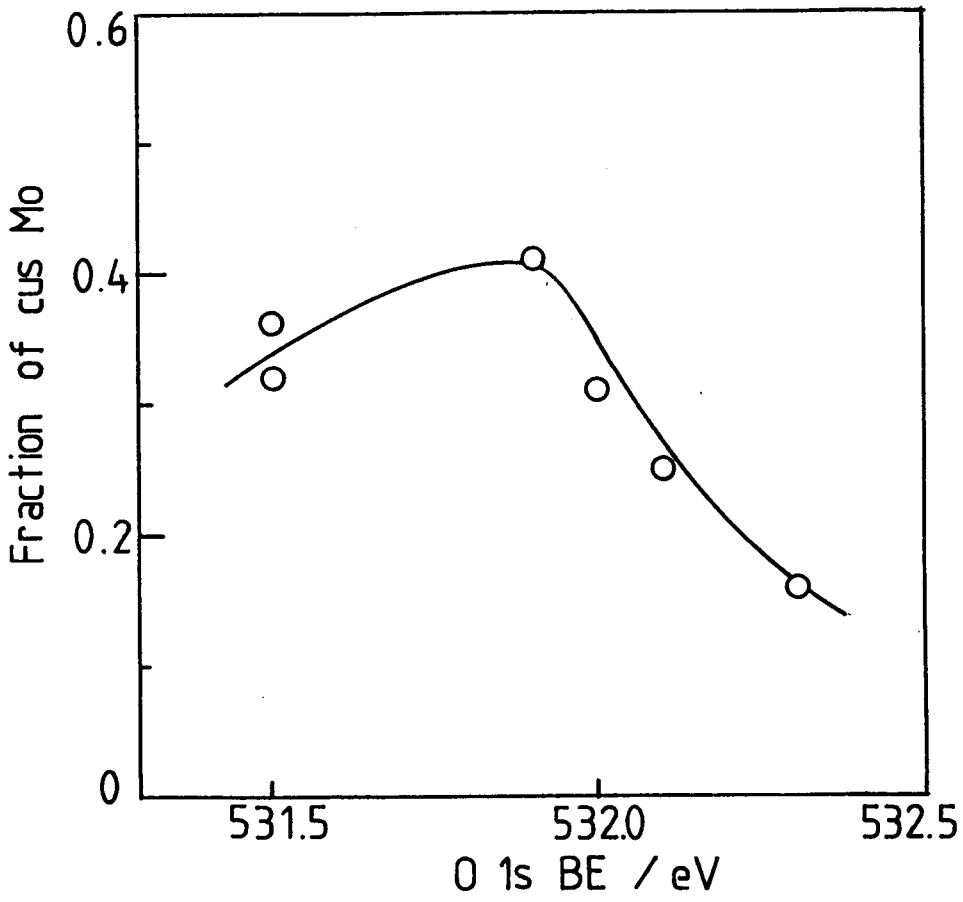

Figure 5 Fraction of cus Mo as a function of O1s binding energy.

References

1) D.S.Zingg, L.E.Makowsky, R.E.Tischer, F.R.Brown, and D.M.Hercules, J.Phys.Chem., 84, 2898 (1980).

2) C.P.Li and D.M.Hercules, J.Phys.Chem., 88, 456 (1984).

3) Yu.I.Yermakov, B.N.Kuznetsov, and V.A.Zakharov, "Catalysis by Supported Complexes", Elsevier, Amsterdam, 1981.

4) D.C.Bailey, and S.H.Langer, Chem.Rev., 81, 109 (1981).

5) Phillips,J. and J.A.Dumesic, Appl.Catal., 9, 1 (1984).

6) P.Gallezot, G.Coudurier, M.Primet, and B.Imelik, "Molecular Sieves II" (J.R.Katzer, Ed.) ACS Symp. Ser. Vol.40, 1977, p144.

7) T.M.Tri, J.-P.Candy, P.Gallezot, J.Massardier, M.Primet, J.C.Vedrine, and B.Imelik, J.Catal., 79, 396 (1983).

8) S.Abdo, and R.F.Howe, J.Phys.Chem., 87, 1713 (1983).

9) S.Abdo, and R.F.Howe, J.Phys.Chem., 87, 1722 (1983).

10) Y.Yon-Sing, and R.F.Howe, J.Chem.Soc.,Faraday Trans.1, 82, 2887 (1986).

11) T.Yashima, T.Komatsu, and S.Namba, Chem.Expess., 1, 701 (1986) and references therein.

12) T.Komatsu, S.Namba, T.Yashima, K.Domen, and T.Ohnishi, J.Mol.Catal., 33, 345 (1985).

13) see Chapter 4

14) R.R.Monchamp and F.A.Cotton, J.Chem.Soc., 1438 (1960).

15) R.A.Fischer, H.-J.Kneuper, and W.A.Herrmann, J.Organometal.Chem., 330, 377 (1987).

16) W.S.Millman and w.K.Hall, J.Phys.Chem., 83, 427 (1979).

Summary

In this thesis, the characterization of dispersed molybdenum sulfide catalysts were investigated in order to reveal the catalytic properties of the molybdenum sulfide based-hydrodesulfurization catalysts. The preparation of highly dispersed molybdenum sulfide catalysts were also examined by using molybdenum hexacarbonyl adsorbed on zeolite or Al_2O_3. The main conclusions concerning the above subjects in this thesis are as follows:

1) On the basis of the H_2S adsorption, molybdenum anions are established to react with surface hydroxyl groups on Al_2O_3 as bidentate ligands similarly to SO_4^{2-} anions, forming a monomolecular layer, when the MoO_3 content is low (< 3 wt%). On a futher increase in the molybdenum content, polymolybdate phases are formed because of the consumption of reactive hydroxyl groups. When the MoO_3/Al_2O_3 catalysts are sulfided, the bare Al_2O_3 surface restores greatly, suggesting a cleavage of Mo-O-Al bonds and rearrangements of molybdenum species. In addition, H_2S adsorption sites were elucidated for the Al_2O_3 surface.

2) Temperature programmed desorption studies of NO have shown the presence of two kinds of coordinatively unsaturated molybdenum sites, doubly and triply, on the sulfided molybdenum catalysts supported on Al_2O_3 or TiO_2 coupled with the IR study of the coadsorption of H_2S and NO. The variations in the TOF of the molybdenum catalysts with the molybdenum content are interpreted

in terms of the unsaturation degree of active sites for the hydrodesulfurization of thiophene and the hydrogenation of 1,3-butadiene.

3) It is shown by using the surface techniques that zinc ions distribute over an alumina surface forming "surface spinel" irrespective of the calcination temperature. Interactions between ZnO and pre-existing molybdate phase induce surface segragation of ZnO. These findings suggest similar interactions between promoters (e.g. CoO) and molybdate phases even in the precursor states.

4) The molybdenum subcarbonyl species thermally stable are established to be $Mo(CO)_3$. The thermal stabilities of the carbonyl species depend strongly on the zeolite cation, suggesting the determining factor to be basic nature of zeolite framework oxygen.

5) The catalytic properties of the molybdenum subcarbonyl species adsorbed on inorganic materials have been explored. It has been found that 1,3-butadiene is selectively hydrogenated to cis-2-butene over the molydenum subcarbonyl species.

And finally,

6) It has been demonstrated that highly dispersed molybdenum sulfides are prepared by reactions between molybdenum subcarbonyl species and H_2S. These sulfide species show high catalytic activities for the hydrodesulfurization of thiophene and the hydrogenation of butadiene.

Bibliography

The works in this thesis have been published in the following papers.

1) "H_2S Adsorption on Al_2O_3, Modified Al_2O_3, and MoO_3/Al_2O_3"
Y.Okamoto, M.Oh-Hara, A.Maezawa, T.Imanaka, and S.Teranishi,
J. Phys. Chem., 90, 2396 (1986).

2) "Physicochemical Characterization of ZnO/Al_2O_3 and ZnO-MoO_3/Al_2O_3 Catalysts"
A.Maezawa, Y.Okamoto, and T.Imanaka,
J. Chem. Soc., Faraday Trans. 1, 83, 665 (1987).

3) "Thermal Decomposition of $Mo(CO)_6$ Encaged in a NaY Zeolite"
A.Maezawa, H.Kane, Y.Okamoto, and T.Imanaka,
Chem. Express, 2, 531 (1987).

4) "Preparation of Sulfided Molybdenum Catalysts from $Mo(CO)_6$"
A.Maezawa, M.Kitamura, K.Wakamoto, Y.Okamoto, and T.Imanaka,
Chem. Express, 3, 1 (1988).

5) "Thermal Stabilities of Molybdenum Hexacarbonyl and Subcarbonyls Encapsulated in NaY and NaX Zeolites"
Y.Okamoto, A.Maezawa, H.Kane, I.Mitsushima, and T.Imanaka,
J. Chem. Soc., Faraday Trans. 1, (1988) in press.

6) "Thermal Stabilities and Catalytic Activities of Molybdenum Carbonyls Encapsulated in Zeolites"
A.Maezawa, H.Kane, Y.Okamoto, and T.Imanaka,
Chem. Lett., 241, (1988) in press.

7) "Highly Selective Hydrogenation of 1,3-Butadiene to cis-2-Butene over Molybdenum Subcarbonyl Species Encapsulated in Alkali-Metal Cation Exchanged Y-Zeolites"
Y.Okamoto, A.Maezawa, H.Kane, and T.Imanaka,
J. Chem. Soc., Chem. Commun., (1988) in press.

8) "Thermal Stabilities and Catalytic Activities of Molybdenum Carbonyls Encaged in a Zeolite and Preparation of Molybdenum Sulfide Catalysts"
Y.Okamoto, A.Maezawa, H.Kane, and T.Imanaka,
"Proceedings of the Nineth International Congress on Catalysis", Calgary, July, 1988, in press.

9) "Stoichiometry of Molybdenum Subcarbonyl Species Encaged in NaY and HY Zeolites"
Y.Okamoto, A.Maezawa, H.Kane, and T.Imanaka,
J. Catal., under submission.

10) "Characterization of Active Sites on Sulfided Molybdenum/Alumina Hydrodesulfurization Catalysts"
A.Maezawa, M.Kitamura, Y.Okamoto, and T.Imanaka,
Bull. Chem. Soc. Jpn., under submission.

11) "Support Effects on the Activity of Molybdenum Sulfide Hydrodesulfurization Catalysts"
A.Maezawa, Y.Okamoto, and T.Imanaka,
in preparation for publication.

Acknowledgements

The studies described in this thesis was carried out at the Department of Chemical Engineering, Faculty of Engineering Science, Osaka University. I am deeply indebted to Prof. Dr. Shiichiro Teranishi and Prof. Dr. Toshinobu Imanaka for their helpful discussions and suggestions. I should like to express my sincere thanks to Dr. Yasuaki Okamoto for his valuable advice, helpful discussions, and continuous encouragement. Without their generous supports, the present studies would have never been accomplished.

I am gratful to Dr. Yuriko Nitta for her thoughtful advice. I should like to expess my appreciation to Mr. Masaru Kitamura and Mr. Hiroshige Kane for achievement of many difficult experiments, and also I heartily appreciate many efforts of Mr. Minoru Oh-Hara, Mr. Isao Mitsushima, and Mr. Koutaro Wakamoto. While I have encouraged by many other menbers of Imanaka Laboratry, I can not find proper words to my gratitude.

Finally, I am deeply thankful to my parents for their deep understanding and continuous encouragement.